TURUN YLIOPISTON JULKAISUJA
ANNALES UNIVERSITATIS TURKUENSIS

SARJA - SER. D OSA - TOM. 1087

MEDICA - ODONTOLOGICA

DEVELOPMENT OF POROUS GLASS-FIBER REINFORCED COMPOSITE FOR BONE IMPLANTS

Evaluation of antimicrobial effect and implant fixation

by

Sara Nganga

TURUN YLIOPISTO
UNIVERSITY OF TURKU
Turku 2013

From the Department of Biomaterials Science, Institute of Dentistry, Faculty of Medicine, University of Turku, Turku, Finland

Supervised by
Professor Pekka Vallittu, D.D.S., Ph.D., C.D.T.
Department of Biomaterials Science
Institute of Dentistry, University of Turku
Turku, Finland

and

Adjunct Professor Niko Moritz, Ph.D.
Department of Biomaterials Science
Institute of Dentistry, University of Turku
Turku, Finland

Reviewed by
Professor Gudmund Skjåk-Bræk, Dr. Techn.
NTNU, Department of Biotechnology
Norwegian University of Science and Technology
Trondheim, Norway

and

Professor Timo Jämsä, Ph.D.
Department of Medical Technology
Institute of Biomedicine
University of Oulu, Finland

Opponent
Professor Serena Best, CEng, MIM, Ph.D.
Cambridge Centre for Medical Materials
Department of Materials Science and Metallurgy
University of Cambridge, UK

The originality of this dissertation has been checked in accordance with the University of Turku quality assurance system using the Turnitin OriginalityCheck service.

ISBN 978-951-29-5514-5 (PRINT)
ISBN 978-951-29-5515-2 (PDF)
ISSN 0355-9483
Painosalama Oy – Turku, Finland 2013

To the One who designed the Original

ABSTRACT

Sara Nganga. Development of porous glass-fiber reinforced composite for bone implants. Evaluation of antimicrobial effect and implant fixation. Department of Biomaterials Science, Institute of Dentistry, University of Turku. *Annales Universitas Turkuensis*, Turku, Finland, 2013.

Cranial bone reconstructions are necessary for correcting large skull bone defects due to trauma, tumors, infections and craniotomies. Traditional synthetic implant materials include solid or mesh titanium, various plastics and ceramics. Recently, biostable glass-fiber reinforced composites (FRC), which are based on bifunctional methacrylate resin, were introduced as novel implant solution. FRCs were originally developed and clinically used in dental applications. As a result of further *in vitro* and *in vivo* testing, these composites were also approved for clinical use in cranial surgery. To date, reconstructions of large bone defects were performed in 35 patients.

This thesis is dedicated to the development of a novel FRC-based implant for cranial reconstructions. The proposed multi-component implant consists of three main parts: (i) porous FRC structure; (ii) bioactive glass granules embedded between FRC layers and (iii) a silver-polysaccharide nanocomposite coating. The porosity of the FRC structure should allow bone ingrowth. Bioactive glass as an osteopromotive material is expected to stimulate the formation of new bone. The polysaccharide coating is expected to prevent bacterial colonization of the implant.

The FRC implants developed in this study are based on the porous network of randomly-oriented E-glass fibers bound together by non-resorbable photopolymerizable methacrylate resin. These structures had a total porosity of 10–70 volume %, of which > 70% were open pores. The pore sizes > 100 μm were in the biologically-relevant range (50-400 μm), which is essential for vascularization and bone ingrowth. Bone ingrowth into these structures was simulated by imbedding of porous FRC specimens in gypsum. Results of push-out tests indicated the increase in the shear strength and fracture toughness of the interface with the increase in the total porosity of FRC specimens.

The osteopromotive effect of bioactive glass is based on its dissolution in the physiological environment. Here, calcium and phosphate ions, released from the glass, precipitated on the glass surface and its proximity (the FRC) and formed bone-like apatite. The biomineralization of the FRC structure, due to the bioactive glass reactions, was studied in Simulated Body Fluid (SBF) in static and dynamic conditions.

An antimicrobial, non-cytotoxic polysaccharide coating, containing silver nanoparticles, was obtained through strong electrostatic interactions with the surface of FRC. In *in vitro* conditions the lactose-modified chitosan (chitlac) coating showed no signs of degradation within seven days of exposure to lysozyme or one day to hydrogen peroxide (H_2O_2). The antimicrobial efficacy of the coating was tested against *Staphylococcus aureus* and *Pseudomonas aeruginosa*. The contact-active coating had an excellent short time antimicrobial effect. The coating neither affected the initial adhesion of microorganisms to the implant surface nor the biofilm formation after 24 h and 72 h of incubation. Silver ions released to the aqueous environment led to a reduction of bacterial growth in the culture medium.

Keywords: Bone substitute material, fiber-reinforced composite, porosity, bioactive glass, silver nanoparticles, antimicrobial activity.

TIIVISTELMÄ

Sara Nganga. Huokoisten lasikuiduilla vahvistettujen yhdistelmämateriaalien kehittäminen luuimplanttisovellutuksia varten. Antimikrobisen vaikutuksen ja fiksaation tutkiminen. Biomateriaalitiede, Hammaslääketieteen laitos, Turun yliopisto. ***Annales Universitas Turkuensis*****, Turku, Suomi 2013.**

Isot luupuutokset, jotka ovat kasvaimien, tulehduksien tai kallon avausleikkauksien seurauksia ovat yksi suurimmista haasteista kallokirurgiassa. Perinteiset keinotekoiset implanttimateriaalit ovat titaania tai erilaisia muoveja ja keraameja. Taannoin kehitetyt biostabiilit lasikuiduilla vahvistetut yhdistelmämateriaalit (FRC:t), jotka sisältävät kertamuovista akryylaatti-muovimatriksia, on otettu käyttöön uutena implanttimateriaalina. FRC:t kehitettiin alun perin hammaslääketieteellisiä sovelluksia varten. *In vitro* ja *in vivo* -testauksien seurauksena nämä yhdistelmämateriaalit on hyväksytty kokeelliseen kliiniseen käyttöön kallokirurgiassa. Tähän mennessä suuria luupuutoksien rekonstruktioita on tehty jo noin 35 potilaalle.

Tämä väitöskirja käsittelee uudenlaisen FRC-teknologiaan pohjautuvan implanttimateriaalin kehitystä kallokirurgiaa varten. Kyseessä oleva monikomponentti-implantti koostuu kolmesta pääosasta: (i) huokoisesta FRC-rakenteesta, (ii) bioaktiivisista lasirakeista FRC-kerrosten välissä sekä (iii) hopea-polysakkaridinanopinnoitteesta. Huokoinen FRC-rakenne edesauttaa luun kasvua implantin sisällä. Bioaktiivinen lasi stimuloi uuden luun muodostumista. Polysakkaridipinnoite estää bakteerien tarttumista ja niiden kasvua implantin pinnalla.

FRC-implantit, jotka kehitettiin tässä tutkimuksessa, perustuvat satunnaisesti orientoituneiden katkokuitujen huokoiseen verkostoon, joka pysyy yhdessä biostabiilin valokovetetun kertamuoviakryylin avulla. Kokonaishuokoisuus näissä rakenteissa on 10-70 tilavuus-%, josta 70% on avohuokosia. Huokosten koot (> 100 µm) ovat biologisesti merkittävissä rajoissa (50-400 µm), mikä mahdollistaa verisuonien ja luun sisään kasvun. Väitöskirjassa luun sisäänkasvu simuloitiin laboratorio-olosuhteissa kipsin avulla. Implantin ja kipsin liitoksen vahvuutta määritettiin mekaanisessa kuormituksessa. Tulokset osoittivat, että mitä huokoisempia implantit ovat, sitä suurempia ovat liitoksen leikkauslujuus ja sitkeys.

Bioaktiivisen lasin vaikutus luuhun perustuu lasin liukenemiseen fysiologisissa olosuhteissa. Kalsium- ja fosfaatti-ionit vapautuvat lasista ja samaan aikaan saostuvat lasin pinnalle ja lähiympäristössä oleviin rakenteisiin muodostaen samankaltaista apatiittimineraalia kuin on luussa. Väitöskirjassa FRC-implantin pinnan biomineralisaatiota bioaktiivisen lasin liukenemisen seurauksena tutkittiin simuloidussa kudosnesteessä (SBF) staattisissa ja dynaamisissa olosuhteissa.

Nanokokoisia hopeapartikkeleita sisältävä, bioyhteensopiva, antimikrobinen polysakkaridipinnoite saatiin aikaan FRC-pinnan voimakkaiden sähköstaattisten vuorovaikutusten kautta. Pinnoite on valmistettu laktoosi-modifioidusta kitosaanista. Laboratorio-olosuhteissa tämä pinnoite pysyi ehjänä seitsemän vuorokautta lysotsyymille ja yhden vuorokauden vetyperoksidille (H_2O_2) altistettuna. Antimikrobinen teho testattiin *Staphylococcus aureuksella* ja *Pseudomonas aeruginosalla*. Tutkimuksessa pinnoitteella todettiin hyvä lyhytaikainen antimikrobinen vaikutus. Mikro-organismit eivät tarttuneet implantin pintaan, eivätkä ne muodostaneet biofilmiä 24 tunnin ja 72 tunnin inkubaation jälkeen. Implanttien pinnoitteista vapautuneet hopeaionit vähensivät bakteerien kasvua kasvatusliuoksessa.

Avainsanat: Luukorvikemateriaali, kuituvahvisteinen yhdistelmämateriaali, huokoisuus, bioaktiivinen lasi, hopeananopartikkelit, antimikrobinen aktiivisuus.

TABLE OF CONTENTS

ABBREVIATIONS

ATCC	American type culture collection
BG	Bioactive glass
BHI	Brain heart infusion (culture medium)
BisEMA	Ethoxylated bisphenol A-glycoldimethacrylate
BisGMA	Bisphenol A-glycidylmethacrylate
CaP	Calcium phosphate
CMF	Cranio-maxillofacial
CFRP	Carbon fiber reinforced polymer
CFU	Colony forming units
Chitlac	Lactose modified chitosan
Chitlac-fluo	Chitlac labelled with fluoresceine isothiocyanate (FITC)
CLSM	Confocal laser scanning microscopy
CT	Computed tomography
CQ	Camphorquinone
DMAEMA	Dimethylaminoethyl methacrylate
DNA	Deoxyribonucleic acid
EDX	Energy-dispersive X-ray spectroscopy
EGDMA	Ethyleneglycol dimethacrylate
ETAAS	Electro thermal atomic absorption spectroscopy
FRC	Fiber-reinforced composite
GlcNAc	N-acetyl-glucosamine
GlcNH2	2-amino-2-deoxy-d-glucose
HA	Hydroxyapatite
H_2O_2	Hydrogen peroxide
ICP-OES	Inductively coupled plasma-optical emission spectrometry
LED	Light emitting diode
LB	Lysogeny broth (culture medium)
MMA	Methyl methacrylate
MRI	Magnetic resonance imaging
nAg	Nanosilver
NPs	Nanoparticles
NMR	Nuclear magnetic resonance (spectroscopy)
PBS	Phosphate-buffered saline
PE	Poly (ethylene)
PEEK	Poly (etheretherketone)
PGA	poly (glycolic acid)

PLA	Poly (lactic acid)
PMMA	Poly (methyl methacrylate)
PTFE	poly (tetrafluoro ethylene)
SBF	Simulated body fluid
SEM	Scanning electron microscopy
semi-IPN	Semi-interpenetrating polymer networks
TEGDMA	Triethyleneglycol dimethacrylate
TSB	Tryptic soy broth (culture medium)
UDMA	Urethane dimethacrylate
UHMW-PE	Ultrahigh molecular-weight polyethylene
45S5	Bioactive glass containing 45 wt% SiO_2

LIST OF ORIGINAL PUBLICATIONS

This thesis is based on the following original articles, which are referred to in the text by the Roman numerals I-IV. The original publications are reproduced with the permission of the copyright holders.

I **Nganga S, Ylä-Soininmäki A, Lassila LVJ, and Vallittu PK** (2011) Interface shear strength and fracture behaviour of porous glass-fibre-reinforced composite implant and bone model material. Journal of Mechanical Behavior of Biomedical Materials 4:1797-1804.

II **Nganga S, Zhang D, Moritz N, Vallittu PK, and Hupa L** (2012) Multi-layer porous fiber-reinforced composites for implants: in vitro calcium phosphate formation in the presence of bioactive glass. Dental Materials 28:1134–1145.

III **Nganga S, Travan A, Donati I, Crosera M, Paoletti S and Vallittu PK** (2012) Degradation of silver–polysaccharide nanocomposite in solution and as coating on fibre reinforced composites by lysozyme and hydrogen peroxide. Biomacromolecules 13:2605-2608.

IV **Nganga S, Travan A, Marsich E, Donati I, Söderling E, Moritz N, Paoletti S and Vallittu PK** (2013) In vitro antimicrobial properties of silver–polysaccharide coatings on porous fiber-reinforced composites for bone implants. Journal of Materials Science: Materials in Medicine. In Press. DOI 10.1007/s10856-013-5022-2.

1. INTRODUCTION

Cranio-maxillofacial (CMF) bone defects demanding reconstructions occur due to contemporary working and living conditions. An increasing number of brain infarction or intracranial haemorrhages require immediate brain decompression with removal of bone segments during craniotomies. Craniotomies have to be performed after diagnoses of traumata, congenital malformations, tumors and hemifacial microsomia or to prevent of the low pressure syndrome (Aitasalo et al., 2009; Engstrand, 2012; Lethaus et al., 2011). Commonly used implant materials for larger defects include bone auto- and allografts, titanium meshes, poly (methyl methacrylate) (PMMA), poly (ethylene) (PE), poly (etheretherketone) (PEEK), hydroxyapatite (HA) and bioactive glasses (BG) or combinations thereof. Discovering the optimal reconstruction material for cranial bone defects is of immediate interest (Engstrand, 2012; Lethaus et al., 2011; Moreira-Gonzalez et al., 2003).

By adding demineralized bone matrix and struts or bioactive ceramics such as BG or HA, investigators aim to include osteoconductive features to cranial implants. BG implants have direct chemical bonding to the bone tissue and osseoinductive properties (Aitasalo and Vuorinen, 2007). Another approach is to design biostable, porous implants structures to allow soft tissue and bone ingrowth, and improve mechanical implant fixation (Chim and Gosein, 2009).

Resorbable tissue engineered materials including growth factors or gene therapy are currently also under investigation for cranial reconstruction, but must prove their potential in clinical reality (Cabraja et al., 2009; Engstrand, 2012). Attempts include, for example, custom-made scaffolds made up of porous sintered HA or slowly degradable polycaprolactone combined with seeded osteogenic cells and growth factors which possibly enable rapid biological integration (Hutmacher et al., 2002; Ripamonti et al., 1999).

Moreover, durable biostable fiber-reinforced composites (FRC), which were originally developed for applications in dentistry, are under consideration as alternative cranioplasty implant material (Tuusa et al., 2007; Vallittu, 1999). The proposed bone substitute material is based on copolymer matrices of PMMA or bisphenol A-glycidylmethacrylate (BisGMA) and triethyleneglycol dimethacrylate (TEGDMA) reinforced with E-glass fibers (Aitasalo et al., 2013; Tuusa et al., 2008). In cell culture and *in vivo* studies, the photopolymerized and postcured BisGMA-TEGDMA resin system has sound biocompatibility and bone formation capability. BG implant coating enhances bone bonding strength (Aho et al. 2004; Ballo at al., 2008 and 2009; Zhao et al., 2009). Additionally, BG showed antimicrobial properties *in vitro* (Leppäranta et al., 2008, Stoor et al., 1998) and *in vivo* (Lindfors et al., 2010).

An alternative approach is to coat the BisGMA-TEGDMA thermoset with bioactive cationic polysaccharides such as lactose-modified chitosan. Polysaccharide coatings, with incorporated immobilized silver nanoparticles (NPs), showed contact-based antimicrobial activity and are biocompatible and not cytotoxic toward eukaryotic cells *in vitro* (Travan et al., 2010, 2011, and 2012).

Infection rates between 2.6 and 22.4 % are reported for alloplastic cranial implants based on PMMA, carbon fiber reinforced polymer (CFRP) or hydroxyapatite placed during cranioplasty with need for implant replacement (Cabraja et al., 2009; Wurm et al., 2004). Denoted infection rates vary as a result of the size of study and the proximity to frontal sinuses of the large skull defects (Cabraja et al., 2009). Previous infections in the region of the implant placement are a significant risk factor for subsequent infections independent on the implant material (Cho and Gosein, 2004). The clinical short term outcome of custom made PEEK implants is promising, while long term evidence is still to be gained (Lovald and Kurtz, 2012). For large and complex shaped cranial defects, custom-made preoperatively manufactured implants are superior to PMMA or HA cement-based implants modelled during surgery, as they lead to reduced operating times and infection rates (Cabraja et al., 2009).

Currently, clinical use with porous, non-resorbable implants, such as based on PMMA, PE (Medpor), hard tissue replacement (a polymeric composite) and HA implants in cranioplasty exists. No increased incidence of infection or other side effects compared to non porous implants was reported (Bruens et al., 2003; Cho and Gosain, 2004).

Limited antimicrobial modifications to prevent infections of cranial bone implants are available. Antibiotic-loaded PMMA, *e.g.* incorporating gentamicin, used successfully in clinical orthopaedics for over 40 years (Hendriks et al., 2004), is not established in field of neurosurgery because of fear of neuro- and oxotoxicity (Ronderos et al., 1992). Within clinical studies, tobramycin as well as cephalosporin loaded implants based on PMMA and hydroxyapatite cements were, however, found to be safe for cranioplasty (Burstein et al., 2006; Pietrzak and Eppley, 2005; Shapiro, 1991). Other researchers proposed a porous colistin loaded PMMA – hydrogel cement to be used as temporal implant for space maintenance in a two stage reconstructions process (Shi et al., 2010). Pre-operatively manufactured, biostable hydrophilic implants were soaked in antibiotic solution prior to implantation during surgery to achieve a limited postoperative release (Eppley, 2002). However, from all these approaches, it is not known if locally administered prophylactic antibiotics significantly reduce infection rates. In relation to this, the present thesis focuses on the development of a FRC implant for cranial reconstruction which is comprised of bioactive and antimicrobial properties.

2. REVIEW OF THE LITERATURE

2.1. Bone as a material

Implant materials developed in this study are intended to replace damaged bone tissue. In this chapter, structure and biological properties of bone are reviewed.

2.1.1. Structure of bone

Bones are major components of the skeleton. As such, they provide protection for soft tissues (*e.g.* cranial, thoracic and pelvic cavity) and permit the maintenance of the body shape and transmission of muscular forces during movements due to their hardness and rigidity (Jee, 2001).

Structurally, bone can be classified as a hierarchical composite material and visualised as a dense sponge containing 10% water (Bonucci, 2000; Jee, 2001). About 60% of the bone matrix consists of inorganic components, namely calcium phosphates (CaPs) as well as magnesium, sodium, potassium, chlorine, iron and carbonate. The organic part consists of collagens (90%) and non-collagen proteins. The mechanical behavior is determined by both the mineral part (inorganic) that is primarily responsible for compressive characteristics, and the collagen structures that mainly define the tensile behavior (Prein et al., 1998).

The cranial bone, being a flat bone, consists of a complex three layer structure with porous cancellous bone in between two layers of dense compact bone. While the compact bone gives the structure the required strength, the cancellous bone serves as energy absorbing layer improving elastic properties (Motherway et al., 2009). The hemispherical shape of cranial bone also contributes to the protection for the central nervous system against direct impact (Prein et al., 1998). The thickness and microstructure of the skull varies with the exact anatomical location and among individuals (**Figure 1**) (Motherway et al., 2009). In contrast to long bones, mechanical properties of cranial bone were found to be transversely isotropic in all directions and on an intermediate level (Wood, 1971). Exemplary values of tensile and bending properties of cranial and long bones are compared in **Table 1**.

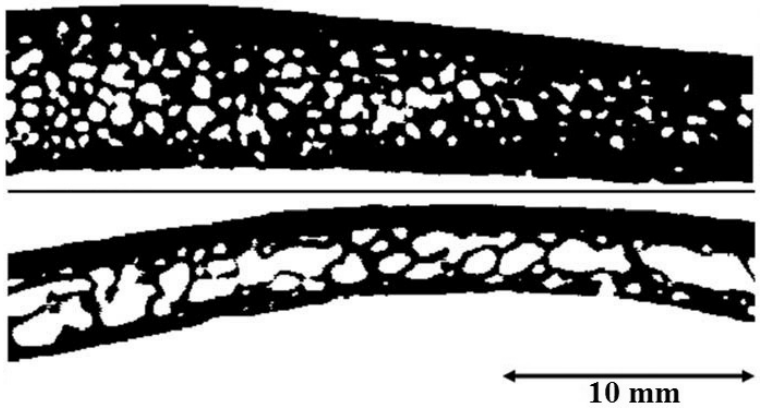

Figure 1: µ-CT cross-sections through cranial bone of two different individuals to illustrate variations in structural porosity and thickness (adopted from Motherway et al., 2009).

Table 1: Mechanical properties of human bone tissues found in the literature (Kokubo 2003; McElhaney et al., 1970; Motherway et al., 2009; Ramakrishna et al., 2001).

Mechanical Property	Cranial bone		Long bone	
	Cortical bone	Composite (compact and cancellous bone)	Cortical bone	Cancellous bone
Tensile strength (MPa)	79.3	43.4	52-133	7.4
Young's modulus (GPa)	1.2	5.4	7-30	0.05–0.5
Max. bending stress (MPa)	n/a	85-128	50-150	n/a

As bone is a self repairing structural material, the mass, shape and mechanical properties can be adjusted to the requirements of the environment and its regeneration after cracks or damages is possible (Jee, 2001). The adaptation of the bone structure to the applied stress condition is known as the Wolff's law (Ramakrishna et al., 2001). The bone formation process is mainly carried out by a sheet of fibrous connective tissue containing undifferentiated cells on the outside of the cortical bone, the periosteum and by osteocytes (bone cells) that lie between the inside layer of cortical bone and cancellous bone. First, during the healing process, a woven cancellous bone is developed as a provisional material which can also be found in the growing embryo (Jee, 2001). Later, it may be replaced by long-term, consistent lamellar bone. Those lamellas are ordered to circular rings forming longitudinally vascular channels which are embedded in the interstitial lamellae. Both the woven and the lamellar type contain osteocytes in small cavities connected to each other by tubular canals. The regulation of the bone maintenance and growth is controlled by the bone cells. These bone cells are called osteoblasts, which form new bone matrix and osteoclasts, which resorb bone and bone lining cells (inactive osteoblasts) (Jee, 2001). The local

calcium ion and oxygen concentration of blood is also part of the regulatory system controlling the constant renewal of bone tissue (Stevens and Lowe, 1997). Therefore, vascularization is required as a prerequisite for the activation of bone cell growth (Jee, 2001).

2.1.2. Bone fractures and healing pathways in cranio-maxillofacial area

Bone fractures are the result of a mechanical overload. The disruption of the bony structure occurs within milliseconds. The degree of fragmentation and the fracture shape depends on the type and rate of loading as well as the energy stored prior to fracturing (Prein et al., 1998).

In the cranial region, which lack long bone and consist of flat bone, closed muscle compartments or penetration of the skin is not as problematic. Particularly in the skull bony walls are thin and tend to remain attached to surrounding soft tissues (Prein et al., 1998). Even in case of stripped soft tissues, the connection to circulation regenerates fast and the chance of infections is minimal. If neovascularization occurs in bone tissue, the union of fractured bones may be observed already after one month. The presence of cancellous bone helps in the rapid recovering of the interrupted blood supply (Prein et al., 1998).

Healing is defined as the restoration of the original integrity (Prein et al., 1998). The healing process can be divided into a self-driven sequence of inductive, inflammatory, reparative and remodeling phases (Prendergast and van der Meulen, 2001). In a clinical context, the healing process is successful if the bone has an adequate anatomic shape and stiffness, and therefore is completely functioning again. This is the case even before the unaltered bone structure on microscopic level is reached (Prein et al., 1998).

The regeneration of the bone tissue can follow a direct or an indirect pathway depending on the mechanical environment. The indirect or so-called “endochondral bone formation” includes a cartilage stage before the real bone tissue is formed through replacement processes. It is mainly observed in long bones and leads to a faster restoration of the original strain and stress values than the direct (so-called “intramembranous”) bone formation. Direct bone formation (membranous ossification) without the cartilage state or external callus occurs in the case of extremely stable fractures such as those in bones shielded from mechanical load and bones of the skull excluding the nasal area. Extensive, interfragmentary motion, especially in long bones may lead to fake joints of cartilage, since bone formation is inhibited (**Figure 2**) (Prein et al., 1998; Prendergast and van der Meulen, 2001).

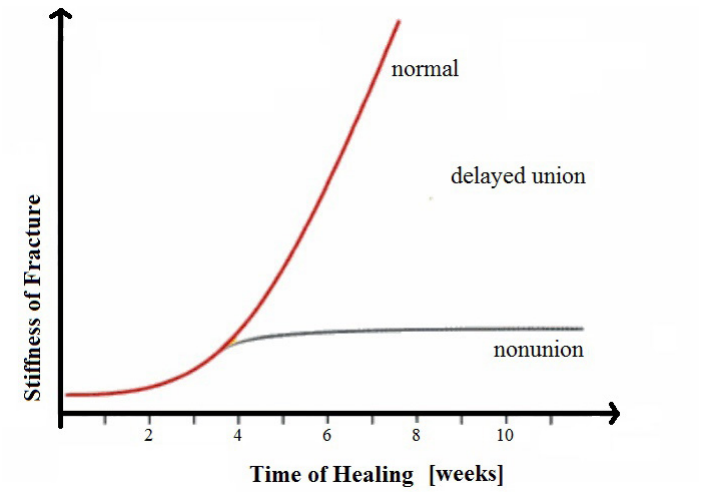

Figure 2: Fracture healing: recovery of the mechanical function. During the fourth and sixth week, a dramatic change occurs from initially low stiffness and strength towards the properties of the normal bone. Overloading of the healing fracture may disturb mineralization processes and delay the unification (adopted from Prein et al., 1998).

2.2. Aspects of bone implant design

This chapter describes the properties of modern implant design which should be considered when developing new implant solutions.

2.2.1. Composite approach

The idea of applying composites as implant materials is feasible because tissues themselves are natural composite materials (Ramakrishna et al., 2001).

A material is referred to as composite if it consists of two or more chemically distinct phases having an interface separating the constituents. This term is used at the atomic level, *e.g.* for metal alloys and for materials consisting of micro- or macroscopically of different phases. In biomaterials science, this concept primarily refers to fiber or particle composites. These composites consist of one or more discontinuous phases, called reinforcement, embedded within a continuous phase called a matrix (Alexander, 1996). In case of fiber reinforced composites the discontinuous phase is usually much stronger and harder than the matrix and its length is much greater than its cross-sectional dimension. The mechanical characteristics of a composite material, such as its toughness, strength, stiffness or fatigue resistance strongly depend on the properties of the single constituents, their volume fraction, interaction and distribution. Further classifications of composites according to the reinforcement geometry include the orientation of fibers (random versus uniform), the fiber length and the number of layers (single *versus* multilayer structure) (Alexander, 1996).

The efficiency of the fiber reinforcement in laminates, the so-called "Krenchel's factor", is influenced by the orientation of the fibers (**Figure 3**). The highest strength and modules in FRCs is reached by unidirectional fiber orientation. However, in this case of anisotropic fiber reinforcement, the sound mechanical properties are limited to the stress applied in the fiber direction. However, the reinforcement capacity of fibers in orthotropic FRCs is divided into two or more different directions which show isotropic mechanical properties. A Krenchel's factor of 0.5 corresponds to the reinforcements with bidirectional (woven) fibers (Vallittu, 2001). This reinforcement influences the strength in all directions to some extent and the prediction of mechanically stronger directions becomes more complex (Alexander, 1996).

Examples of commonly used reinforcing materials include strong polymers (aramid), glass and carbon fibers as well as ceramic particles. Synthetic, non-absorbable polymers, such as polysulfone, ultrahigh molecular-weight polyethylene (UHMW-PE), polytetrafluoroethylene (PTFE), PEEK and PMMA, absorbable polymers, such as poly (lactic acid) (PLA) and poly (glycolic acid) (PGA) or natural polymers, such as purified bovine collagen serve as matrix materials. The use of composites may also lead to an increased biocompatibility of the product (Alexander, 1996).

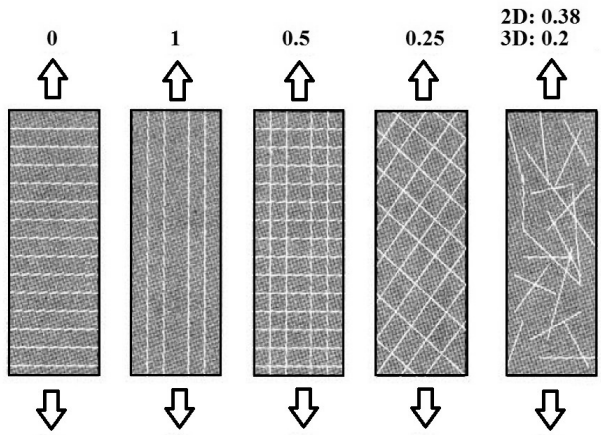

Figure 3: Reinforcement efficiency (Krenchel's factor) of fibers with different fiber orientation in plane (adopted from Vallittu, 2001).

Advantages of using FRCs as implant materials are the low weight and the possibility to tailor mechanical properties equal to those of bone and the simpleness to form desired complex geometries prior to polymerization (Tuusa et al., 2007a; Vallittu 1996 and 1999). Continuous fibers, properly orientated to the direction of loading, behave additionally as crack stoppers (Vallittu, 2001). The plasticity required for the superior moulding properties arise from the use of resin systems for impregnating the reinforcement fibers (Cahn et al., 1992). The complete impregnation of all fibers is a prerequisite for covalent fiber-matrix bonding *via* silane coupling and hydrogen bonds; these allow stress transfer

from the matrix to the fibers. Proper impregnation also prevents sorption of water or oxygen which both inhibits radical polymerization of the acrylic resin inside the composite. To ensure sufficient impregnation, a thick, viscous resin and fibers with poor resin wettability should be avoided (Vallittu 1996, 1999 and 2001).

Improved fiber impregnation and handling properties can be ensured by using so-called "semi-interpenetrating polymer networks" (semi-IPN) of two independent polymers. In everStick® products (StickTech Ltd., Finland) for example, glass fibers are pre-impregnated with a polymer-monomer-gel to improve the composite flexibility and the adhesion of added resin monomers penetrating into the polymer network (Vallittu, 2001).

2.2.2. Biomimetics

Biomimetics, a term first used by Otto Schmitt in 1969, is used as a synonym of "biomimesis," "biomimicry," or "biologically inspired design." It can be defined as "the study of the formation, structure, or function of biologically produced substances and materials and biological mechanisms and processes especially for the purpose of synthesizing similar products by artificial mechanisms which mimic natural ones" (Vincent et al., 2006).

Bone, being a natural composite, makes the prior mentioned composite approach an example of the applied principle of biomimetics. Biomimetic inspired implant materials may also resemble bone in terms of either the hierarchical micro- and nanostructure, the chemical composition of main components or the interconnected porosity (Liao et al., 2004). Material combinations proposed within a tissue engineering approach are based on polymer – ceramic nanocomposites (Liao et al., 2004, Ródenas-Rochina et al., 2013).

In context of implant development, a biomimetic process is defined as a procedure during which a biologically active bonelike apatite layer is deposited on a metallic or polymeric implant material. Methods applied include chemical treatments or physical adsorption (Kokubo et al., 1999).

2.2.3. Biocompatibility

Biocompatibility is one of the basic requirements for implant materials. It can be defined as the "ability of a biomaterial to perform with an appropriate host response in a specific application" (Williams, 1987). Wintermantel distinguished further between surface and structural compatibility of an implant. "Surface compatibility refers to suitable chemical, biological and physical properties of the implant surface, while structural compatibility implies the optimal adaptation to the mechanical behavior of the host tissues" (Wintermantel and Ha, 1998). Implant materials must be compatible with blood if they will be immersed in circulation. Test methods to evaluate biocompatibility vary with materials and applications. However, even when a material itself is biocompatible, the medical device has to be tested separately (Hanson and Harker, 1996).

2.2.4. Tissue implant interactions

The process of tissue attachment to implant materials is dependant on the tissue response at the interface and the chemical reactivity of the implant material. Four types of attachment are usually distinguished: inert; biostable (microporous inert implant); bioactive; and bioresorbable behavior. First, biologically nearly inert behavior is characterized by no chemical or biological bonding and the formation of a fibrous capsule (*e.g.* Al_2O_3 or titanium alloys). Second, in the case of microporous inert implants, such as metals with HA coating, a biological fixation is established by bone ingrowth and mechanical attachment into pores (Hench, 1996). Pore sizes, larger than 50 μm, are necessary to allow maintenance of the healthy tissue (Itälä et al., 2001). The third type is the bioactive fixation. The dense, non-porous surface-reactive materials of this group elicit a specific biological response resulting in a chemical bonding to the tissue. Examples of such are BG, BG ceramics, dense HA or bioactive composites. Bioresorbable materials belonging to type four include tri calcium phosphate, calcium sulfate, PLA or PGA. These materials degrade gradually and are replaced by the host tissue (Hench, 1996).

Maintaining implant strength long enough to match regeneration and resorption rates of metabolic acceptable substances are of importance during the evaluation of implant materials (Hench, 1996). In literature, there are different terms describing different aspects of the bone bonding process. At first, osteoinduction must occur, and osteoinduction is defined as a process by which osteogenesis is induced. Cells are activated and differentiate to preosteoblasts. Subsequently, osteoconduction proceeds. Osteoconductivity of a surface refers to the ability of bone growth on the surface or down into pores (Albrektsson and Johansson, 2001).

Osseointegration was introduced by Brånemark in 1952 as "the formation of a direct interface between an implant and bone, without intervening soft tissue." A proper attachment to bone ensures successful load transfer and inhibits relative implant movement from the bone (Brånemark, 1977 and 1983). Therefore, movements with negative effects, such as stress shielding or micromotion at the implant interface, need to be avoided already directly after implantation (Prein et al., 1998; Søballe et al., 1992).

2.2.5. Antimicrobial strategies for bone implants

Newer, more efficient antimicrobial strategies are demanded as infections associated with surgical implants are chronic complications (Darouiche, 2003). Although implants are generally sterilized and antiseptic techniques are applied, it is common after surgery that pathogenic microorganisms infiltrate and contaminate surgical areas by replacing the normal flora (Campoccia et al., 2006; Schierholz and Beuth, 2001). Following local infections are difficult and costly to treat with systemic or local antibiotics since they are caused by bacteria that protect themselves from host defence system and antibiotics by a biofilm (Darouiche, 2003; Hardes et al., 2007). The following chapter reviews some of

the local treatment strategies presently developed in order to prevent implant-associated infections and to reduce the need of revision surgeries.

2.2.5.1. Course of an implant infection

Planctonic bacteria, such as *Staphylococcus aureus* and coagulase-negative staphylococci (e.g. *Staph. epidermidis*), are pathogens that infect the implant surface. Infection might develop after contamination during surgery, during the stay in hospital or later caused by local infections elsewhere in the body (Buscher et al., 2009). Microorganisms may remain in a dormant state several years before colonizing the implant surface (Buscher et al., 2010). After implantation, the device is in contact with body fluids and immediately covered by a layer of adsorbed protein (Buscher et al., 2009). The first step towards an implant infection is the reversible adhesion of microorganisms followed by permanent attachment and colonization. Once attached, certain strains begin to deposit a slime layer which is an exopolysaccharide matrix, called the glycocalix. Within these so-called "biofilms," bacteria are protected against host defense mechanisms and systemically administered antibiotics (Lucke et al., 2003).

2.2.5.2. Local antimicrobial strategies

The first step to avoid implant centered infections is to maintain a high level of hygiene before and during surgery to minimize the bacterial burden (Schierholz and Beuth, 2001). Furthermore, systemic antibiotics, such as vancomycin or cefazolin, are routinely administered prior to and after cranial surgery, even though there is no evidence of an effect on infection rates (Wylen et al., 1999).

Other preventive strategies address "the race for the surface" concept first described by A. Gristina in 1987. This is the competition between tissue integration and biofilm formation on the implant surface (Buscher et al., 2010). Antimicrobial fortification of an implant surface should inhibit biofilm formation and may include the following properties: (1) being anti-adhesive; (2) having biocide-release activity; and (3) yielding antimicrobial actions after contact. Frequently two of these strategies are combined to overcome limitations of having just one property (Ho et al., 2004). Fewer bacteria will adhere to implants with an appropriate hydrophobicity, surface charge and roughness as well as on polymer brush coatings (Buscher et al., 2010). Common antibiotics locally released from implant surfaces against *S. aureus* implant infections are gentamicin, rifampin, cefuroxime, vancomycin, tobramycin, and ciprofloxacin. The efficacy of combinations is known (Monzon et al., 2001; Walenkamp and Vree, 1981). Compared to the administration of systemic antibiotics, which is standard after implantation surgeries, far less systemic side effects arise from a local antibiotic treatment typically applied at a several orders of magnitude higher concentration (Schierholz and Beuth, 2001). In addition to traditional antibiotics, also disinfectants, such as chlorhexidine and quaternary ammonium compounds, or metal ions, such as copper, zinc or silver / silver

sulfadiazine, have been introduced as implant coatings (Buscher et al., 2010; Jaeger et al., 2005; Stanić et al., 2010). The advantages of a contact active material are its long lasting antimicrobial activity and also it minimizes the adverse effects on mammalian cells in response to leaching agents (Gosheger et al., 2004; Travan et al., 2011). However, the circle of action is limited to the surface itself, so that infections within the nearby tissues are not treated (Moojen et al., 2009).

One other way to win this "race for the surface" is to encourage tissue integration and prevent osteomyelitis (Pietrzak and Eppley, 2005). This indirect antimicrobial strategy applies mainly to the prevention of late implant infections caused by a minor trauma or wound breakdown. A viable biologic tissue implant interface, ensured by bone ingrowth or soft-tissue ongrowth, efficiently prevents bacterial colonization and subsequent infections, as reported for bone cements in cranioplasty (Gilardino et al., 2009). For implants encapsuled by fibroblasts, there is the effect of immunosuppression at the implant surface which must be considered (Schierholz and Beuth, 2001).

2.2.5.3. Silver as antibacterial agent

Silver is well known for its broad-spectrum antimicrobial activity and its low toxicity to mammalian cells (Hardes et al., 2007). The antimicrobial activity of silver ions is proportional to their concentration, while chemically stable metallic silver and poorly soluble compounds, such as silver acetate and silver chloride, show only limited antimicrobial efficacy (Schierholz et al., 1998). Ho et al. (2004) presumed that elementary silver acts either as contact active material or as source of released silver ions. Lok et al. (2007) pointed out that silver NPs need to have a partially oxidized surface, thus the ability to adsorb Ag^+ ions, to exhibit antibacterial activities. Silver, in its ionic state or as NPs, replace metal ions like Ca^{2+} or Zn^+ and bind to proteins *via* thio-, amino-, imidazole-, carboxylate- and phosphate groups. As these functional groups are exposed in the extracellular portion of the bacterial membrane proteins, silver ions have the ability to kill a broad spectrum of bacteria. In addition, the silver ions bound to bacterial DNA affect cellular oxidation processes and block the respiratory chain (Morones et al., 2005; Schierholz et al., 1998). Bacteria are not prone to develop resistance to silver (Hardes et al., 2007). Antiviral and antifungal characteristics of silver NPs have also been reported (Lu et al, 2008; Kim et al., 2009).

Coatings with silver alone or silver hydrogels are in clinical use for catheters, sutures, wound dressings, heart valve sewing rings and endoprostheses (Darouiche, 1999; Hardes et al., 2007; Wilkinson et al., 2011).

Possible adverse effects and toxicity of silver NPs for eukaryotic cells are discussed with controversy. Researchers suggest that particle size and a dose dependant risk of cell death are adverse effects, because there is no physical barrier hindering the uptake of leaching silver NPs into cells (Albers et al., 2013; Chen et al., 2008).

2.2.6. Porosity

Porosity in solid materials may occur either only at the surface or throughout the complete bulk material in the form of individual spacings and openings of interconnected pores (Jansen and von Rectum, 2004). Specific porous structures are analyzed by indicating pore geometry, interconnectivity, size, orientation, and branching. Depending on their size, the pores are labelled as either micro- (width <100 μm) or macro-pores (width >100 μm) (Taboas et al., 2003). The term total porosity P_t refers to the total volume fraction of empty space in the specimen. It is calculated using the quotient of the actual volume of the material and the total volume V_s/V_t (**equation 1**). In practice often the equivalent quotient of the actual and theoretical density ρ/ρ_{th} is used to determine the porosity (**equation 2**) (Ho and Hutmacher, 2006):

$$P_t\,(\%) = 1 - (V_s/V_t) * 100\% \qquad \text{(equation 1)}$$

$$P_t\,(\%) = 1 - (\rho/\rho_{th}) * 100\% \qquad \text{(equation 2)}$$

Total porosity is divided into the concepts of open and closed porosity depending on the interconnectivity of a porous specimen (Dlapka et al., 2010). Open porosity describes the situation in which the pores are connected directly to the surface. It is the only functional biologically active part of the porosity. In the case of fully interconnected global pores, only existing big and complex shaped pores reach the end of the whole specimen. Isolated pores distributed in the matrix represent the closed porosity. Porosity is investigated through penetration methods: mercury; gas; flow pycnometry; or the evaluation of micro-computed tomographies (micro-CT) or scanning electron microscopy (SEM) images. Plane porosity is used for more exact descriptions of the dependence between strength of the material and its porous microstructure analyzed at cross-sectional fracture surfaces (Dlapka et al., 2010; Ho and Hutmacher, 2006).

As with other surface irregularities, pores are known to guide many types of cells and help tissue repair. It is, therefore, important to analyze functional porosity (interconnected open porosity), which allows for tissue ingrowth by transferring body liquids and providing space for growing cells. Closed porosity may be biologically active only after degradation processes and it primarily leads to the reduction of the mechanical properties and homogeneity of the implant (Jansen and von Rectum, 2004). For bone ingrowth pore sizes, the range of 75-250 μm, are favorable, whereas ingrowth of fibrocartilageous tissue is effectively promoted by 200-300 μm pores. In connection to this, porous scaffolds are of interest for applications in tissue engineering products, artificial skin, drug delivery, artificial blood vessels and bone and cartilage reconstructions. With the help of a specifically designed surface microtexture, it is possible to prevent epithelial downgrowth, inflammatory response, and fibrous encapsulation and to increase vascularity of the healing process. The detailed theory

of the contact guidance of cells by artificial surfaces is currently under investigation (Jansen and von Rectum, 2004).

2.3. Biomaterials for craniofacial implants

2.3.1. Requirements for skull bone reconstructions

Biomaterials, applied as bone reconstructions in the maxillo-facial area next to brain tissues, need to fulfil special requirements. Implanted components should not evoke any toxic or adverse reaction in the neural tissue of the brain, the calvarial bones, nor in the periosteal soft tissues. Moreover, the implants have to protect the underlying brain, provide durable, mechanically stable and a cosmetically satisfying reconstruction of the anatomical contours. The ideal implant material should be non-thermal conducting, radio-transparent, nonmagnetic, lightweight, simple to prepare, easily applicable and inexpensive. An individualized production process is needed to obtain implants with customised geometries ensuring perfect fit in the bone defect (Cabraja et al., 2009; Chiarini et al., 2004; Kuttenberger et al., 2001).

The reconstruction of cranial bone defects is required if the defect exceeds a critical size (Schmitz and Hollinger, 1986) or if a significant deformity or dysfunction of the defect site is observed. Best options for implant material need to be evaluated for each specific case depending on the defect size and the patient's condition (Kuttenberger et al., 2001; Moreira-Gonzalez et al., 2003). For small defects of 10-50 cm^2 in size, removed skull bone grafts or non-customized titanium meshes are suitable for reconstruction while larger defects of 50 to over 100 cm^2 require customized reconstruction with preserved autogenous bone or synthetic materials reviewed in the following paragraphs (Lethaus, 2011).

2.3.2. Traditional material choices for craniofacial reconstruction

2.3.2.1. Bone grafts

Historically established materials for cranial reconstructions are auto- and allografts, resembling closely the natural bone structure (Moreira-Gonzalez et al., 2003). An autograft is "a transplanted tissue or organ transferred from one part of a body to another part of the same body," while allografts (also called homografts) consist of tissues or organs transplanted between unrelated individuals of the same species (Ramakrishna et al., 2001). Known drawbacks of this approach are the risk of infections and immunological reactions, fast bone resorption, limited graft sizes and preparation delay due to the donor site morbidity (Matsuno et al., 2006; Moreira-Gonzalez et al., 2003).

2.3.2.2. Metallic implants

An alternative is to use synthetic alloplastic materials such as biocompatible metals, ceramics or polymers (Kuttenberger et al., 2001). Until 1986, plates and screws for maxillo-facial implants were commonly made of stainless steel and chromium-molybdenum alloys because they were strong, ductile and biocompatible for fixation (Prein et al., 1998). However, problems such as corrosion, leaching of ions and infections occurred (Wurm et al. 2004). Today, these metals are replaced by titanium materials which are extremely insoluble in water and physiologically inert. As titanium has a thin oxide layer on its surface leading to a high resistance to corrosion, a second surgery for implant removal is no longer necessary. Additionally, the replacement of combinations of bone or cartilage grafts is possible using dynamic meshes (Kuttenberger et al., 2001; Prein et al., 1998). The disadvantage of all metallic implants is stress shielding by the implant and consequent bone underloading and degradation processes due to mechanically much greater stiffness of the implant in comparison to the bone (Prein et al., 1998; Zhao et al., 2009). Furthermore, the implantation of metals makes the use of magnetic resonance imaging (MRI) difficult or even impossible (Ramakrishna et al., 2001). For metal implants that do not match the exact anatomic defect shape, there is the need to improve the implant attachment to the bone by bioactive ceramic coatings *e.g.* made up of aluminium oxide (Al_2O_3), HA or BG ceramics (Hench, 1996; Moritz et al., 2003; Tang et al., 2010).

2.3.3. Bioactive glasses and ceramics

Ceramics, glasses and glass-ceramics are inorganic and non-metallic materials. Different degrees of crystallinity are achieved by different temperature ranges and progressions during the procession (Hench, 1996; Rawlings, 1993).

Fully ceramic CMF implants are available and are made of Al_2O_3, HA and HA-PLA composite cements (Hench, 1995). As for bioactive ceramics, such as CaP and calcium sulphate, especially CaP are of great interest as substitute materials because of their composition similar to HA, the primary mineral component of bone (Hench, 1996).

The first surface active glass that had the ability to bind covalently to bone and soft tissues in aqueous environments *via* a bone-like apatite layer was discovered by L. Hench in 1971 (Hench et al., 1971). This glass belongs to the class of BGs containing Na_2O, CaO, P_2O_5 and SiO_2. The observed bioactivity is limited to certain glass compositions marked as region A with grey color in **Figure 4**. Glasses within compositions in the region B are nearly inert silica glasses (*e.g.* window or bottle glass), which build a fibrous capsule at the tissue-implant interface. Compositions in region C are resorbable within 10-30 days. Glasses of region D are technically not practical and are not tested as biomaterials.

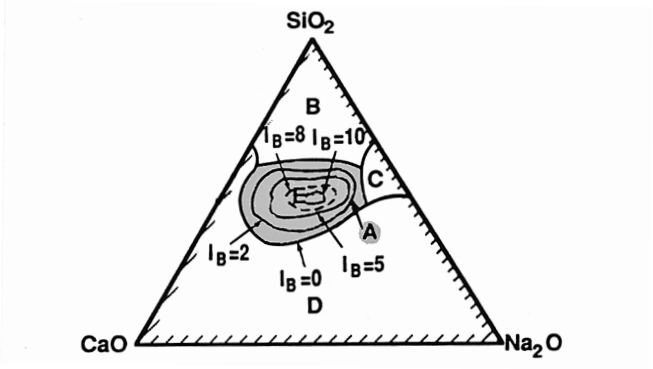

Figure 4: Ternary phase diagram showing the bone and soft tissue bonding of bioactive glasses and glass-ceramics of the system SiO_2-Na_2O-CaO. All compositions have constant 6 wt% of P_2O_5. Lines mark compositions with same index of bioactivity I_B (adopted from Hench, 1996).

BG, whose features of are less than 60 mol% SiO_2, high Na_2O and CaO contents, has a CaO:P_2O_5 ratio higher than 5:1, as the number of bridging oxygen ion in the structure is crucial for the bioactive behavior (Ducheyne, 1987). The most common glass 45S5 consists of 45 wt% SiO_2 as a network forming component and 6 wt% P_2O_5, 24.5 wt% CaO and 24.5 wt% Na_2O. Lines in the diagram (**Figure 4**) mark compositions with the same index of bioactivity ($I_B = 100 / t_{0.5bb}$). The index of bioactivity indicates the time within which more than 50% of the interface bonding is created. This level of interface bonding is critical to generate a bond to bone. $I_B = 4$ represents the optimum of the time dependant bonding strength. The thickness is of the interface layer is changing while the bonding is established (Hench, 1996).

The mechanisms of BG bonding to the bone involve a series of physicochemical reactions: at first alkali ions (Ca^{2+}, Na^+ and K^+) from the glass surface exchange for hydrogen or hydronium ions (H^+ or H_3O^+) from the body fluid (of aqueous solution). Hydroxyl ions then attack silica network and dissolve it by breaking its Si-O-Si bonds and forming Si-OH groups at the glass surface (Rawlings, 1993). This step is regulated by the amount of silica groups and the pH of the liquid. Following condensation and repolymerization of Si-OH ends in a SiO_2-rich layer on the BG surface. In addition, migrated Ca^{2+} and PO_4^{3-} ions from the glass form a gel-like phosphate-calcia rich film on top of the SiO_2 layer within the first minutes. The amorphous CaO-P_2O_5 film is crystallized to polycrystalline apatite during the next few weeks. The bonding to tissues is established by incorporation of collagen fibril and other proteins of fibroblasts produced by osteoblasts during the agglomeration of apatite crystals (Rawlings, 1993).

The bone like apatite formation, *in vitro,* is commonly investigated by immersing samples of interest in simulated body fluid (SBF) (Kokubo and Takadama, 2006). However, the reaction rates of BG depend strongly on the experimental setup. Changes in BG sample dosage, shape and size, porosity or surface morphology affect the kinetics

of BG reactions as the ratio of the BG surface area to solution volume changes (Arstila et al., 2006; Balas et al., 1998; Greenspan et al., 1994; Jones, 2001). The agitation rate of the system has also an impact on the *in vitro* reaction of BG (Rámilla and Vallet-Regí, 2001).

BGs, in the form of solid plates and particles of different sizes are already a well established implant material in clinical use in the CMF area. Bioactivity, and osteoconductive and bacteriostatic behavior of BGs are reported (Aitasalo et al., 2001; Gosein, 2004; Heikkilä et al., 1995). BGs also have angiogenesis promoting properties (Lindfors et al., 2010).

A limiting factor of full ceramic and glass implants is their intrinsic brittleness, which does not allow manipulation of the fixations to stabilize bone fragments in proper alignment and makes it difficult to adjust the shape of the device after production (Wurm et al., 2004). Craniofacial implants out of ceramic – polymer composites depict an alternative to overcome this limitation: examples include PE-BG, PMMA-BG, PEEK-HA or PEEK-TPC among others (Kurtz and Devine, 2007; Peltola et al., 2012, Swords, 2006).

2.3.4. Synthetic polymers and composites

2.3.4.1. PMMA

Commonly, the most frequently used reconstruction material in maxillo-facial area is PMMA because of its inert and non-thermoconductive characteristics. Moreover, complex shapes of acceptable strength can be easily produced. Drawbacks of PMMA implants, especially in case of implant completion during surgery, are high temperatures during polymerization that cause thermal necrosis in bone tissues as well as the eventual remaining and leaching of toxic monomers (Moreira-Gonzalez et al., 2003).

To overcome these drawbacks and to achieve an improved tissue compatibility, composite bone cements containing HA or BG, in a methacrylate resin matrix commercially used in dentistry have been proposed (Aho et al., 2004; Sanus et al., 2008; Tuusa et al., 2007a). Promising clinical cranioplasty results were reported when the acrylic bone cement, namely "Cortoss™" was placed on the dura mater and polymerized during surgery (cement composition: 30% BisEMA, BisGMA, TEGDMA resin, 70% glass-ceramic filler) (Sanus et al., 2008).

2.3.4.2. Dental resin systems

Monomers used in dental resin include MMA, BisGMA, TEGDMA, urethane dimethacrylate (UDMA) and various combinations thereof (**Figure 5**) (Imazato et al., 2001; Peutzfeldt, 1997; Vallittu, 2001). In practice, the highly viscous, hydrophobic monomer BisGMA is mixed with the flexible hydrophobic monomer TEGDMA to reduce the viscosity and stiffness of the final polymer and enable the resin handling

(Darvell, 2002). Other possible monomer fillers used to dilute the highly viscous BisGMA are ethyleneglycol dimethacrylate (EGDMA) and aliphatic or aromatic urethane dimethacrylates. In addition to the monomers, there is a low amount of so-called "starter chemicals" required for the photopolymerization reaction at room temperature in the resin mixture. An α-1.2 di-ketone such as benzil or camphorquinone (CQ), which absorbs light energy in the wavelength range of 440-480 nm and forms an excited triplet state, serves commonly as a free radical initiator. An amine reducing agent such as DMAEMA is added to accelerate the reaction (Cahn et al., 1992). When the mixture is cured with an intensive visible blue light at around 470 nm wavelength from a LED or a quarz-halogen lamp, at least two free radicals are generated – one coming from the reducing agent and one from the ketone (Cahn et al., 1992; Darvell, 2002). The rate of polymerization depends on the exposure time, the thermal energy within the system, and the light intensity reaching the sample surface. The greater the proportion of BisGMA in the resin, the higher is the amount of residual non-reacted vinyl double bonds and thus, the lower degree of conversion (ratio of potentially reactive versus reacted double bonds of a monomer) (Cahn et al., 1992).With a lower degree of conversion more residual monomers may leach out in wet *in vivo* environment and potentially cause irritation of tissues or allergic reactions (Ruyter, 1995).

For the biostable, fully cured FRC structures used in this study (E-glass fibers impregnated with a resin mixture based on the monomers BisGMA, TEGDMA and starter chemicals CQ and DMAEMA), a degree of monomer conversion above 60% has been reported (Imazato et al., 2001; Uctasli et al., 2005). Therefore, in animal studies, the resulting minimal release of residual monomers did not cause any cytotoxic side effects (Zhao et al, 2005). The sterilization process of FRCs includes autoclavation at 121°C for 20 minutes (min) at 0.1 MPa pressure (Tuusa et al., 2008).

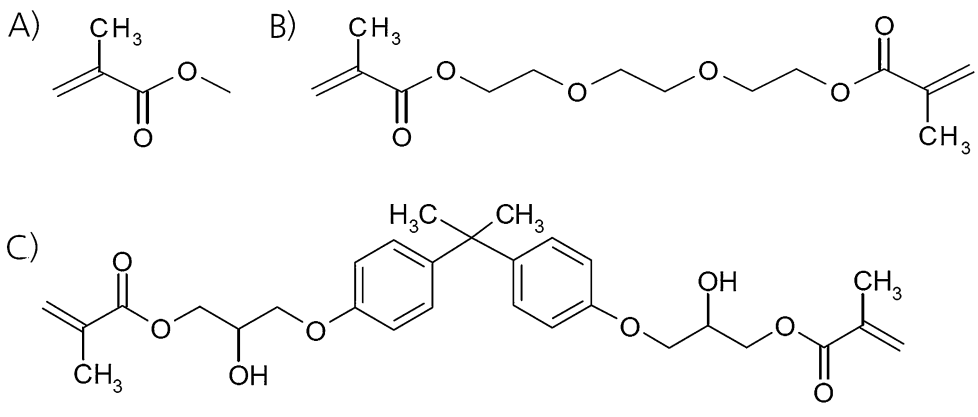

Figure 5: Chemical structure of resin monomers: A) Methyl methacrylate (MMA); B) Triethyleneglycol dimethacrylate (TEGDMA); C) Bisphenol-A-glycidyl dimethacrylate (BisGMA).

2.3.4.3. Fiber reinforcements

Among other reinforcing fibers, glass-fibers are the most widely used reinforcement material both for thermoplastic and thermosetting composites due to their relatively low costs and in exceptional tensile, compression, and impact properties. Further, the strong corrosion resistance and low moisture absorption paired with esthetic properties and the sound adherence to matrix polymers through silane coupling agents are beneficial for dental applications (Alexander, 1996; Murphy, 1998). The term E-glass refers to electrical grade glass. The range of E-glass compositions (in wt%) is 52-56 SiO_2, 12-16 Al_2O_3, 5-11 B_2O_3, 15-25 CaO, 0-5 MgO, 0.5-2.0 $Na_2O + K_2O$, 0-0.1 TiO_2 (Murphy, 1998). Glasses with calcium alumino borosilicate compositions are particularly durable (Zhao et al., 2009) and specified for the reinforcement of plastics (Murphy, 1998).

Polyethylene fibers are also good candidates for reinforcing acrylic resin as the pairing shows minimal water uptake with resin adhering well to the fibers even without coupling agents. For applications in dentistry the use of carbon and aramid fibers combined with PMMA resins is restricted due to poor aesthetics and difficulties in polishing (Chow et al., 1993). PEEK is well compatible with the carbon fibers and experimental PEEK implants have a superior fatigue resistance (Kurtz and Devine, 2007). Increased osteconductivity and implant integration can be achieved using BG fiber reinforcement with partial exposure to tissue fluids (Marcolongo et al., 1998, Puska et al., 2006).

2.3.5. Modern FRC implant designs tested in clinical studies

The following section describes design elements of the new developed FRC implants intended for use in cranial defect reconstruction.

The novel FRC is made of a randomly oriented chopped silanized E-glass veil impregnated within the BisGMA/TEGDMA polymer matrix. Porous FRC is prepared by removing excessive resin, so that 75–81 wt% resin remained in the structure. According to ongoing micro-CT analyses by Ylä-Soininmäki A. et al., this procedure results in a total porosity of 39–49 vol% with more than 70% of functional (open) porosity (**Table 3**). As pore sizes were above 100 μm the requirements for possible bone ingrowth were met according to the literature (Itälä et al., 2001).

A structural implant design was previously introduced using partially porous BisGMA/MMA/PMMA-resin impregnated FRC laminates (Tuusa et al., 2008). The multicomponent laminate specimens, used in the present study, were made from two layers of BG granules entrapped between three layers of porous FRC (**Figure 6b**).

Figure 6a shows the model implant at an implant site, whose anatomical details are simplified. Various tissue layers and the scalp, on top of the implant and the skull bone, are not marked in the scheme. The implant size and shape varies according to the patient's needs; the thickness of the implant has to be adjusted to the thickness of the remaining adjacent bone. The screws (D) made of biodegradable polymers, such as PGA and PLA or biostable titanium, provide the initial implant fixation. However, in case of exact fitting and

implant stabilization by the overlying scalp, these screws are not necessary. The upper dense FRC layer (E), interfacing cortical bone, is designed to act as a strong impact resistance layer protecting the nervous tissue underneath. The porous FRC structure including BG granules as bioactive component (F) mimicks the structure of cancellous bone and should promote new bone formation. The hydrophilicity of the BG granules leads to an enhanced blood flow into the porous part of the implant (Nganga et al., 2011). As BG partly dissolves in contact with body fluids (Zhao et al., 2009), the structural FRC layers are kept in place by everStick ® fibers bundles (StickTech Ltd., Turku, Finland). Antimicrobial coatings are to be applied on FRC surfaces to prevent implant infections.

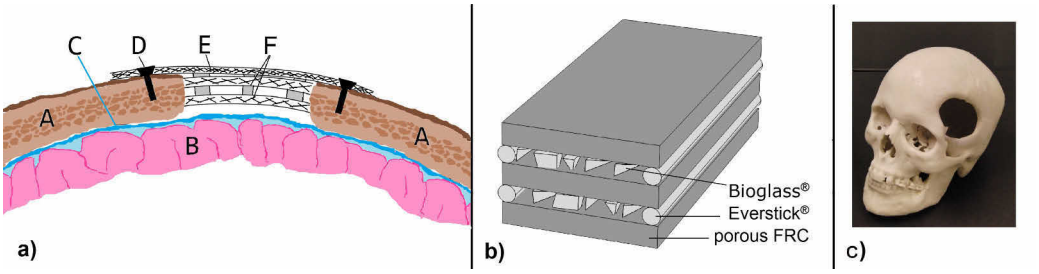

Figure 6 (a) Scheme of cranial implant design: A – intact bone; B – brain tissue; C – dura mater; D – screws for implant fixation; E – dense and F – porous FRC layers with everStick® space holders (gray) and BG (not marked) in between layers. (b) Scheme of *FRC3* specimen. (c) Gypsum model of a skull defect which was used during implant preparation.

The implant model described above is deployed in ongoing clinical studies with promising outcome in 15 patients during a four year follow-up (Aitasalo et al., 2012 and 2013). For the indirectly manufactured implants, first, a preoperative model of the skull defect is fabricated by rapid prototyping based on the patient's 3D CT-data (**Figure 6c**). Then this model is used to prepare a precise patient-specific implant by hand laminating process. (Aitasalo et al., 2009 and 2013; Seitz et al., 2004). In future, automated implant fabrication might include the shaping of implants from a FRC block based on the patient's own anatomical data.

2.3.6. Polysaccharides

The polysaccharide chitosan, described hereafter in more detail, is not intended to be used as craniofacial implant materials as such, but depicts an interesting coating option to add functional properties to an implant surface.

Polysaccharides, carbohydrate molecules with the general formula $C_x(H_2O)_y$, incorporate plenty of –OH functional groups which allow various chemical modifications and solubility in aqueous medium (Baldwin and Kiick, 2010). Biocompatible and biodegradable macromolecules are involved in cell signaling, and in tissue addressing and transport mechanisms.

2.3.6.1. Chitosan and derivatives

Chitosan, as an abundant linear cationic polysaccharide derived from the deacetylation of chitin, is composed of 2-amino-2-deoxy-d-glucose (GlcNH2) residues with a various amounts of N-acetyl-glucosamine groups (GlcNAc) at a random position (**Figure 7**), (Molinaro et al., 2002). Antimicrobial activity in acidic conditions (Simoncic and Tomsic, 2010) and the promotion of wound healing by chitosan occures. Therefore, chitosan is used as a biomaterial in scaffolds, hydrogels and drug delivery systems in various modifications (Kumar, 2000). Those modifications of the amino groups present in the glucosamine units include; acylation (Kubota et al., 2000), alkylation (Yang et al., 2005), carboxymethylation (Muzzarelli et al., 1982), and quaternarization (Murata et al., 1996) of native chitosan.

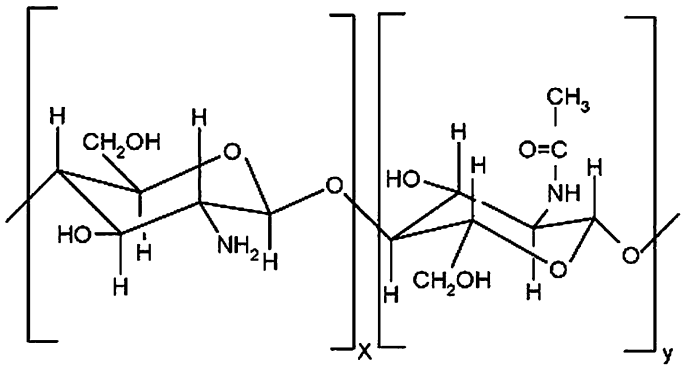

Figure 7: Structure of chitin and chitosan. Chitin is composed predominantly of GlcNAc units (y). Chitosan is composed predominantly of GlcNH2 units (x) (adopted from Retuert et al., 2000).

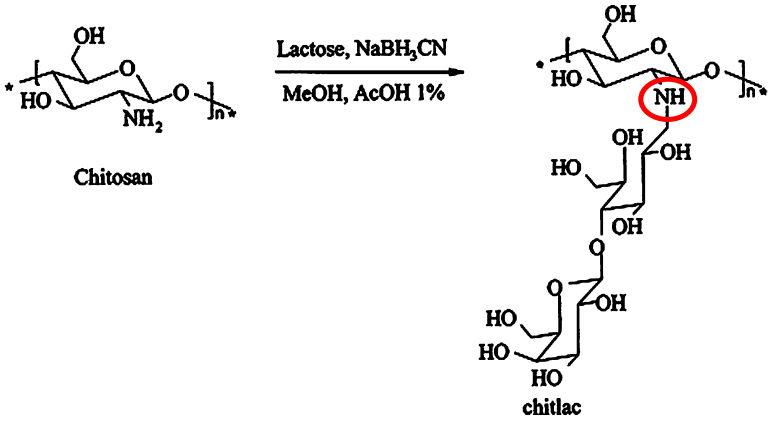

Figure 8: Synthesis of chitlac via N-alkylation of chitosan with lactose. Red circle: coordination point of Ag in chitlac (adopted from Donati et al., 2005).

Donati and co-workers (Donati et al., 2005) produced lactose-modified chitosan (here after: chitlac) by grafting lactose to chitosan *via* a reductive N-alkylation (**Figure 8**). This stimulates growth and collagen production *in vitro*. Due to the presence of lactitol side chains, this derivative overcomes limitations of native chitosan by being highly soluble in physiological conditions and miscible with anionic polysaccharides (Travan et al., 2009). The cationic chitlac forms stable coatings on activated substrates with negative surface charge through polyeletrolyte complexes (Travan et al., 2010). In addition, silver NPs can effectively be stabilised in the chitlac structure by the coordination of nitrogen atoms (**Figure 8**). Therefore, chitlac-nAg is proposed as antimicrobial bioactive implant coating that promotes bone cell proliferation and inhibits bacterial proliferation (Marsich et al., 2013; Travan et al., 2009 and 2011). A combination of chitlac-nAg and alginate was used to create antimicrobial hydrogels (Donati et al., 2007; Travan et al., 2009).

3. AIMS OF THE PRESENT STUDY

Investigations, within this PhD project, aimed to develop a coating system on FRC implants for bone replacements in calvarial or craniofacial defects with sustained antimicrobial and bioactive features. Therefore, the need of revision surgeries will be reduced. The new designed coating containing antimicrobial silver, in the form of NPs stabilized in chitlac, should be biostable and release only minimal amounts of silver to avoid toxic side effects. The polysaccharide coating exposes amino groups of chitlac on the surface that are likely to interact with carboxyl and sulphate groups of the extracellular matrix. This is a trigger for biological implant tissue interaction. BG granules and pores are incorporated into FRC implants to allow bone ingrowth and an additional bioactive fixation of the implant. It is expected, that the combination of BG granules and a silver-polysaccharide coating leads to a superior antimicrobial performance than implants containing one of the active components.

The specific aims of the four studies were:

- to analyze interface shear strength and fracture behavior of porous glass-fiber-reinforced composite implant and bone model material **(Study I).**
- to assess the formation of a calcium phosphate layer on the BisGMA-TEGDMA resin of the FRC implant with incorporated BG granules, *in vitro,* upon static or dynamic immersion in SBF **(Study II)**.
- to study, *in vitro,* the degradation of silver–polysaccharide nanocomposite, in solution and as coatings on FRC, by lysozyme and hydrogen peroxide which simulate inflammatory reactions **(Study III)**.
- to examine, *in vitro,* the antimicrobial behavior and the inhibition of bacterial adhesion and *in situ* biofilm formation by chitlac-silver-nanocomposite coating on dense and porous FRC **(Study IV).**

4. MATERIALS AND METHODS

4.1. Materials

The materials used for fabrication of test specimens in this series of studies are listed in **Table 2**.

Table 2: Materials used for specimen preparation in this series of studies.

Material	Type of Material	Manufacturer
E-glass-fiber Tissue[a] GFT-56G8-100	E-glass-fiber sheet	Ahlstrom Glassfiber Oy, Kotka, Finland
Bis-phenyl-A-glycidyl dimeth-acrylate (BisGMA)	Resin monomer	EssChem, Seaham, County Durham, Great Britain
Triethyleneglykol dimethacrylate (TEGDMA), 95%	Resin monomer	Sigma-Aldrich GmbH, Buchs, Switzerland
Dimethylaminoethyl meth-acrylate (DMAEMA), 98%	Activator	Aldrich Chemie GmbH, Steinheim, Germany
Camphorquinone (CQ), 97%	Photoinitiator	Sigma-Aldrich GmbH, Buchs, Switzerland
EverStick ® C&D[b], Ø 1.5 mm, ~4000 fibers	Preimpregnated glass fiber bundle	StickTech Ltd., Turku, Finland
EverStick ® ortho[b], Ø 0.75 mm, ~2000 fibers	Preimpregnated glass fiber bundle	StickTech Ltd., Turku, Finland
GC Fujirock ® EP	Type 4 dental stone (gypsum)	GC Europe N.V., Leuven, Belgium
Bioglass® 45S5[c], granules, 100-250 µm, lot 221-226-20-Jun07	Bioactive glass	Mo-Sci Health Care LLC. Rolla, MO, USA
Bioglass® 45S5[c], granules 300-500 µm	Bioactive glass	Åbo Akademi, Turku, Finland

[a] Electrical grade glass, fiber diameter: 10 µm, fiber length: 8 mm, nominal basis weight: 100 gm^{-2}, acrylic binder (with silane coupling agent) 11%, (89% fibers); the orientation of the non-woven fibers in the veil is semi-random, with preferred orientation in thickness. Ahlstrom Glassfibre Oy, Kotka, Finland, 0.91 mm thick sheet.
[b] Silanated E-glass-fiber of type tex 600 impregnated with a photopolymerizable resin system.
[c] Bioglass of following chemical composition (wt%): SiO_2: 45, Na_2O: 24.5, CaO: 24.5, P_2O_5: 6.

Further reagents used were 2-[N-morpholino] ethanesulfonic acid (MES), 1-ethyl-3-[3-(dimethylamino) propyl] carbodiimide (EDC), N-hydroxy-succinimide (NHS), 7-amino-1,3-naphtalene disulfonic acid (7-ANA), fluorescein isothiocianate (FITC), and lysozyme (from chicken egg white), which were purchased from Sigma-Aldrich. Hydrogen peroxide (H_2O_2, 35%) was purchased from Riedel-de Haën, Seelze, Germany.

Synthesis of chitlac. The polysaccharide coating was prepared from chitlac (lactose-modified chitosan, CAS registry number 85941-43-1). The procedure to synthesize chitlac starting from a highly deacetylated chitosan (residual acetylation degree approximately 18%, (viscosity average) relative molar mass approximately 7×10^5) has been reported by Donati et al. (2005). The chitlac sample was composed of glucosamine residue ~20%, N-acetylglucosamine ~18% and 2-(lactit-1-yl)-glucosamine ~62%, as determined by means of ^{1}H NMR (nuclear magnetic resonance spectroscopy). The chemical structure of chitlac-nAg complex is shown in **Figure 8** (Travan et al., 2010).

4.2. Methods

4.2.1. FRC preparation (S-I to S-IV)

Resin and FRC specimen with different degrees of porosity and size were prepared as described below. Specimen geometries, used for the different parts of the study, are summarised in **Table 3**.

Photopolymerizable polymer resin consisted of equal parts of the monomers BisGMA and TEGDMA, as well as the photo initiator CQ (0.7 wt%) and the activator DMAEMA (0.7 wt%). For plain resin samples, the mixture was poured into moulds and polymerized by light curing. Subsequently, the specimens were ground (LaboPol-21 Grinding Machine, 300 rpm, Struers A/S, Rødovre, Denmark) to their final dimension and the surfaces were polished with the series of SiC papers with the grit increasing up to #4000 (FEPA).

The photo-initiated polymerization of the specimens was carried out in three stages to ensure minimal content of residual monomers. Firstly, the specimens were pre-cured by a dental hand cure device (Elipar® S10 LED curing light, 3M/ESPE, Seefeld, Germany) with an exposure time of 120 seconds (s) (intensity: 1200 mW/cm², wavelength: 430-480 nm). Secondly, the specimens were post-cured in a vacuum light oven (Visio Beta vario, 3M/ESPE, Seefeld, Germany) for 15 min in ambient temperature and thirdly in a light oven (Targis Power, Ivoclar Vivadent AG, Schaan, Lichtenstein) for 25 min at a temperature of 95°C.

For FRC specimens, non woven E-glass fiber tissue was impregnated with the resin mixture and left for 48 hours (h) in dark. Four specimen groups with different porosities (total porosity of 9-68%) were prepared by altering the amount of polymer resin (53-92 wt%, cf. **Table 3**). Therefore, excessive resin was removed by compressing the specimen (*FRC p2* and *FRC p3*) or blowing with hot air at 70 °C for 10 min (*FRC p1*) before light curing. The amount of polymer resin in the composites was controlled by weighing (PS303-S DeltaRange®, Metler Toledo AG, Greifensee, Switzerland) the E-glass veil before adding the polymer and after the FRC polymerization was completed.

Table 3: Composition and geometry of FRC specimen groups with varying porosity listed according to the part of the study. (Details of specimen used in S-II are listed in Table 4). Table partly adopted from S-I.

Group name	wt% Resin	Total porosity [%][a]	Specimen geometry and name, Number of Study (S)
Original E-glass tissue	0	56 - 66	Cylinder ø 8.45-mm, h = 5.5 mm **S-I**
FRC p1	53 - 57	54 - 68	Cylinder ø 8.45-mm, h = 5.5 mm **S-I**
FRC p2	75 - 81	39 - 49	Cylinder ø 8.45-mm, h = 5.5 mm **S-I** Porous FRC (single layer) *(FRC2)* **S-II** FRC laminate with BG *(FRC3)* **S-II** Porous FRC disc, Ø 9-mm (*pF*) **S-III, S-IV**
FRC p3	85 - 87	15- 32	Cylinder ø 8.45-mm, h = 5.5 mm **S-I**
FRC p4	89 - 92	9 - 25	Cylinder ø 8.45-mm, h = 5.5 mm **S-I** Dense FRC disc, Ø 9-mm (*dF*) **S-III, S-IV**
Resin	100	N.A.	Resin block *(FRC1)* **S-II** Resin disc, ø 9-mm **S-III, S-IV**

[a] In an ongoing study by A. Ylä-Soininmäki et al. the total porosity was analyzed by means of micro-CT imaging (Skyscan 1072, Skyscan N.V. Kontich, Belgium). Analyses of different volumes of interests in the reconstructed 3D-images revealed a functional part of the porosity (open porosity) of generally above 70 vol% for all groups. The average pore size was larger than 100 µm. The reinforcing E-glass fibers in the specimens were covered by polymer resin.

Dense FRC discs (*FRC p4*, **S-III/S-IV**) were prepared by vertically segmenting a light cured FRC block, which was made up by piling of ten impregnated E-glass-tissue layers. Surfaces to be coated were polished with the series of SiC papers with the grit increasing up to #2400 (FEPA). Porous FRC discs (*FRC p2*) were cut out from single tissue layers. Before use, specimen were cleaned by sonication in ultrapure water (milliQ quality), and left to dry at room temperature. Specimen for immersion tests (**S-II**) were additionally cleaned by sonication for 5 min, washed with ethanol and stored in a desiccator.

For FRC cylinders (push-out specimen, **S-I**) nine impregnated E-glass-tissue layers for each porosity group were piled up before light curing. Fully polymerized FRC blocks of 7-mm in height were ground in dry state (micromotor, Ultimate 500K, NSK Nakanishi, Inc., Tochigi, Japan) into cylindrical shapes of diameter 8.45 ± 0.15-mm. They were then embedded into gypsum in moulds having a diameter of 25-mm (powder-to-liquid ratio of 100 g/20 mL as recommended by the manufacturer). A vibrator plate (Vip 24, Silfradent, S.Sofia (FC), Italy) was applied for 3 min during initial setting to ensure the filling of all pores connected to the surface and to avoid air bubbles within the gypsum. Excess gypsum, on the top and bottom side was removed by grinding with SiC paper grit #800 (FEPA) to the final sample thickness of 5.5 ± 0.01-mm (dimension in z-direction in **Figure 9**). After that, the samples were left to set at room temperature for 24 h. Dimensions of push-out specimen were chosen according to the thickness of the human skull bone and established diameters of previous tests (Mattila et al., 2006, Motherway et al., 2009).

For *FRC p2* and *FRC p4*, additional push-out specimens with everStick® C&D pins were prepared to model the situation of initial implant fixation with surgical screws before and after bone ingrowth, respectively (**Figure 9b** and **Figure 10**). Three holes of 1.25-mm in diameter were drilled with a dentist's drill at an angle of 45° in each sample on the FRC-gypsum interface area. The pins were fixed by light curing after placing them into the holes.

FRC laminate specimen (*FRC3*, **S-II**) were designed as model for a cranial implant. The laminate was prepared by putting fiber bundles (everStick® Ortho) as spacers between two pieces of *FRC p2* (*FRC2*, **S-II**) (**Figure 11b**) so that a layer of BG granules could be incorporated. Each of the two BG layers per specimen contained 45S5 Bioglass® granules of the 100-250 μm fraction, 60 ± 5 mg for smaller specimens (10 x 10 x 4 mm^3) and 200 ± 10 mg for larger specimens (9.3 x 30 x 4 mm^3). The BG content of both smaller and larger *FRC3* was around 38% of the total specimen weight. The two sides of the *FRC2* pieces along the spacers were sealed with additional resin prior to final light curing. In previous tests, the packed arrangement of the granules in between the *FRC2* layers enabled wetting throughout the composite structure (Nganga et al., 2011).

4.2.2. Surface activation and coating of FRC surfaces (S-III, S-IV)

FRC specimens were activated and coated as previously described by Travan et al. (2010 and 2011). The FRC specimens (*pF* and *dF*) were immersed in HCl 12 M at 80°C for 7 h, in order to expose on the surface of the material COO^- functional groups by hydrolysis of the methacrylate esters. Thereafter, specimens were removed, rinsed with deionized water (3 x 50 mL), with NaOH 0.1 M (50 mL) and with water again (50 mL) and finally air dried overnight.

For the dip coating, the activated specimens were immersed for 24 h in wells containing 0.5 mL coating solution (4 g/L chitlac in deionized water), and subsequently rinsed in deionized water for 5 min under agitation. Then the FRC specimens were dried under hood overnight.

Chitlac coating solutions containing silver NPs were prepared by reducing silver ions with ascorbic acid according to the following procedures: After dissolving chitlac in deionized water at the concentration of 4 g/L, the resulting solution was mixed with $AgNO_3$ solution to a final $AgNO_3$ concentration of 1 mM. Ascorbic acid ($C_6H_8O_6$) solution was added at final concentration of 0.5 mM. After 4 h, a yellow-orange stable colloidal solution was obtained.

4.2.3. Push-out tests and test analyses (S-I)

The push-out tests were performed on a universal materials testing machine in compressing mode (Lloyd Model LRX, Lloyd instruments Ltd, Fareham, England). The load was applied on the central part of the specimen with a constant speed of 1 mm/min until specimen failure. The clearance of the hole of the support jig was at least 0.8-mm for all specimen (**Figure 9**), (Dhert and Jansen, 2000). A load-displacement curve and

the maximum shear force [N] for at least nine samples per group were recorded with the associated instrument software (Nexygen™). The work until the point of maximum load (W_{max}) and rupture work (W_{RP}) were determined and their difference $W_D = W_{RP} - W_{max}$ calculated to evaluate the fracture toughness (Varin et al, 2001).

Fracture modes were visually evaluated with help of light microscopy images (stereomicroscope MDG 17, Wild Heerbrugg AG, Switzerland, with camera software Leica Qwin Leica microsystems DI, Cambridge, Great Britain). Lateral fracture surfaces were used to determine the area fraction of the gypsum-FRC interface. Penetration depths of gypsum into the pores were determined from cross sectional images of the FRC cores using ImageJ (National Institute of Mental Health, US). Within this study, the term cohesive fracture was applied to fracture lines which left gypsum on the FRC core.

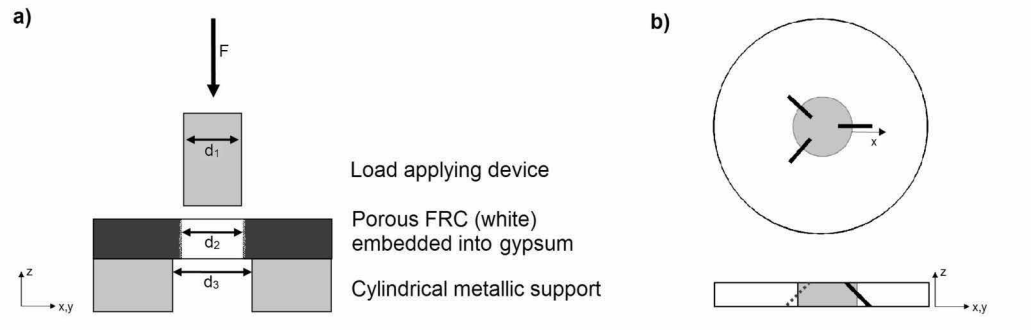

Figure 9: (a) Set-up of push-out test: dimensions: d_1=7.89-mm, d_2=8.45±0.15-mm, d_3=11.17-mm, (b) schema of test specimen with pins. Figure partly adopted from S-I.

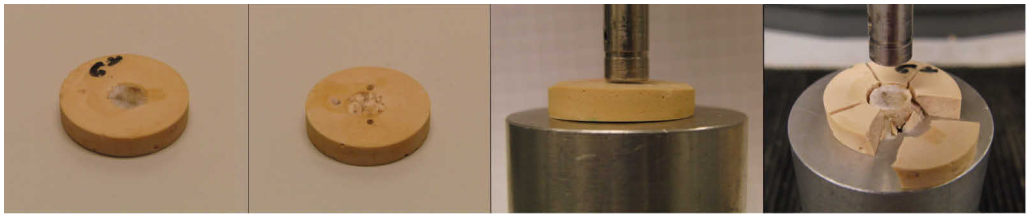

Figure 10: Specimen of push-out test with pins of porosity group 2 (from left to right: picture of top side; picture of bottom side; specimen during testing; and after carrying out the test). Figure partly adopted from S-I.

4.2.4. In vitro SBF Immersion (S-II)

The ability of BG granules to induce CaP formation on the composite surfaces was explored during immersion in SBF in static as well as dynamic conditions. To prepare SBF according to Kokubo's formulation (c-SBF) (Kokubo and Takadama, 2006) following reagents were dissolved consecutively into deionized water: NaCl, $NaHCO_3$, KCl, K_2HPO_4*$3H_2O$, $MgCl_2$*$6H_2O$, $CaCl_2$*$2H_2O$, and Na_2SO_4. The fluid was buffered at physiological pH 7.40 at 37°C with $(CH_2OH)_3$ CNH_2 and 2M-HCl.

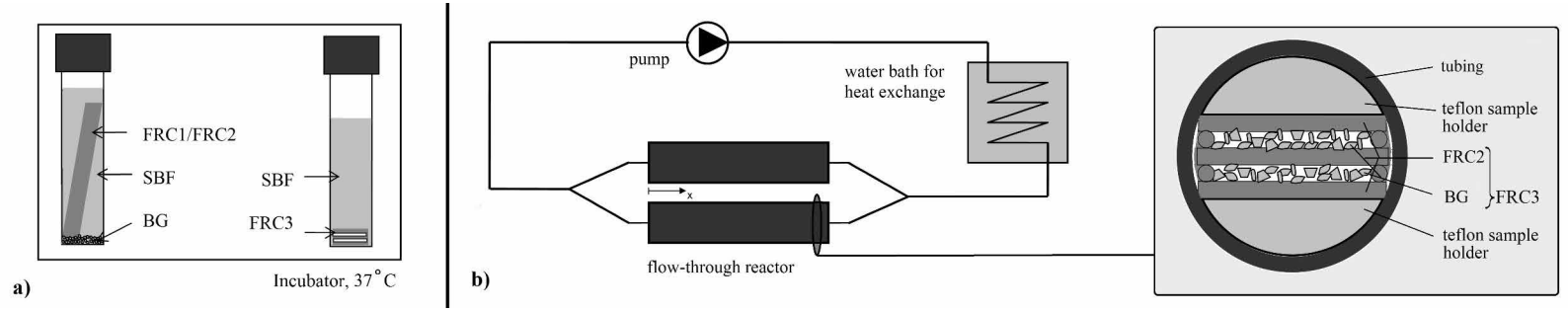

Figure 11: Scheme of static (a) and dynamic (b) immersion test set-up: left: pump system, right: Cross section of *FRC3* specimen in tube reactor. Figue adopted from S-II.

Table 4: Specimen groups used in each static and dynamic immersion test. Immersion times were 3 and 7 days in the static test and 7, 14 and 28 days in the dynamic test. N: Number of tests of each immersion time. In the dynamic test, two specimens were immersed in parallel. Table adopted from S-II.

Test	Group name	N	Specimen		Volume (mL)	SBF Immersion with BG granules	Flow rate (mL/min)
			Type	Size (mm^3)			
Static	SBF control	2 / 2	none	n/a	7	no	n/a
Static	FRC1 control	0 / 2	*FRC1*	9 x 59 x 2.9	7	no	n/a
Static	FRC2 control	0 / 2	*FRC2*	9 x 60 x 1	7	no	n/a
Static	BG	1 / 1	none	n/a	7	yes	n/a
Static	FRC1+BG	2 / 2	*FRC1*	9 x 59 x 2.9	7	yes	n/a
Static	FRC2+BG	2 / 5	*FRC2*	9 x 60 x 1	7	yes	n/a
Static	FRC3	1 / 1	*FRC3*	10 x 10 x 4	5	yes*	n/a
Dynamic	FRC3	2 / 2 / 1	*FRC3*	9.3 x 30 x 4	22 (circulated)	yes*	13

*BG granules were part of the *FRC3* specimens

In the static test condition, *FRC1* and *FRC2* specimens were immersed in 7 mL SBF with and without BG granules (Bioglass® 45S5, 100 mg/mL, 300-500 μm fraction). *FRC3* specimens were incubated in horizontal orientation in 5 mL SBF (static test) or within a circulating SBF flow through the structure (dynamic test). For details see **Table 4** and **Figure 11**.

The aim of the static test was to investigate the effect of the distance between the composite surfaces and BG granules on the *in vitro* behavior. Therefore BG granules at the bottom of the polypropylene flasks and the vertically oriented *FRC1* or *FRC2* specimen were placed in contact to each other. The specimens were incubated at 37°C for either 3 and/or 7 days with gentle agitation (120 rpm in shaking incubator Stuart S1500) evoking movement of solution and glass granules. The level of pH was recorded at 37°C at various time points (pH meter: MP225, Mettler Toledo).

For the test in dynamic condition, a closed reactor system was built up of a peristaltic pump (type Isomatec Reglo Quick, IDEX Health & Science GmbH, Wertheim, Germany) and two parallel specimen chambers made of reinforced PE with an inner diameter (d_I) of 9.4-mm. A water bath was connected to maintain a temperature of 37°C. The flow rate of the 22 ml SBF was determined as 13 ml/min at the main connector tubing (Tygon ST ® 3603, Saint-Gobain Performance Plastics, US) with d_I = 3.2-mm and estimated as 3 mL/min in each of the specimen chambers. A uniform flow of liquid was ensured by covering both ends of *FRC3* specimen with filter paper kept in place by PE holders. A pre-immersion of *FRC3* in SBF in vacuum for 10 min served to displace air out of the specimen. During the second half of the pre-immersion time, the specimens were attached to the flow system, which was then cleaned by pumping in ethanol, H_2O (twice)

and finally SBF. After that, the specimens were incubated in circulating SBF for 7 d, 14 d or 28 d. After every 7 d the SBF was exchanged and the pH measured.

Further analyses of the SBF included inductively coupled plasma-optical emission spectrometry (ICP-OES, Optima 5300 DV, Perkin Elmer) to determine ionic concentrations of Ca, P, K, Mg, Na, P, and Si. Therefore SBF samples of 0.5 mL were taken from static and dynamic tests.

Effects of the immersion on FRC specimen were followed by weighting the specimen in dry state before and after the treatment and characterization by SEM. The processing of FRC specimen after specific immersion times included washing steps in H_2O (twice), and ethanol (once) followed by drying overnight at 60°C in an oven and storage in a desiccator.

4.2.5. Characterization of precipitation layers (S-II)

Precipitation layers on FRC specimen were examined in top and cross-sectional view by SEM (Gemini 1530, LEO Oberkochen /Carl Zeiss, Germany) coupled with energy-dispersive X-ray spectroscopy (EDX, UltraDry Silicon Drift Detector, Thermo Scientific, Madison,Wisconsin, US). FRC for cross-sectional analyses were prepared by embedding the specimen in epoxy resin (EpoFix®, Struers A/S) filled with carbon active p.a. (Merck, Darmstadt, Germany) to enhance contrast against the BisGMA/TEGDMA resin. Epoxy blocks were cut along the along the main axis of FRC and cross-sectional surfaces polished with SiC paper up to 4000 grit and gold coated.

For specimen from static immersion test SEM images were taken at various positions (at 0, 3, 8, 11, 22, 33, 44, 58-mm distance from the bottom end). In addition, the reaction layers on the surfaces of BG granules were analyzed. *FRC3* from the dynamic test were imaged in cross-section at 0, 15 and 30-mm distance from the solution inlet surface of the specimen.

4.2.6. Determination of chitlac degradation (S-III)

4.2.6.1. Chitlac degradation in solution

Time dependant changes of specific viscosity were recorded to study degradation kinetics of chitlac in solution in presence of either lysozyme or H_2O_2. Flow times through a capillary (diameter 0.53-mm) were detected at T=37°C with an Ubbelohde type viscometer connected to a Schott-Geräte AVS/G automatic apparatus and the reduced specific viscosity η_{sp} / c calculated (c is the solute concentration) (Donati et al., 2007; Nordtveit et al., 2004). Three separate solutions of chitlac, enzyme, and oxidizing agent were prepared by dissolving the reagents in PBS solution (pH 7.4) at room temperature. All solutions were then filtered through a 0.45 μm Millipore filter for clarification.

Prior to measurements, the reactive agents were heated at 37°C and then mixed with the chitlac solution to attain final concentrations of: A) 1.26 g/L chitlac with 3.5% H_2O_2 or B) 1.4 g/L chitlac with 1 000 units/mL lysozyme, respectively.

4.2.6.2. Degradation of chitlac coating on FRC by lysozyme

Chitlac was labelled with fluoresceine isothiocyanate (FITC) as a fluorescent tag (hereafter: chitlac-fluo) to allow quantitative analyses of the total chitlac amount in coating on FRC substrates (Donati et al., 2005; Travan et al. 2010). The spectrofluorimeter signal was calibrated with the help of chitlac-fluo solutions in deionized water in the concentration range from 0.25 to 4 g/L. *FRC p2* and *FRC p4* specimens, both with and without chitlac-fluo coating were incubated in 0.5 mL PBS or PBS containing lysozyme (20 000 units/mL, adapted from Lee et al., 1995) at 37°C for either three or seven days in a row, or for three days with liquid exchange after each 24 h. Spectrofluorimeter signals of supernatants of the coating solutions and of the degradation assay were collected in triplicates in order to study the chitlac mass deposit on the specimen surfaces and released upon enzymatic attack.

4.2.6.3. Degradation of chitlac-nAg coating on FRC by H_2O_2

The amount of silver incorporated in the chitlac coatings was quantitatively analyzed by means of Electro Thermal Atomic Absorption Spectroscopy (ETAAS) with Zeeman background correction. A Thermo M series AA spectrometer equipped with a GF95Z Zeeman Furnace and a FS95 Furnace Autosampler (Thermo Electron Corporation, Cambridge, UK) were used for analyses.

The oxidative degradation of chitlac-nAg by H_2O_2 was studied as follows: First, chitlac-nAg coated specimens were immersed in 0.5 mL of deionized water with and without addition of 3.5% H_2O_2 (adapted from Chang et al., 2001) or 0.0035% H_2O_2 for 24 h at 37°C (8 replicates). Non-treated chitlac-nAg coated specimens served as control group. After incubation, specimens were removed, rinsed with 0.5 mL milliQ water in well and subsequently washed in 50 mL of milliQ water and dried. To solubilize the silver content, each specimen was put in a 15 mL tube with 3.0 mL of nitric acid (69% v/v; Sigma-Aldrich, Milan, Italy). Then, the tubes were heated in a boiling water bath for 1 hour, sonicated for 15 min and left 24 h at room temperature before adjusting the volume to 10.0 mL with deionized water. The concentration of the silver solutions was measured at a wavelength of 328.1 nm and analyzed against measured values of standard solutions (range: 0-10 µg/L) obtained by dilution of silver standard solution at 10 000 µg/mL. A five-point standard curve with a correlation coefficient at least 0.9995 was used for the analytical measurements. The limit of detection at the operative wavelength was 0.1 µg/L.

4.2.7. Antimicrobial performance of silver-polysaccharide coatings (S-IV)

The antimicrobial behavior of the silver-polysaccharide nanocomposite coatings on dense and porous FRC structures was investigated *in vitro* by applying three protocols; adhesion tests, antimicrobial efficacy tests, and biofilm tests. All experiments were carried out using the bacteria strains *Staphylococcus aureus* (ATCC 25923) (gram+) and

Pseudomonas aeruginosa (ATCC 27853) (gram-) as species commonly causing implant related biomaterial infections.

4.2.7.1. Bacterial adherence

The bacterial adherence was tested to simulate the affinity of microorganisms to the implant surface directly after implantation. A protocol adapted from previous work (Tanner et al., 2000) was applied for the microorganisms (*S. aureus* and *P. aeruginosa)* on uncoated and coated FRC specimens.

The bacteria were precultured from a frozen glycerol preparation and inoculated in 45 mL brain heart infusion medium (BHI; Bacto™ Brain Heart Infusion, Becton, Dickinson & Company, Le Pont de Claix, France) of 16 h at 37°C. After harvesting the bacteria by centrifugation (4 000 rpm, + 4°C, 10 min, Centrifuge 5810R, Eppendorf, Hamburg, Germany), they were washed once with phosphate-buffered saline (PBS) (diluted from Dulbecco's Phosphate-Buffered Saline (D-PBS) 10x, Invitrogen). Then cells were resuspended in PBS at a concentration of ~0.35 at A550, which corresponded to ~1×10^7 colony-forming units (CFU) (Spectrophotometer BioSpec-mini DNA/RNA/protein analyzer, Shimadzu Biotech, Japan). The suspension was gently sonicated and vortexed to homogenize the solution. Then, the specimens were placed in test tubes (BD Falcon, 14 mL, Ref 352001, US) with 5 mL of bacterial suspension. After rolling (Coulter mixer, Coulter electronics limited, England) at room temperature for 30 min, the specimens were washed three times in abundant physiological saline and gently dried without touching the surface. Thereafter, the bacterial samples from the specimen surfaces were collected for analysis of viability (three replicates) or fixed for analysis by SEM (one specimen).

The bacteria attached to the surface of the specimens were collected with micro brushes into microtubes (2 ml, Sarstedt, Numbrecht, Germany) containing 900 µL of Tryptic Soy Broth (TSB, Bacto™ Tryptic Soy Broth, Becton, Dickinson & Company) with 10% glycerol. Thereafter, the bacteria were sonicated (~5 s with tipsonicator UP 50 H Ultrasonic Processor, Hielscher, Teltow, Germany cycle 1, amplitude 100%), serially diluted in physiological saline (10 µL of 1:10, 1:100, and 1:1000) and cultured on blood agar plates. CFU measurements were done after 16 h of culturing at 37°C. The values reported are the mean ± standard deviation of all relevant dilutions of the three replicates.

4.2.7.2. Antimicrobial efficacy test

Antimicrobial efficacy tests, simulating the performance of the coatings, in the case of bacterial contamination during surgery, were performed according to a modified protocol of the Japanese Industrial Standard method (JISZ 2801:2000) (Travan et al., 2011).

Mid-log phase cultures of *S. aureus* or *P. aeruginosa* in LB-medium (lysogeny broth, Sigma-Aldrich Co. LCC., US) were centrifuged at 3 000 rpm for 5 min and resuspended in 30% LB-medium diluted with PBS at the final concentration of $5x10^8$ CFU/mL. Then,

10 µL of bacterial suspension were deposited on coated and uncoated *dF* specimens; 20 µL of bacterial solution were deposed on the coated and uncoated *pF* specimens. Thereafter, the specimens were covered with UV-sterilized polymer sheets (10 x 10 mm) (Wako Pure Chemical Industries, Ltd., Richmond, VA, US) and incubated for 3 h at 37°C in saturated humidity. The covered specimens were immersed in 2 mL of high salt solution (10 mM Na-phosphate, 400 mM NaCl and 10 mM $MgCl_2$) and vortexed for 30 s to allow the detachment of bacteria from the specimens. After serial dilutions in PBS (up to 10^4), the bacterial suspensions were plated on LB agar and incubated for 16 h at 37°C and the number of viable bacteria was studied. The tests were performed in three replicates.

4.2.7.3. Biofilm formation

For biofilm tests bacteria of the two strains were precultured in TSB from glycerol stock solutions according to the procedure used in the bacterial adherence test. After washing, and culturing in PBS for 16 h, the bacteria were resuspended in fresh TSB medium with 1% (wt/vol) glucose and diluted to ~10^6 CFU/mL. 1 mL of bacteria suspension was added to the specimens in 24-well plates and incubated for 24 h and 72 h at 37°C in a humidified atmosphere. For late biofilms (72 h incubation), the medium was replaced with fresh medium every 24 h. At the end of the incubation period, the culture medium was discarded and all specimens were washed four times in PBS to remove planctonic bacteria. After serial dilutions in PBS, the bacterial suspensions were plated on LB agar and incubated for 16 h at 37°C, and the number of viable bacteria was studied. The tests were performed in three replicates. One specimen was used in SEM analysis. Confocal microscopy was applied to visualize biofilms after 72 h incubation (two replicates).

4.2.7.4. Biofilm visualisation by confocal laser scanning microscopy

In the analysis by confocal laser scanning microscopy (CLSM), the adherent biofilms were stained with Film tracer™ FM® 1-43 green biofilm cell stain (Invitrogen Life Science) (Houot and Watnick, 2008). The staining solution was prepared by diluting 10 µL stock solution into 0.990 mL dimethyl sulfoxide (DMSO), followed by dilution of 0.1 mL into 0.9 mL in sterile ultrapure water. Thus, the final stain concentration was 1 µg/mL. Prior to staining, the specimens were washed in deionized water to avoid interaction of the stain with PBS ions. After removal of the deionized water, 50 µL of staining solution was added on two wet biofilm specimens at a time. Then specimens were incubated for 30 min in the dark (practically up to 45 min) and rinsed with sterile ultrapure water to remove excess stain. Finally, specimens were covered by polymeric cover slips and biofilms analyzed in confocal laser scanning microscope (CLSM, type Nikon C1). Three-dimensional images of surface areas of 100 µm² or 200 µm² were collected in slices of 0.3 µm distance covering a depth (z-axes) of up to 22 µm at a wavelength of 488 nm. The biofilm thickness was measured from the CLSM images at

three or more different locations and averaged with the software *Image J* (W. Rasband, National Institute of Health, US).

4.2.7.5. Scanning electron microscopy

SEM (JSM 5500, JEOL Ltd., Tokyo, Japan) was used to assess the distribution and morphology of bacterial colonies on substrate surfaces. After washing, bacteria were fixed on the test surfaces by immersing the specimens into fixing solution (PBS containing 5.7% of formaldehyde and 8% glutaraldehyde) for 5 min. Thereafter, the specimen were washed in deionized water, dried with an ascending series of ethanol (50%, 70%, 96% and absolute ethanol) and stored in desiccator prior to SEM analysis.

Specimens with fixed bacteria were attached to metal holders by carbon tape and sputter-coated with gold. SEM images were taken at various magnifications (250x, 500x, 1000x, 2500x and 5000x) in central and peripheral regions of the specimens.

4.2.8. Statistical analysis (S-I to S-IV)

To study differences amongst the behavior of sample and treatment groups, statistical analyses were performed using the SPSS (Statistical Package of Social Science, SPSS Inc., Chicago, USA) software. The equality of variances was analyzed by Levene test and where appropriate, the equality of means test with Independent-samples T-test. Data which did not follow normal distribution was analyzed by a Kruskal-Wallis Test and Mann-Whitney U-test. Univariate ANOVA (analysis of variance), followed by Tukey's honesty significant difference test, was applied to compare the influence of two independent factors on the measured variable. The level of statistical significance was considered to be 0.05.

5. RESULTS

5.1. Push-out test (S-I)

5.1.1. Load-deflection curves

The shear strength of the interface between mechanically interlocked gypsum and porous FRC specimen increased significantly with an increased degree of FRC porosity (**Table 5**). FRC samples with a total porosity of 54-68% (*FRC p1*) cracked at a maximal load of 1147 ± 271 N, which indicated an interface strength twice as big as that of specimen with 9-25% total porosity (*FRC p4*) ($p<0.05$). The lowest push-out forces were observed for *FRC p3* and *FRC p4* specimens and showed statistically similar properties ($p=0.84$). Further, ANOVA revealed no effect of the pins on recorded push-out forces ($p=0.39$). The factors porosity and addition of pins, were found to be independent. Micro roughness of the interface of *FRC p2* specimen had also no impact on the interface strength (data not shown).

Along with the maximum load, the rupture process was affected by the FRC porosity. For *FRC p1* specimen, the cracking noise was observed during the time point of maximum load, followed by a prolonged fracturing of the gypsum. In contrast, fractures in less porous interfaces happened mostly abruptly, leading to lower W_D values (**Table 5**). In case of *FRC p2*, the rupture process was twice as fast after the insertion of fixation pins into the samples, while no influence of the pins was seen for *FRC p4*. Deflections curves of *FRC p4* showing zigzag patterns on the ascent slope specimen pointed to an unstable cracking progress. In the case of $W_{D,}$ statistical differences were confirmed *via* Kruskal-Wallis Test ($p<0.001$), as the Levene Test failed.

Table 5: Results of push-out test; Values depict average ± standard deviation. Table adopted from S-I.

Group Name	Total porosity [%]	Maximum Push-out Load [N]	W_D (mJ)	Number of Samples
FRC p1	54 - 68	1146.6 ± 270.8	114.9 ± 80.8	10
FRC p2	39 - 49	760.8 ± 113.8	30.7 ± 12.7	11
FRC p3	15- 32	525.7 ± 163.8	5.7 ± 1.4	12
FRC p4	9 - 25	515.3 ± 177.0	4.5 ± 1.7	9
FRC p2_pins	39 - 49	778.8 ± 194.6	17.0 ± 6.6	11
FRC p4_pins	9 - 25	395.3 ± 98.3	4.4 ± 2.3	9

5.1.2. Analyses of fracture modes and gypsum penetration

All fractures observed during push-out testing were cohesive thus splitting the gypsum ferrule and leaving the FRC core undamaged. The amount of gypsum remaining at the FRC surface increased with increasing FRC porosity. For specimens withstanding push-out forces of 800 N or higher, parts of the gypsum pushed off the sample support due to the fracture impact. Gypsum ferrules of specimen with pins ruptured into three main parts corresponding to the stress concentration at the weak points surrounding the pins. Frequently, small pieces of gypsum underneath the pins remained attached to the FRC core (cf. **Figure 10**). Generally, observed fracture modes varied even within specimen groups and the insertion of pins did not lead to a specific drift of fracture patterns.

In micrographs of the lateral fracture surface on the FRC side (**Figure 12**), the fraction of the lateral area of FRC cores of porosity groups *p1, p2, p3,* and *p4*, into which gypsum penetrated, was assessed to be 70%, 45%, 15%, and 2%, respectively. The plot of the maximal push-out loads *versus* those area fractions revealed a parabolic trend in material behavior.

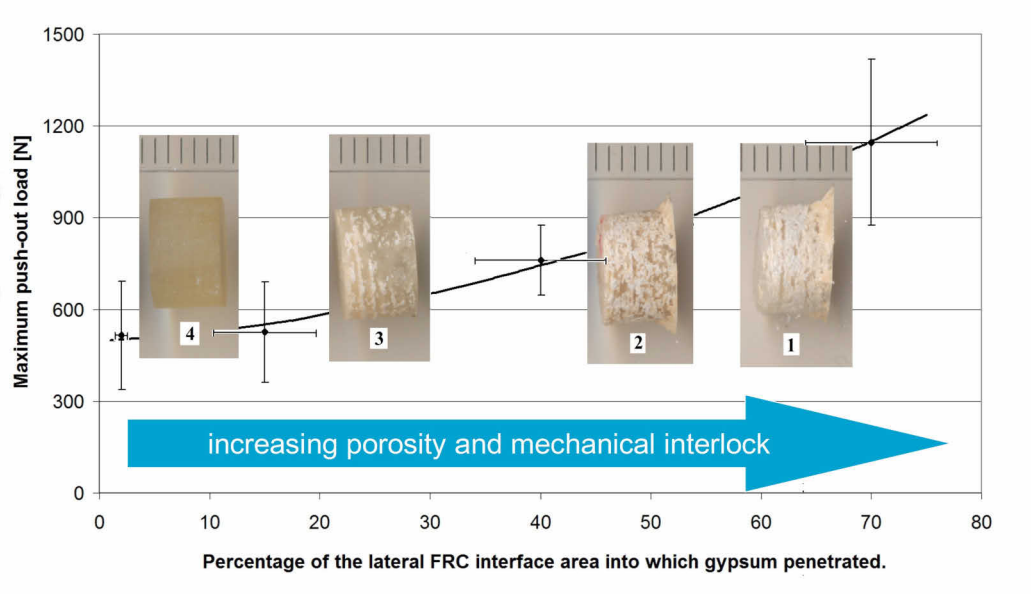

Figure 12: Results of push-out test: plot of maximal push-out forces versus percentage of lateral area with gypsum penetration. The lateral interface area penetrated by gypsum was calculated from micrographs of push-out samples cores of *FRC p1* to *FRC p4* after removing surrounding gypsum (scale marking in mm). Figure adopted from S-I.

Figure 13 reports penetration profiles of gypsum into the interconnected porosity of FRC cores. As expected, the penetration depth increased in line with FRC porosity. In case of *FRC p1*, the E-glass tissue layers did not stick together properly, thus allowing gypsum to penetrate through the whole FRC structure. The own weight of gypsum and applied vibration during initial setting led to increased gypsum penetration depths at the lower part

of the specimen. The penetration depth was at least 0.5-mm for *FRC p1* and *FRC p2*, and 0.3-mm for *FRC p3* at the place of surface pores. At some places gypsum penetrated up to 2-mm into those FRC structures. The dense *FRC p4* did not allow gypsum to penetrate in.

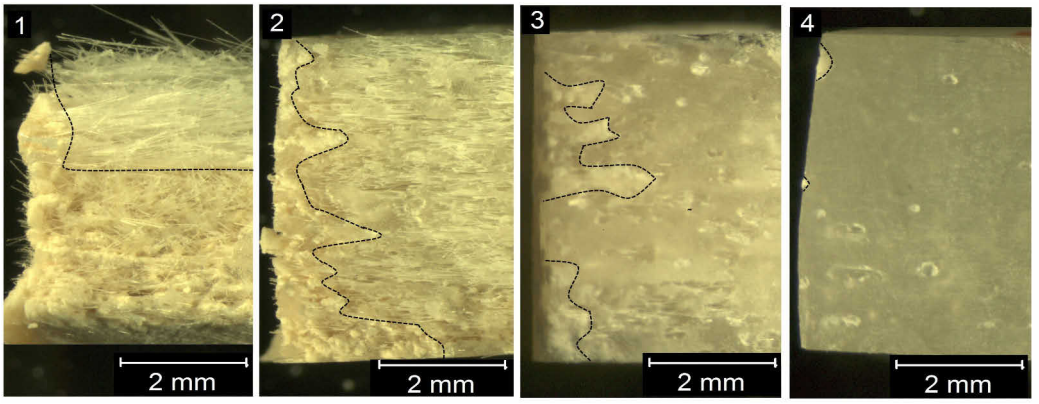

Figure 13: Cross-sections of FRC specimen of different porosity (*FRC p1* to *FRC p4*); dashed lines indicate gypsum penetration depth profiles in the FRC blocks. The structures on the right-hand side of the profiles depict pores not reached by gypsum. Figure adopted from S-I.

5.2. Characterization of precipitation layers (S-II)

Immersion tests of this study showed the ability of BG to conduct the known bioactive reactions and to induce CaP precipitation at the FRC surfaces in both static and dynamic conditions.

5.2.1. Precipitation layers in the static test

SEM-EDX analyses of the static test revealed a precipitation layer with a cauliflower structure indicating CaP all over the surfaces of *FRC1* and *FRC2* that were immersed together with BG granules in SBF (**Figure 14**). The thickness of the precipitation layer increased with immersion time and was thicker for *FRC1* (up to 0.8-µm) than for *FRC2*. After seven days, the CaP layer covered almost the whole *FRC1* surface, whereas *FRC2* was only partly coated. As seen from the precipitation profiles (**Figure 15**), the layer thickness declined from the bottom towards the top of the specimen, but increased again at the upper end of the specimen. A statistically significant increase of the surface area covered by CaP was observed on the bottom parts of *FRC2* (x = 0 to 30-mm) between three and seven days of immersion. As expected, specimen incubated without BG granules did not show any signs of CaP precipitation.

The presence of *FRC1* or *FRC2* in the SBF had an influence on the reaction layers found on the BG granule surfaces (300-500 µm) at the bottom of the flasks. The typical reaction layers containing CaP, silica (Si) and mixed CaP/Si were formed on BG surfaces incubated in SBF for one week in a thickness of 5 µm. Upon incubation with FRC

specimen present, the reaction layers developed on the BG granule surfaces were thinner and mainly out of Si with few spots of CaP (**Figure 16**). Detailed results of the EDX analyses are shown in Figure 7 of the original publication (**S-II**).

When *FRC3* specimen were immersed in static condition, incorporated BG granules (fraction 100-250 μm) developed a Si-rich, a CaP/Si – mixed, and occasionally thin CaP layer. On the resin surface next to the reacted BG granules, precipitated a thin CaP layer (**Figure 17**). However, on E-glass fibers and in the center of the laminate specimen, no precipitation could be detected.

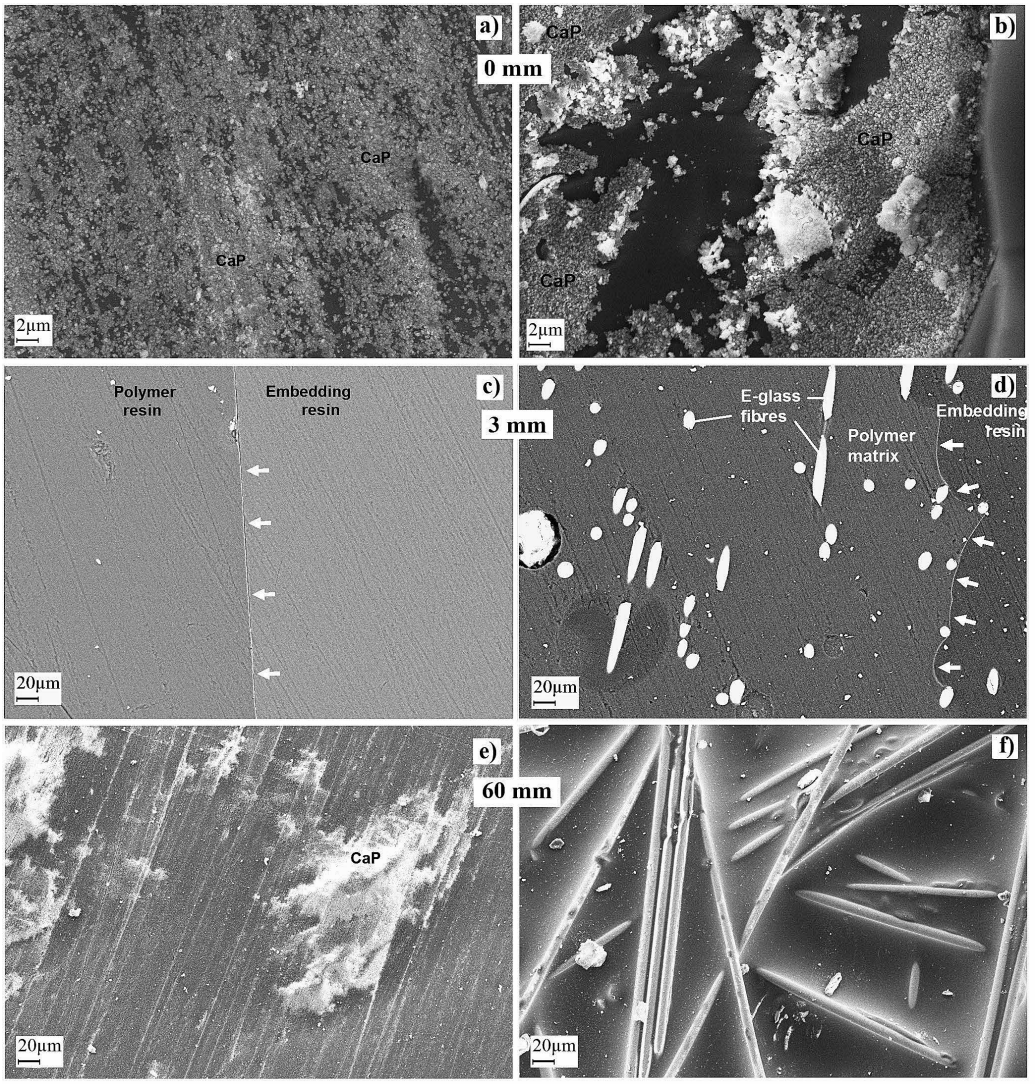

Figure 14: SEM micrograph of *FRC1* (left) and *FRC2* (right) specimen after seven days immersion in static conditions with BG: specimen surface at position x = 0-mm (a,b), and 60-mm (e,f); cross-sections at position x = 3-mm (c,d), white arrows indicate CaP on resin.

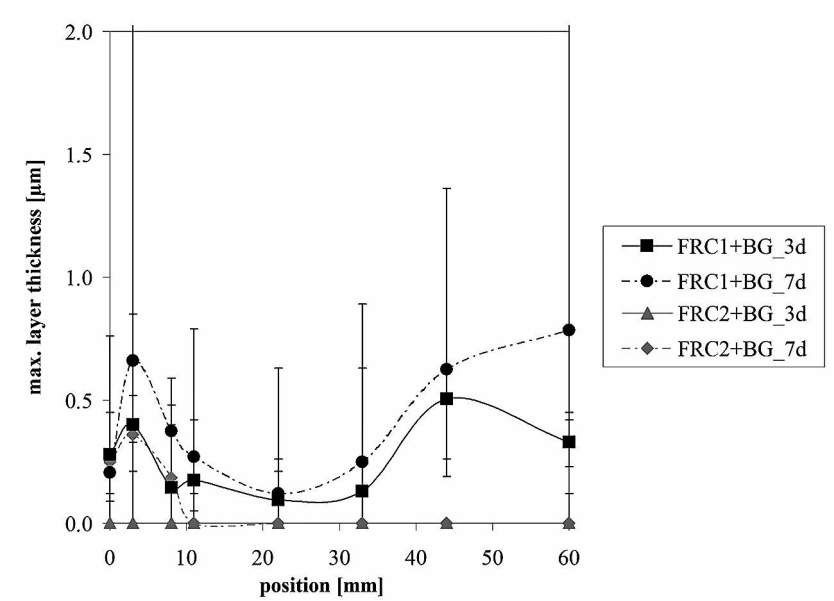

Figure 15: Maximal thickness of precipitation layers on *FRC1* and *FRC2* after static immersion test for three and seven days dependant on the sample area based on cross sectional SEM images: As the data did not follow normal distribution, the diagram depicts calculated medians together with minimum and maximum values of at least four measurements. Lines are drawn to guide the eye. Figure adopted from S-II.

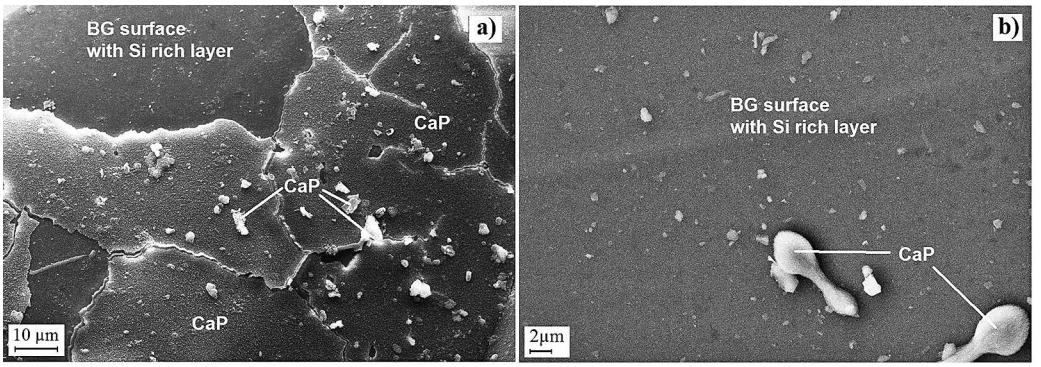

Figure 16: SEM micrograph of BG granules surface after seven days immersion in static conditions without (a) and with *FRC2* specimen (b). Figure adopted from S-II.

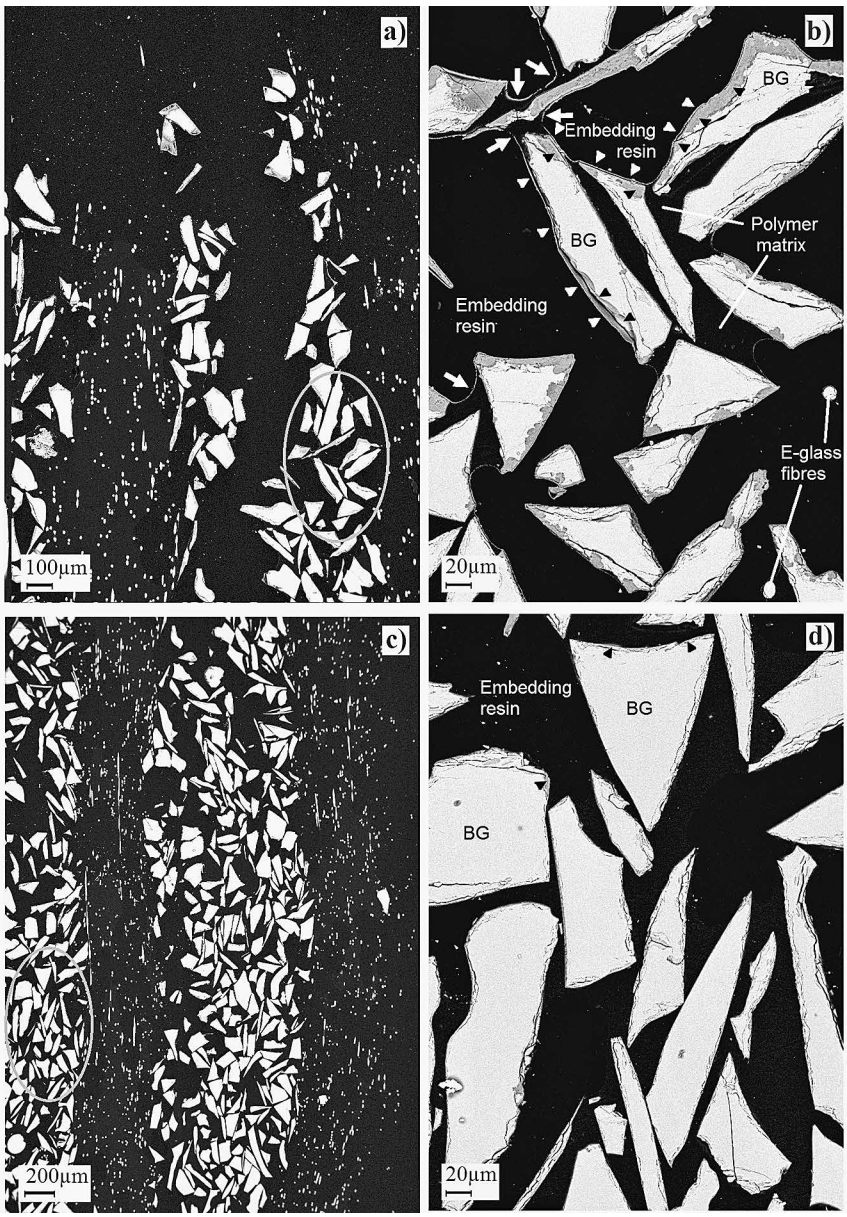

Figure 17: SEM micrograph of *FRC3* after seven days of static immersion: cross section at the margin (a and b) and the central part (c and d) of the specimen. White arrowheads indicate Si rich layer, black arrowheads CaP/Si mixed layer and white arrows CaP on resin. Circles mark area of detail figures on the right. Figure adopted from S-II.

5.2.2. Precipitation layers in the dynamic test

For *FRC3* incubated in circulating SBF, CaP precipitation was induced at some places of the *FRC2* surfaces reached by the solution throughout the implant structure (**Figure 18**). On incorporated BG granules, similar patterns of reactions layers were detected as in the

case of static immersion. The thicknesses of CaP layers increased with incubation time, particularly at the inlets and outlets of the specimen.

Disintegration of a part of the BG granules from the specimen inlets and outlets indicated in SEM images (**Figure 18**) was confirmed by a slight weight loss during immersion (**Table 6**). However, BG granules were not observed in reactor tubes upon removal of the specimen (in static and dynamic tests). Changes in specimen weight might also be affected by the deposition of precipitation layers.

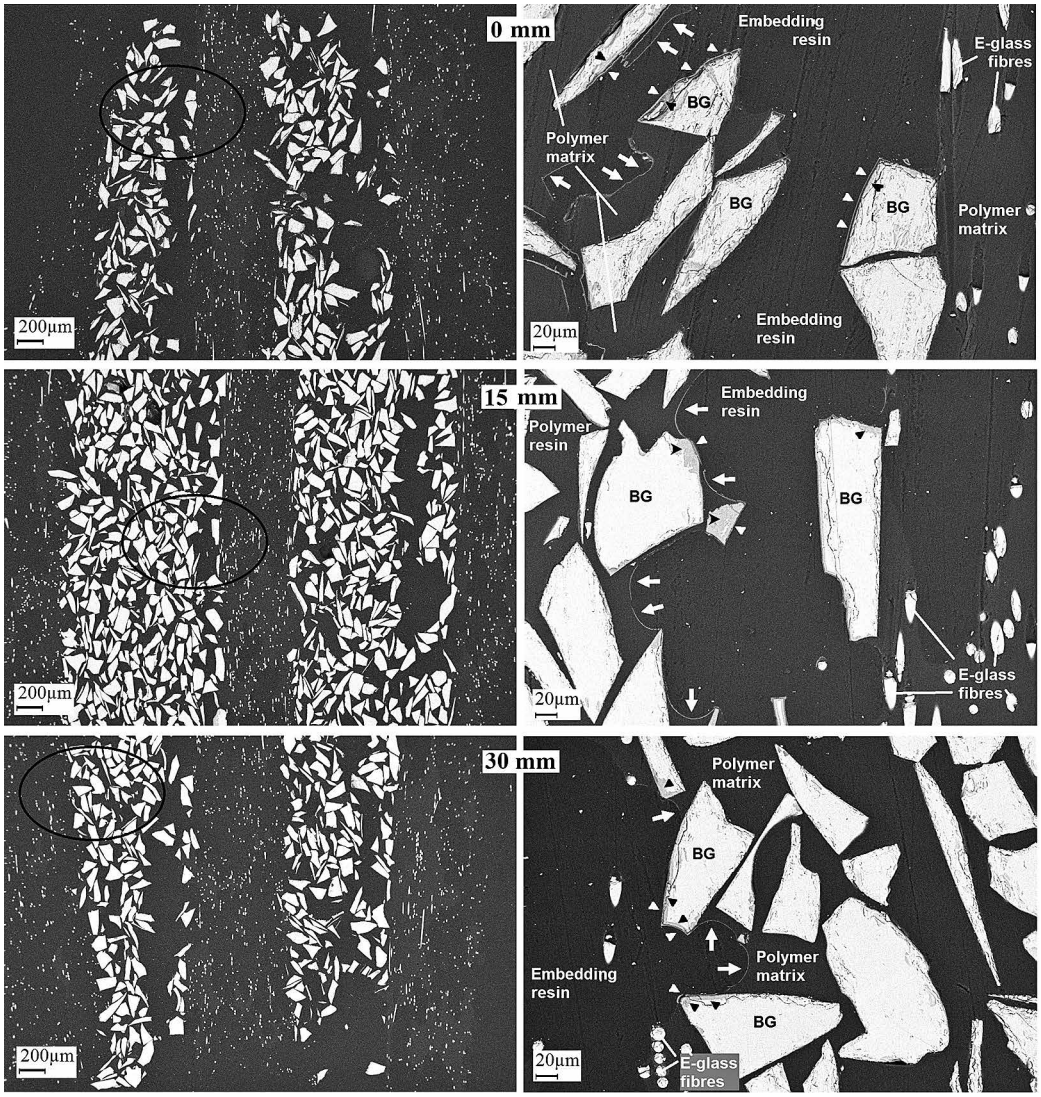

Figure 18: SEM micrograph of *FRC3* after seven days immersion in dynamic conditions: cross section at positions x= 0, 15, and 30-mm for the magnifications 30x (left) and 250x (right). White arrowheads indicate Si rich layer, black arrowheads CaP/Si mixed layer and white arrows CaP on resin. Circles mark area of detail figures on the right.

5.2.3. Analysis of SBF supernatants

Findings of ICP-OES analyses of the SBF supernatants were consistent with the picture received from SEM-EDX results. The dissolution of silicon and sodium ions from the BG granules induced the formation of precipitation layers, consuming phosphate ions. A portion of magnesium ions of the SBF was also integrated in the CaP layer. For details see **Table 7**.

Detected pH values of the SBF corresponded to the anticipated trend (**Figure 19** and **Table 6**). The pH level of SBF controls was constant during one week of static immersion, while the pH of sample solutions with incubated FRC specimen and BG granules increased by 1 ± 0.2 units (mean ± standard deviation). For *FRC1* and *FRC2* immersed alone, a slight pH decrease of 0.1 units was detected. For the circulating SBF of the dynamic test, the weekly increase of pH diminished over time.

Table 6: pH changes of SBF and weigh loss of *FRC3* during immersion in static and dynamic conditions (average and standard deviation (in parentheses)), N.A. = not analyzed. For groups with two samples (*) the range indicates the distance between the two values. In the dynamic tests, both *FRC3* specimens immersed in parallel were weighted separately, while only one SBF sample was withdrawn from dynamic test reactor at a time. Table adopted from S-II.

Group name (nr of tests)	Immersion time (days)	pH change	Weight loss (mg)	Weight loss (%)
		Samples of static immersion test		
FRC3 (1)	3	0.79	10.5	3.51
FRC3 (1)	7	1.24	6.4	2.10
		Samples of dynamic immersion test		
FRC3 (2)	0 - 7	1.14 (0.01)*	16.1 (6.0)	1.53 (0.58)
FRC3 (2)	8 - 14	1.05 (0.25)*	29.3 (16.5)	2.85 (1.58)
FRC3 (1)	15 - 21	0.75	N.A.	N.A.
FRC3 (1)	22 - 28	0.65	36.2 (13.0)*	3.52 (1.25)*

Table 7: Concentration of ions (mg/L) in mixed SBF after various times of immersion in static, and dynamic conditions. The emission lines (nm) for each ion in the ICP-OES analyses are also given. Values depict averages and standard deviations (in parentheses) out of the indicated number of samples. For groups with two samples (*) the range indicates the distance between the two values. < LOQ indicates values below the limit of detection (for P and Si ions in each case 4 mg/L). Table adopted from S-II.

Group name (nr of samples)	Immersion time (days)	Concentration of the ions (mg/L) in sample solutions					
		Ca (317.9)	K (766.5)	Mg (285.2)	Na (589.6)	P (213.6)	Si (251.6)
SBF controls							
SBF control (2)	0	78.3 (4.0)*	183.5 (0.0)*	32.4 (1.8)*	3333 (115)*	33.7 (1.1)*	< LOQ
SBF control (2)	7	79.2 (5.2)*	186.3 (2.8)*	31.4 (0.8)*	3200 (0)*	28.7 (6.1)*	< LOQ
SBF control (1)	14	80.2	184.7	31.1	3200	28.7	< LOQ
Samples of static immersion test							
FRC1 control (2)	7	86.7 (2.6)*	192.6 (0.9)*	33.4 (0.2)*	3400 (0)*	29.3 (3.9)*	< LOQ
FRC2 control (2)	7	82.5 (1.6)*	188.1 (3.5)*	32.5 (0.5)*	3200 (0)*	30.5 (0.6)*	< LOQ
BG (1)	3	163.3	192.7	29.2	3600	13.4	43.6
BG (1)	7	123.7	195.2	25.7	3800	< LOQ	60.6
FRC1+BG (2)	3	172.5 (38.0)*	190.8 (5.3)*	26.0 (0.5)*	3500 (141)*	6.0 (0.1)*	48.0 (24.6)*
FRC1+BG (2)	7	131.9 (82.0)*	190.4 (2.8)*	23.2 (1.1)*	3700 (141)*	< LOQ	63.1 (7.2)*
FRC2+BG (2)	3	145.7 (3.3)*	190.4 (3.9)*	27.8 (0.0)*	3400 (0)*	16.6 (0.1)*	33.5 (0.1)*
FRC2+BG (5)	7	166.1 (20.2)	191.3 (2.2)	26.9 (1.9)	3680 (109)	5.3 (0.1)	49.5 (6.3)
FRC3 (1)	3	184.5	229.6	29.3	3800	< LOQ	61.0
FRC3 (1)	7	189.2	215.0	25.4	4000	< LOQ	64.7
Samples of dynamic immersion test							
FRC3 (2)	0 - 7	166.7 (23.6)*	192.7 (1.4)*	26.5 (1.5)	4000 (0)*	< LOQ	67.1 (4.3)*
FRC3 (2)	8 - 14	214.1 (5.2)*	194.0 (5.6)*	30.2 (3.7)*	3900 (141)*	< LOQ	63.5 (0.2)*
FRC3 (1)	15 - 21	184.8	195.7	32.7	3800	< LOQ	61.1
FRC3 (1)	22 - 28	165.0	198.2	32.7	3800	< LOQ	58.3

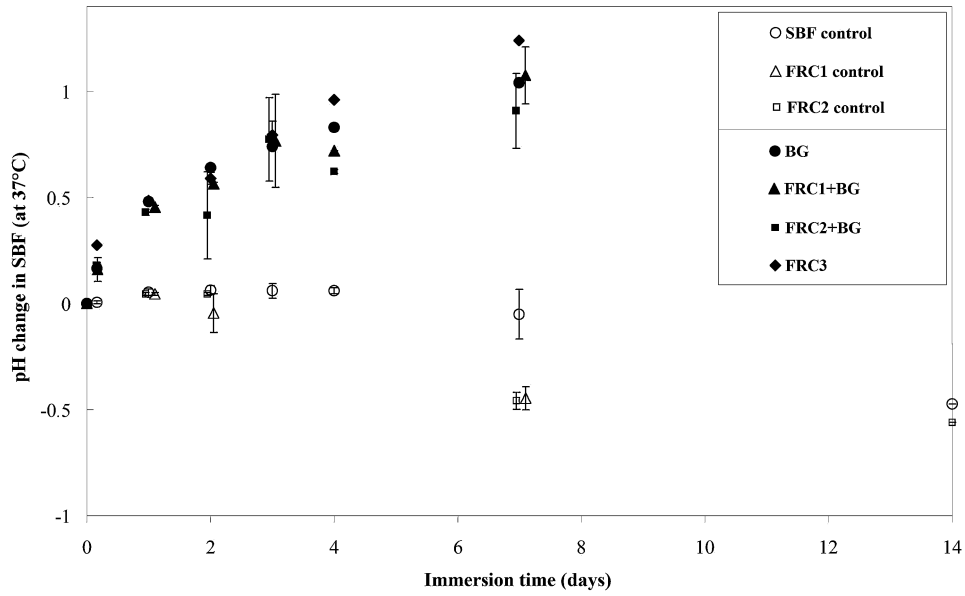

Figure 19: Diagram showing pH changes during immersion test in static conditions (average of two measurements). Bars indicate minimum and maximum values of two measurements. Figure adopted from S-II.

5.3. Chitlac degradation in solution and as coating on FRC substrates (S-III)

Exposure of chitlac solutions to lysozyme and H_2O_2 led to rapid degradation of the polysaccharide. The relative specific viscosity of chitlac in solution decreased to 35% and 18% of the original value after three hours of enzymatic degradation by lysozyme, and chemical degradation by H_2O_2, respectively (**Figure 20a**). The degradation rate for chitlac by lysozyme was found to be 3.1×10^{-4} g^2/dL^2 /min from the initial slope of the experimental data reported in **Figure 20b**. After a rapid viscosity decrease in the beginning the degradation rate slowed down. Plots of Δ (1/(η_{sp} /c)) over the degradation time (**Figure 20b**) show Michaelis–Menten kinetics of the enzymatic cleavage reaction of the β-1,4 N-acetylglucosamine linkages. In the case of the oxidant H_2O_2, the depolymerizaton reaction of chitlac followed a linear trend indicating first-order kinetics or pseudo-first order kinetics with a reaction rate of 6×10^{-4} g^2/dL^2 /min.

In contrast to the results in solution, the chitlac coating on FRC substrates was very stable against enzymatic (lysozyme) degradation. The chitlac-fluo mass adsorbed on activated dense and porous FRC samples was about 1.95 ± 0.07 mg/disc independent of the sample type close to the theoretical maximum of 2 mg/disc present in the coating solution. Changes in fluorescent signal of coated samples due to incubation in PBS with lysozyme compared to that in pure PBS were generally insignificant ($p>0.05$). The

detected values of mass loss were smaller than 0.05% and 0.25% for coated dense and porous FRCs respectively, after seven days of incubation. Chitlac did not form a coating layer on non activated specimens. The ETAAS analysis revealed no significant silver release from chitlac-nAg coatings ($p>0.13$) into deionized water containing 3.5% H_2O_2 within 24 h. The amount of silver incorporated in the coating for dense and porous specimens was 518±117 ng/disc and 127±54 ng/disc, respectively (**Figure 21**).

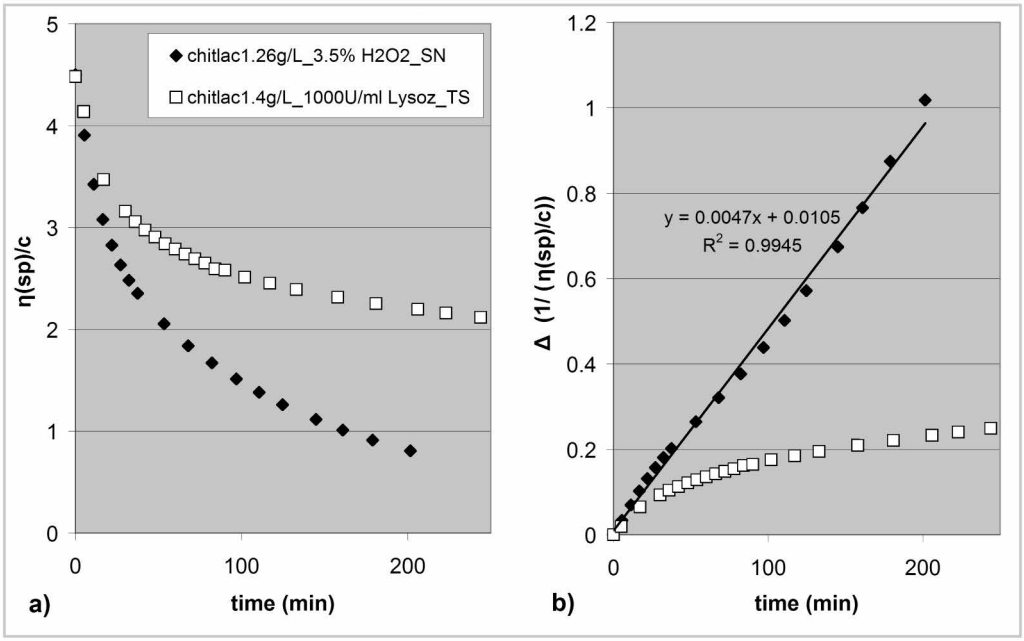

Figure 20: Degradation of chitlac in solution with H_2O_2 and lysozyme: (a) reduction of specific viscosity and (b) variation of the inverse of the specific viscosity over time for chitlac (1.26 g/L) in the presence of H_2O_2 (black symbols) and lysozyme (white symbols) in PBS at 37°C. Figure adopted from S-III.

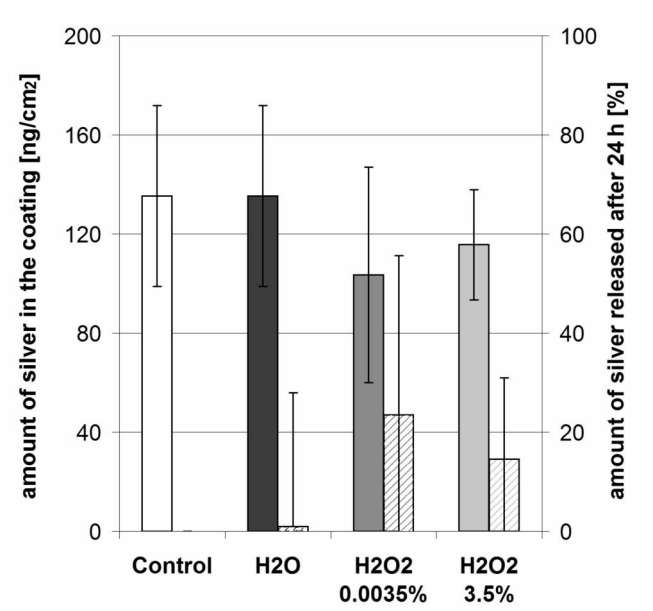

Figure 21: Degradation of chitlac-nAg coating by H_2O_2: amount of silver remaining on the coating after 24 h immersion (plain bars) and percentage of silver release (dashed bars). Figure modified from S-III.

5.4. Antimicrobial behaviour of silver-polysaccharide coatings (S-IV)

5.4.1. Bacterial adherence

In the adherence test, the initial adhesion was measured, which is the interaction between the cell surface and the material surface. Significantly less *S. aureus* ($p<0.05$) attached to the dense specimens than the porous specimens, while no differences were observed for *P. aeruginosa*. In these experimental conditions, the chitlac-nAg had no impact on the bacteria binding process. Observations of SEM images (Figure 2 of the original publication (**S-IV**)) were in line with the culturing results shown in **Table 8**.

5.4.2. Antimicrobial efficacy test

In the test for antimicrobial activity in a small volume of LB-medium, the chitlac-nAg coatings were highly effective for both (dense and porous) substrates against both bacteria strains. Bacteria were efficiently inactivated with direct contact to antimicrobial silver-polysaccharide coatings as the CFUs/mL dropped by at least 4 orders of magnitude ($p<0.01$, **Table 8**). With both *S. aureus* and *P. aeruginosa*, there were no statistically significant differences between dense and porous specimens.

Table 8: Bacterial adherence and antimicrobial efficacy tests of chitlac-nAg coatings: Results of colony counts. Values depict averages and standard deviations (in parentheses), (*dF* – dense FRC, *pF* – porous FRC, for details see Table 3).

Group name	Bacterial adherence test [log CFU/sample]		Antimicrobial efficacy test [log CFU/1mL]	
	S. aureus	*P. aeruginosa*	*S. aureus*	*P. aeruginosa*
pF	5.50 (0.15)	5.48 (0.16)	6.44 (0.87)	6.45 (0.17)
pF-nAg	5.37 (0.51)	5.48 (0.15)	1.43 (1.73)	0 (0)
dF	4.45 (0.19)	5.28 (0.21)	6.27 (0.69)	6.39 (0.25)
dF-nAg	4.48 (0.26)	5.40 (0.13)	0 (0)	0 (0)

5.4.3. Biofilm formation

In the biofilm tests, the formation of early (24 h) and late (72 h) biofilms on substrates was barely affected by the antimicrobial coating. On porous FRC, the *S. aureus* biofilm formation after 72 h was significantly increased compared to dense FRC ($p=0.02$), while the porosity did not affect *P. aeruginosa* biofilms. Further, the chitlac-nAg coating had no effect on the biofilm formed on the specimens, but in the medium, the growth of planktonic cells was reduced by 2 log CFU by dissolved silver ions.

In agreement with these results, conducted SEM analysis did not indicate biofilm inhibition by chitlac-nAg coating. Single, adherent bacteria were able to interact and aggregate in colonies. In case of *P. aeruginosa,* abundant extracellular polysaccharide slime developed. For *S. aureus,* the round shaped bacterial cells formed multilayered clusters hold together by extracellular components. CFU data and SEM images are represented in Figure 4 and 5 of the original publication (**S-IV**).

In CLSM images, a reduced *S. aureus* biofilm thickness was found on chitlac-nAg coated dense FRC specimens compared to uncoated specimens ($p=0.01$; **Figure 22** and **Figure 23**). For *P. aeruginosa,* no effect of the coating was detected. On porous substrates, dead cells and slime were accumulated in pores leading to a higher detected biofilm thicknesses.

Analyses of SEM and CLSM images were undermined by partly removed biofilm during the washing and preparation procedure. Particularly for the dense substrates, biofilms sloughed off easily, leading to high standard deviations that hampered the quantification of the biofilm mass (Lawson et al., 2010).

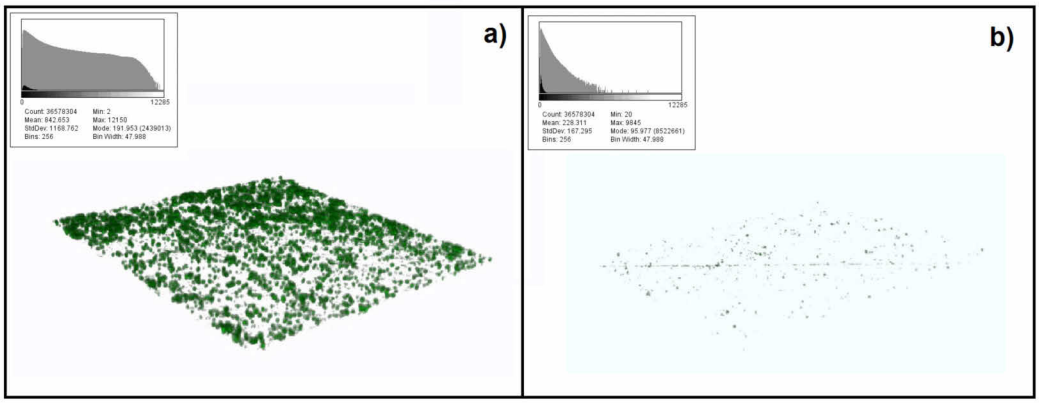

Figure 22: CLSM images of late biofilms (72 h incubation), image area 100 x 100 x 10.8 µm³; 3D volume and histogram, a) *S. aureus* on dF, b) *S. aureus* on dF-nAg.

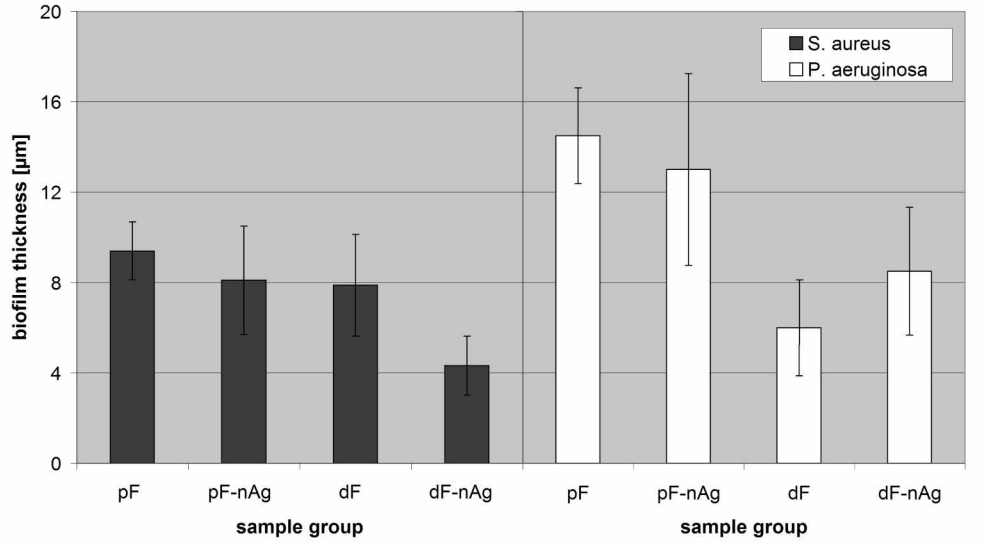

Figure 23: Thickness of late biofilms (72 h incubation) measured in CLSM images. Figure adopted from S-IV.

6. DISCUSSION

6.1. General discussion

Within this series of *in vitro* studies bioactive and antimicrobial modifications of biocompatible FRC implants for craniofacial reconstruction have been investigated.

6.1.1. Bioactive implant modification

Porosity and BG granules were introduced to the multi-component FRC implants to enable mechanical implant attachment to the surrounding bone via biological and bioactive interaction. A proper bone attachment and osseointegration of an implant enables load transfer and lowers the risk of implant rejection and implant associated infections (Campoccia et al., 2006; Gilardino et al., 2009). In an ongoing study, Ylä-Soininmäki et al. showed tensile properties and porosity of the FRC structure to be applicable as cranial implant material.

In the first part of the present thesis (**S-I**), the mechanical properties of the implant interface to gypsum (used as a bone substitute material) were investigated to simulate the effect of bone ingrowth into the macroporous structure. The push-out model confirmed the mechanical interlocking of gypsum and the porous structure, thus the possibility for bone ingrowth.

Secondly, immersion tests in SBF were conducted to study the formation of a bone-like apatite layer on the implant surface induced by incorporated BG granules (**S-II**). This CaP precipitation on the FRC surface is essential to establish bone bonding (Cao and Hench, 1996) and therefore to enhance the biological implant fixation. Whether the observed mineralization (CaP formation) on the FRC surface, initiated by reactions of BG granules, is sufficient to promote initial bone bonding *via* cell ingrowth, is to be verified in further experiments.

Applied BG granules, potentially, also contributes to local antimicrobial effects in the implant structure (Zhang et al., 2010). However, this effect is dependent on the particle size and local ion concentration. Within this series of studies no adequate *in vitro* model was found to support the antimicrobial activity of BG inside the laminate.

6.1.2. Antimicrobial implant modification

For multi-component implants, comparable to the model described in this thesis, there are different ways of silver incorporation which can create antimicrobial activity in order to prevent implant associated infections. Silver has been incorporated into implant materials as component of the methacrylate resin matrix (Cheng et al., 2011), within ceramic fillers such as zeolites or silica gel microspheres (Kawahara et al. 2000, Yoshida et al., 1999), or

as part of sol-gel derived BG powder or BG foams (Blaker et al., 2004, Jones et al. 2006). Coating systems, applicable on polymer surfaces, include the deposition of elemental silver *via* ion beam processes (Brutel et al., 2000), silver hydrogel coatings (Darouiche, 1999), and nanosilver layer by layer polyelectrolyte systems (Grunlan et al., 2005; Malcher et al., 2008).

Of the mentioned alternatives, contact-based antimicrobial activity of silver was reported only by Yoshida et al., 1999, who, however, found a limited release of silver ions from silica gel after 6 month storage in water. For cranial implants, a contact-based antimicrobial system is essential due to the implant site in proximity to the brain, which belongs to the organs known for their sensitivity to nanosilver exposure (Tang et al., 2009). An alternative way of creating contact-based antimicrobial activity is the addition of antimicrobial monomers or quaternary ammonium compounds covalently anchored to the FRC structure (He et al., 2012).

In the present study, a contact active, silver-polysaccharide-based coating was investigated, as synergistic effects of the biological implant recognition of chitlac and the antimicrobial effect of silver have been reported (Travan et al., 2012).

In study III (**S-III**), the degradation behavior of the chitlac-nAg coating was analyzed *in vitro* in conditions simulating inflammatory reactions at the physiological implant site. Specifically, the degradation by lysozymes and the oxidant hydrogen peroxide (H_2O_2) was studied, since these molecules are released in high concentrations by macrophages during healing of bone implant sites (Vårum et al., 1997; de Oliveira-Marques et al., 2007). As anticipated, the polyelectrolyte coating was very stable, while immobilised nAg particles followed independent release kinetics into aqueous solution dependant on the electrolyte concentration (Marsich et al., 2013).

Therefore, the antimicrobial efficacy of the coatings observed against *S. aureus* and *P. aeruginosa* was dependent on the microbiological test set-up (**S-IV**). The contact-active films showed an excellent short time antimicrobial effect (one drop of bacteria solution), whereas no inhibition of bacterial adherence was observed on the implant surface when specimens were immersed into agitated bacterial solution. During biofilm tests, silver ions released to the aqueous environment led to a reduction of bacterial growth in the culture medium incubated with the coated specimen.

6.2. Interface shear strength of porous FRC and bone model material (S-I)

Results of the push-out tests (**S-I**) confirmed that increasing the degree of FRC porosity led to an enhanced mechanical interlocking at the gypsum-FRC interface resulting in higher measured push-out forces and fracture toughness. Applied pins failed to model the initial mechanical implant fixation, as they had no significant effect on the interface shear strength with gypsum. For further experiments (**S-II** and **S-IV**), porous structures of type *FRC p2* were used for this group because this type had sufficient structural stability and simple preparation was combined with a high level of interconnected porosity.

For *FRC p4*, serving as negative control, the push-out resistance was mainly caused by frictional forces as the lack of significant porosity inhibited mechanical interlocking. In case of FRC cores with higher levels of porosity, the observed fracture behavior was a result of mechanical interlock. For the parts of the fracture line at the gypsum-FRC interface, frictional forces were dominant, while the compressive strength and brittleness of penetrated gypsum determined the fracture resistance for cohesive fracture lines passing through the bone model material (Darvell, 2002) (**Figure 24**). For proper analyses of the push-out results, a porous implant surface strongly affects the multi-axial stress distribution at the interface. The basic condition of evenly load distribution throughout interfacial region is not fulfilled (Thompson et al., 1999), thus calculations of shear strength, elastic modulus and total energy absorption were not feasible (Mattila et al., 2006). However, analyses of the work from the time point of maximal load to rupture (W_D) were adequate to demonstrate the prolonged fracture process with increasing macro porosity and to estimate fracture toughness. A quantitative regression analyses to describe the parabolic trend of maximum push-out load with increasing area fraction of gypsum penetration (**Figure 12**) was not undertaken because a fifth data point was missing.

Results of pull-out and push-out tests reflect also mechanical properties of bone / bone model material as their definition implies the fracture of the bone surrounding the implant during the experiment (Brånemark *et al.,* 1998). From a clinical perspective, the push-out shear strength of the implant interface still provides valid information about how strongly an implant is anchored in the bone. By using computer simulation similarly as reported by Shirazi-Adl and Forcione (1992), it would be possible model the multi-axial stress situation in the hybrid interface and get an insight on the different shares of leading to observed push-out strength.

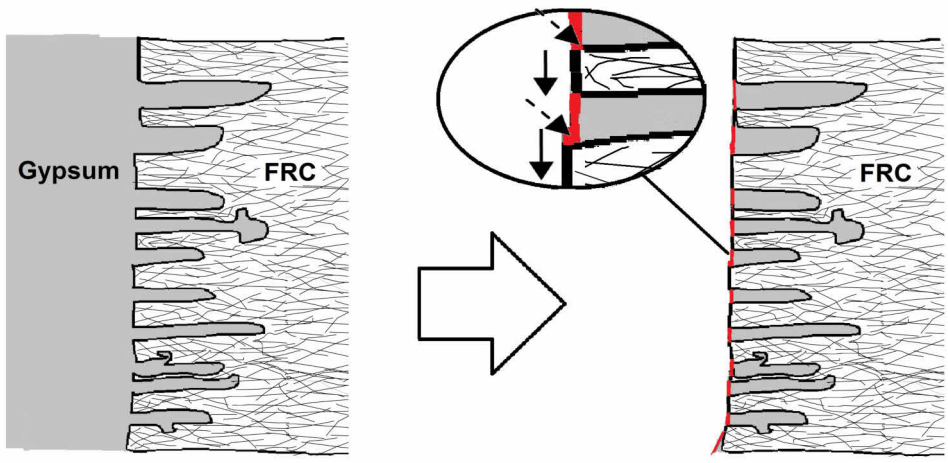

Figure 24: Schema of gypsum penetrating into porous FRC: schema of situation before and after push-out test, plain arrows show the direction of real shear force, dashed arrows the direction of partly compressive shear forces; red line marks the part of the fracture surface inside the gypsum (The bulk porosity of FRC is not represented). Figure adopted from S-I.

Bone model materials, such as gypsum, acrylic cements or PU foams are applied during mechanical implant testing to avoid inhomogeneous properties of preserved natural bone specimen (Ballo et al., 2007; Cristofolini et al., 1996; Sommers et al., 2007). Nevertheless, bone model materials can not reproduce directly the process of bone ingrowth including the temporarily established weak surface layer before bone mineralization (Andersson et al., 1992). In the present model of completed bone ingrowth, previously established to analyze surface porous PMMA-based FRCs (Mattila et al., 2006), gypsum fills all available surface pores as a result of capillary and vibrational forces. Mattila et al. (2006) reported the highest push-out forces of 2149 ± 263 N for grooved control samples with a thickness of 10-mm. In accord with this, maximal loads recorded in the present study were of 1147 ± 271 N for 5.5-mm thick samples. The limiting factor was in both cases the compressive strength of gypsum being 53 MPa stated by the manufacturer or rather the diametral tensile strength of 2.5 MPa reported by Hersek et al. (2002). The results show that porous FRC was stronger than gypsum. Further, the present results contain only limited information on the absolute behaviour of FRC in the *in vivo* environment.

To improve the push-out model, a stronger and less brittle bone model material could be used which resembles the anisotropic mechanical properties of natural long bones (see **Table 1**). Moreover, the initial implant fixation could be modelled by a grooved implant interface instead of placing pins introducing heterogeneous stress distribution (Mattila et al., 2006).

Mattila et al. (2009) proved, with using an *in vivo* rabbit model, the functionality of the porous FRC at the interface to bone. After a follow-up time with bone ingrowth of 12 weeks push-out forces were 283 ± 55 N for surface porous FRC-implants, 131 ± 22 N for titanium implants and only 14 ± 11 N in case of non-porous polymer controls. These values are consistent with present *in vitro* results.

6.3. *In vitro* bioactivity of FRC implants containing bioactive glass (S-II)

In this *in vitro* study BG granules incorporated to the implants were found to evoke CaP formation on the surface of porous FRC structures in static and dynamic test conditions. This was expected as similar precipitation reactions of BG in SBF have been previously reported for other polymeric materials (Abe et al., 1990; Marcolongo et al., 1997).

A precondition for the apatite nucleation on polymers is the enhancement of supersaturation of SBF by silicon and calcium ion release from BG (Kokubo et al., 1991). Heterogeneous nucleation, the initial step of the precipitation at the solid surface, occurs once the local pH of the medium exceeds the isoelectric point of the surface. After the adsorbtion of Ca^{2+} ions to the surface, which stimulates further adsorbtion of HPO_4^{2-} ions, CaP crystals grow spontaneously in SBF (Duan et al., 2004). In dynamic conditions, the attainment of local threshold ion concentrations and CaP precipitation is

postponed compared to the static experimental condition (Duan et al., 2004; Rámila and Vallet-Regi, 2001).

For BG surfaces, the presence of the FRC surfaces lessened the precipitation of CaP (**Figure 16**). Similar results have been reported for degradable polymer composites (Lu et al., 2005). However, as the specimens used in our study were biostable, we think that the larger combined surface area of BG and *FRC1/FRC2*, on which the CaP precipitation occurred, led to the reduced thickness of the CaP layer formed on BG granules compared to the precipitation layer formed on BG granules incubated alone.

As for the granule size of BG, different aspects need to be considered. By using BG with a distinct particle size, porosity is created in the edges between the particles. Interconnected pores of suitable size may serve as chambers for cell differentiation which might be crucial for the *in vivo* bone bonding behavior (Ducheyne and Qiu, 1999) For BG granules of 150-170 µm in size, the Ducheyne and Qiu (1999) observed additional chamber formation in eroded, fully reacted BG after 3 to 6 month after implantation. In the present study, the BG size of 100-250 µm was used according to the thickness of laminate layers. The BG granules of that size were best retained in the structures and ensured wetting throughout the layers (Nganga et al., 2011).

In the static test, the agitation reduced local concentration gradients along the specimen surfaces so that, in contrast to the configuration reported by Abe et al. (1990), similar precipitate structures where observed on the back and front sides of specimens. However, CaP layers on the *FRC2* surface were thickest next to BG granules and the portion of the surface area covered by CaP varied greatly (**Figure 15**). These findings indicated that the establishment of a continuous CaP layer is assured by a complete BG layer throughout the entire laminate structure.

In this study, an accurate direct comparison of the result obtained for *FRC2* specimens incubated with BG granules and *FRC3* containing embedded layers of BG granules was not possible as the effective ratios of surface area of the BG granules to the volume of SBF differed. Variations of the local pH and ion concentration gradients are some of the reasons leading to patterns in CaP precipitation. While the formation of a quite uniform CaP layer was observed on free standing *FRC2* surfaces, the CaP precipitation on *FRC2* surfaces within *FRC3* laminate layers was more pronounced at restricted spots reached by the agitated SBF.

Dynamic immersion systems are a common approach to study the reactivity of bioactive glasses and ceramics in *in vitro* conditions simulating the implant site (Duan et al., 2004; de Aza et al., 2007, Queiroz et al., 2003). Continuous flow or circulatory flow systems with large SBF reservoirs are able to maintain physiological pH level and ion concentrations over a long time period (de Aza et al., 2007; Deng et al., 2005). The present flow system was designed to guaranty the SBF flow through the porous structure of *FRC3,* similar to the approaches of Deng et al. (2005) and Yue et al. (2011). The SBF was circulated and only periodically exchanged, so that it could be assumed that the local threshold ion concentrations for precipitation reactions were exceeded during the

experiment. As a result, the pH level was not kept constant, but precipitation due to SBF flow within the composite could be demonstrated.

The formation of the apatite layer *in vivo* is expected to be delayed compared to the kinetics observed *in vitro,* as the local physiological pH will not change to the same extent (de Aza et al., 2007). Moreover, adherent serum proteins present *in vivo* prevent the apatite nucleation (Bohner and Lemaitre, 2009). Those are possible reasons for the absence of apatite on the polymer implant surfaces next to the BG granules coating in experimental cranial defects after a twelve week study period (Tuusa et al., 2007a). However, in both *in vitro* and *in vivo* conditions, an enhanced osseointegration of FRC implants containing BG granules has been observed (Ballo at al., 2008; Zhao et al., 2009).

6.4. Chitlac degradation in solution and as coating on FRC substrates (S-III)

Degradation kinetics of chitlac in colloidal solution resembled degradation patterns previously reported by Nordtveit et al. (1994) for unmodified chitosan with various degrees of deacetylation. For the enzymatic cleavage reaction by lysozyme the degradation rate decreased over time. This can be ascribed to the decline of specific binding sites of lysozyme (hexameric sequences along the polysaccharide chain) more than to the presence of oligomers which act as enzyme inhibitors. In case of H_2O_2, the random chemical decomposition of the polysaccharide chains followed (pseudo) first order kinetics (Nordtveit et al., 1994; Chang et al., 2001), because the flexible lactose side chains of the grafted polysaccharide do not hinder chitlac degradation in solution (**Figure 20**).

Chitlac, as a coating on FRC substrates was very stable against enzymatic (lysozyme) degradation, because specific binding sides of the polysaccharide chains were not any longer accessible within the polyelectrolyte complexes formed on the polymer surface. Minimal release of chitlac during incubation of porous FRC can be explained as a wash-out effect of unspecifically bound chitlac from surface pores.

The degradation of the chitlac-nAg coating due to H_2O_2 was studied indirectly by detecting the released amount of silver from the coating *via* ETAAS. In this study, deionized water was used as medium to avoid artifacts of insoluble silver complexes formed with ions present in aqueous media. The polysaccharide layer including the silver NPs was not affected during incubation, even though the applied H_2O_2 concentration (3.5%) was at a 100 000 times higher level than the typical physiological extracellular concentration (**Figure 21**) (Stone and Yang, 2006). Therefore, the coating is expected to show long term stability likewise at the implant site *in vivo,* despite inflammatory reactions taking place during the healing process.

The detected total silver content of the specimens (below 600 ng/disc) was well below the reported levels evoking cytotoxicity towards mammalian bone cells, which are above 64 µg/mL (0.048 mM Ag^+ release) (Albers et al., 2013).

Similar to the behavior of present chitlac coatings, Yuan et al. (2008) reported long term stability for chitosan coatings bound *via* silane-glutaraldehyde molecules on titanium surfaces, which were incubated for five weeks in the presence of lysozyme.

6.5. Antimicrobial efficacy of silver-polysaccharide coatings (S-IV)

In this *in vitro* study, the antimicrobial efficacy of chitlac-nAg coating, which had been established previously (Travan et al., 2009 and 2011; Marsich et al., 2013), was studied on dense and porous FRC implants. The silver-polysaccharide coating is intended to act as a stable, antimicrobial film which inhibits bacteria adhesion and biofilm formation in direct contact to the implant (Darouiche, 1999).

In addition to the degradation test described in previous paragraph (**S-III**), the release of silver from chitlac-nAg coated specimen was investigated during immersion in 0.9% (wt/wt) NaCl (Marsich et al. 2013). Here, a sustained release of >90% of the silver load from intact chitlac layers was observed after seven days, accompanied by a decline of antimicrobial activity (**Figure 25**). The variations of the results can be ascribed to factors controlling the strength of silver complexation in the polyelectrolyte film and therefore the ion release. Of major importance are the concentration of electrolytes in the medium, pH, temperature, and presence of organic matter (Stebounova et al., 2011).

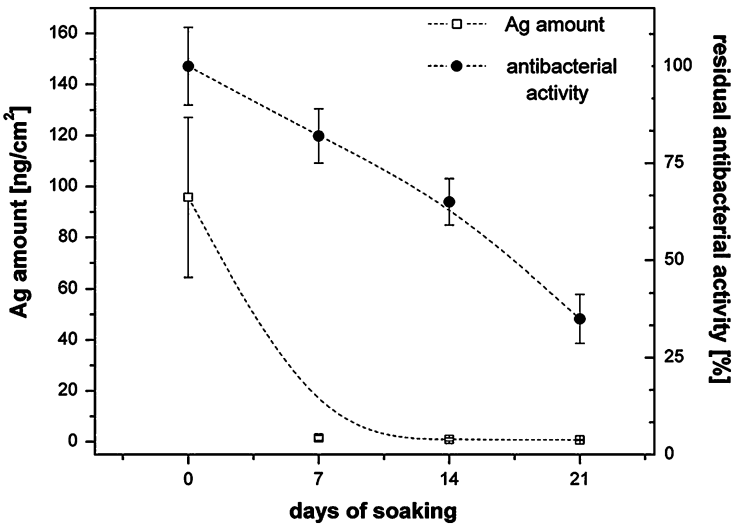

Figure 25: Silver release and persistence of antibacterial effect of chitlac–nAg coatings over time (Figure by E. Marsich, reproduced with Permission) (Marsich et al., 2013).

The results of the three applied microbiological protocols used in the study varied. The volume and exchange rate of bacterial suspension into which the specimens are immersed determines the dissolution kinetics and the local concentration of released silver ions.

The initial adhesion is determined by the interaction between the surfaces of the cell and the material upon contact. To understand the process of adhesion on a microscopic level the physicochemical and thermodynamic interactions due to specific surface characteristics of the microbe and the substrate must be acknowledged (Bos 1999). The incubation medium may also affect the affinity of the bacteria to test surfaces. In pure growth medium (TSB), Barton and co-workers (Barton et al., 1996) reported the amount of bacteria adhering to be halved compared to adherent bacteria cultured in PBS. In the present adhesion test, the silver dissolution led to a reduction of its concentration on the sample surface with following reduction of contact bactericidal activity (see **Table 8**). Compared to the clinical situation the liquid volume and flow are overrated, thus the material's antimicrobial efficacy underestimated.

The antimicrobial test was applied to simulate the performance of the coatings in the case of bacterial contamination of the implant. A low volume of concentrated bacterial suspension was applied between the surface of the specimen and plastic sheet. Therefore, the local silver concentration at the surface of the specimen was high enough to elicit a strong antibacterial activity (**Table 8**). The material efficacy might be slightly overestimated as body fluids at the implant site are exchanged continuously (Jee, 2001).

In the biofilm test, afore mentioned silver release explains the observation of bacterial growth inhibition in the supernatant medium without biofilm inhibition on surfaces of the specimen. This result is reasonable as the antibiotic concentration required for bactericidal activity against sessile organisms can be several orders of magnitude higher than for planktonic bacteria (Dunne, 2002). The difference in behavior of *S. aureus* and *P. aeruginosa,* both being early colonizers during implant infection, might be related to the type specific variation in slime production (Costerton et al., 1999).

Quantitative analyses methods used to study biofilm formation showed a limited applicability for the antimicrobial coating system. Deficits displayed visually in biofilm parts removed and were manifested in high standard deviations in the confocal data.

In this study, porosity introduced to FRC specimens led to an increased number of bacteria adhering (see **Table 8**), which is a result of the larger effective sample surface area compared to the flat polished surfaces. It is well known that rough surfaces attract more bacteria because of surface irregularities (Busscher et al., 2010, Tanner et al., 2001). The substrate material might also affect the durability of the antimicrobial effect, which needs, however, further investigation.

In comparison to the situation *in vivo,* this *in vitro* model represents a simplified situation. Serum protein coating of implant surfaces present under physiological conditions led to a recent *in vitro* study which showed a significant reduction of the antimicrobial activity of silver for *S. aureus* and *P. aeruginosa.* However, a sufficient anti-biofilm activity was maintained (Marsich et al, 2013). The use of a biofilm bioreactor would further enable the simulation of the interaction of multiple microbial species, macrophages, and osteoblast-like cells dependant on the medium flow next to

the implant surface (Lawson et al., 2010; Subbiahdoss et al., 2011) before testing the antimicrobial performance *in vivo* (Malaisrie et al, 1998).

6.6. Future Prospects

The aim of this series of studies was to develop a coating system on FRC implants with sustained antimicrobial and bioactive features. Investigations of this series of studies verified bioactive and short term antimicrobial features of suggested implant modifications separately. Further studies need to address the synergistic effect after combining BG granules and silver-polysaccharide coating in FRC implant structures. In practice, silver-polysaccharide coatings need to be completed before the placement of BG, as BG granules are likely to dissolve during the polymer surface activation process with HCl. Alternatively, another localized way of surface activation which enabels the polyelectrolyte attachment must be developed in order to simplify the implant fabrication process. In the future, these efforts could lead to the development of an implant material that has multiple functionalities (specific coatings) on different spots of the surface.

As for the FRC laminates structures containing BG mechanical properties need to be evaluated, especially flexural strength and impact resistance. Effects of the BG granules size on the bioactive and antimicrobial implant performance are also of interest.

Concerning the polysaccharide coating, further research need to be performed to develop a sole contact-based active antimicrobial coating system with prolonged contact-based activity. One approach to improve the stabilization of the silver NPs within the coating is the formation of a polyelectrolyte multilayer coating with alternate deposition of chitlac-nAg and oppositely charged alginate (Donati et al., 2007; Grunlan et al., 2005). This is to build barrier against ionic interactions with body fluids.

As the present series of studies included only *in vitro* experiments, these results need to be verified *in vivo*. This is especially important to gain further knowledge about processes occuring during the bone ingrowth with and without bacterial contamination and to determine the overall physiological response to the implant.

7. CONCLUSIONS

1) Porous FRC structures obtained by removal of excess resin promote the fixation between bone and implant *via* mechanical interlock. In a push-out model a twofold increase of the interfacial bond strength to bone model material was observed with an increase of the total FRC porosity by 43% (**S-I**).

2) BG granules entrapped with the FRC laminate structure are able to enhance the osseointegration of the implant. Both in the static and dynamic *in vitro* conditions, BG granules were able to conduct known bioactive reactions as well as to induce CaP formation on the surface of FRC (**S-II**).

3) Cationic polysaccharide coatings bound *via* strong electrostatic interactions to functionalized implant surfaces are very stable against degradation during inflammatory reactions during the healing process. Immobilized silver NPs coordinated to charged groups within the polysaccharide molecule are stable in deionized water, but quickly dissolve in presence of aqueous solutions containing electrolytes (**S-III**).

4) The contact-active silver-polysaccharide coating on FRC implants exhibits an adequate short term antimicrobial activity against *Staphylococcus aureus* and *Pseudomonas aeruginosa*, but the initial adhesion of microorganisms to the implant surface is not affected by the antimicrobial coating. Released silver ions from the coating reduce the bacterial growth in the culture medium surrounding the implant (**S-IV**).

ACKNOWLEDGEMENTS

This research was carried out at Turku Clinical Biomaterials Centre of the Department of Biomaterials Science, Institute of Dentistry, University of Turku, Finland, during the years 2011 to 2013. Part of the work was performed at Department of Life Sciences, University of Trieste, Italy during a lab visit in 2011.

My sincere thanks go to Professor Pekka Vallittu for giving me the opportunity to work in his team and his encouraging guidance during my PhD studies. I would like to express my deep gratitude to my second supervisor Adjunct Professor Niko Moritz for interesting discussions, hands-on suggestions to the lab work and sharing experiences on biomaterials research.

For the practical support, especially with mechanical testing and statistic analysis, I would like to thank Lippo Lassila. Appreciation goes to Anne Ylä-Soininmäki and Riina Mattila for good cooperation during the development of porous FRC.

I would like to thank co-workers from Åbo Akademi, namely Adjunct Professor Leena Hupa and Di Zhang, for their guidance and support during planning and performing of immersion tests and analysis of bioactive glass reactions. The help of Linus Silvander during SEM/EDX analyses was highly appreciated.

Special thanks goes to co-authors Professor Sergio Paoletti, Ivan Donati, Andrea Travan, and Eleonora Marsich from Department of Life Sciences, University of Trieste, Italy for the invitation to Italy, the welcoming atmosphere during my stay, fruitful discussions and kind assistance during lab work. Without their contribution it would not have been possible to analyze polysaccharide coatings within this study. Matteo Crosera (from Department of Chemical and Pharmaceutical Sciences, University of Trieste, Italy) is thanked for is help during the analyses of silver ions concentrations.

Further, I am grateful to Adjunct Professor Eva Söderling for guidance during biofilm studies and sharing her microbiological expertise. Liisa Valtonen and Oona Hällfors are acknowledged for their work during microbiological experiments.

In addition, I would like to thank the involved personnel of Institute of Dentistry and TCBC, namely Tarja, Hanna, Minttu, and Sevi for helping in practical matters. Sincere thanks also go to all other colleagues and members of TCBC team for ensuring a pleasant working atmosphere. They include; Yulia, Anne, Aous, Jasmina, Mervi, Sufian, Ferhan, Paula, Kaisa, Leila and Jingwei among others. Kaisa, Paula and Kati are acknowledged for their companionship during conference trips.

Thanks goes to members of the supervisory board Professor Timo Närhi (University of Turku), Adjunct Professor Eva Söderling (University of Turku), Professor Horst Fischer (RWTH Aachen, Germany) and Professor Sergio Paoletti (University of Trieste, Italy)

for reviewing and commenting annual progress reports. Michael Nganga and Robert M. Badeau, Ph.D. are thanked for proofreading the language of the thesis.

Thanks to the reviewers of the thesis, Professor Gudmund Skjåk-Bræk from the Department of Biotechnology, NTNU, Norwegian University of Science and Technology, Norway and Professor Timo Jämsä from the Department of Medical Technology, University of Oulu, Finland. I would also like to thank Professor Serena Best from the Department of Materials Science and Metallurgy, University of Cambridge, UK for accepting the invitation to function as my opponent at the public examination.

I am grateful for the financial support from the Academy of Finland. The work was part of the BioCity Turku Biomaterials Research Programme. Further financial support came from the Finnish National Doctoral Programme of Musculoskeletal Disorders and Biomaterials (TBDP) and resources from the Institute of Dentistry, University of Turku.

Finally, I would like to thank my friends in Finland and Germany for their support and above all, my thanks go to my husband, my daughter, and all other family members for their unlimited love and support.

Turku, August 2013

Sara Nganga

Sara Nganga

REFERENCES

- Abe Y, Kokubo T, Yamamuro T (1990) Apatite coating on ceramics, metals and polymers utilizing a biological process. J Mater Sci Mater M 1:233–238.
- Aho AJ , Hautamäki M, Mattila R, Alander P, Strandberg N, Rekola J, Gunn J, Lassila LVJ, Vallittu PK (2004) Surface porous fiber-reinforced composite bulk bone substitute - In vitro studies and in vivo evaluation in segment defect. Kluwer Academic Publishers, Cell and Tissue Banking 5:213-221.
- Aitasalo K, Kinnunen I, Palmgren J, Varpula M (2001) Repair of orbital oor fractures with bioactive glass implants. J Oral Maxil Surg 59:1390-1395.
- Aitasalo K, Vuorinen V (2007) Bioactive glass in fronto-orbital and skull surgery. 8th European Skull Base Society Congress and 15th German Skull Base Society Congress. Skull Base 2007; 17, doi: 10.1055/s-2007-984150.
- Aitasalo K, Peltola M, Vuorinen V, Vallittu P (2009) Novel composite implants in craniofacial reconstruction. 9th European Skull Base Society Congress. Skull Base Suppl 1, 19:11-12.
- Aitasalo K, Rekola J, Piitulainen J, Vallittu PK (2012) Craniofacial bone reconstruction with a novel bioactive composite implant. J Neurol Surg B 73 - A099.
- Aitasalo KMJ, Piitulainen JM, Rekola J, Vallittu PK (2013) Craniofacial bone reconstruction with bioactive fibre-reinforced composite implant. Head Neck Accepted manuscript online. doi: 10.1002/hed.23370.
- Albers CE, Hofstetter W, Siebenrock KA,Landmann R, Klenke, FM (2013) In vitro cytotoxicity of silver nanoparticles on osteoblasts and osteoclasts at antibacterial concentrations. Nanotoxicology 7:30-36.
- Albrektsson T, Johannsson C (2001) Osteoinduction, osteoconduction and osseointegration. Eur Spine J 10 Suppl 2: s96-101.
- Alexander H (1996) Composites. In: Biomaterials Science - an introduction to materials in medicine. edited by Ratner BD, Hoffman AS, Schoen FJ, Lemons JE, Academic Press. p 94-104.
- Andersson OH, Liu G, Kangasniemi K, Juhanoja J (1992) Evaluation of the acceptance of glass in bone. J Mater Sci Mater M 3:145-150.
- Arstila H, Tukiainen M, Hupa L, Ylänen HO, Kellomäki M, Hupa M (2006) In vitro reactivity of bioactive glass fibers. Advances in Sci and Technol 49:246-251.
- Balas F, Pérez-Pariente J, Vallet-Regí M (1998) Relationship between bioactivity and textural parameters in glasses. In: Bioceramics 11. Edited by LeGeros RZ, LeGeros JP. River Edge, NJ: World Scientific. p 125-128.
- Baldwin AD, Kiick KL (2010) Polysaccharide-modified synthetic polymeric biomaterials. Biopolymers. Pept Sci 94:128–140.
- Ballo AM, Lassila LV, Vallittu PK, Närhi TO (2007) Load bearing capacity of bone anchored fiber-reinforced composite device. J Mater Sci Mater M 18:2025-2031.
- Ballo AM, Kokkari AK, Meretoja VV, Lassila, LVJ, Vallittu PK, Närhi TO (2008) Osteoblast proliferation and maturation on bioactive fiber-reinforced composite surface. J Mater Sci Mater M 19:3169−3177.
- Ballo AM, Akca EA, Ozen T, Lassila L, Vallittu PK, Närhi TO (2009) Bone tissue responses to glass fiber-reinforced composite implants – a histomorphometric study. Clin Oral Implants Res 20:608−615.
- Barton AJ, Sagers RD, Pitt WG (1996) Bacterial adhesion to orthopedic implant polymers. J Biomed Mater Res 30:403-410.
- Blaker JJ, Nazhat SN, Boccaccini AR (2004) Development and characterisation of silver-doped bioactive glass-coated sutures for tissue engineering and wound healing applications. Biomater 25:1319-1329.
- Bohner M, Lemaitre J (2009) Can bioactivity be tested in vitro with SBF solution? Biomater 30:2175–2179.
- Bonucci E (2000) Basic composition and structure of bone. In: Mechanical testing of bone and the bone-implant interface. CRC Press, Boca Raton, p. 3-21.
- Bos R, van der Mei HC, Busscher HJ (1999) Physico-chemistry of initial microbial adhesive interactions—its mechanisms and methods for study. FEMS Microb Rev 23:179–230.
- Brånemark P-I (1983) Osseointegration and its experimental studies. J Prosthet Dent 50:399-410.
- Brånemark P-I, Hansson BO, Adell R, Breine U, Lindström J, Hallén O, Öhman A (1977) Osseointegrated implants in the treatment of the edentulous jaw. Stockholm: Almqvist and Wiksell. p 132.
- Brånemark R, Ohrnell LO, Skalak R, Carlsson L, Branemark PI (1998) Biomechanical characteri-

zation of osseointegration: an experimental *in vivo* investigation in the beagle dog. J Orthop Res 16:61-69.

- Bruens ML, Pieterman H, de Wijn JR, Vaandrager JM (2003) Porous polymethylmethacrylate as bone substitute in the craniofacial area. J Craniofac Surg 14:63-68.

- Brutel De La RA, Dossche KM, Birnbaum DE, Hacker R (2000) First clinical experience with a mechanical valve with silver coating. J Heart Valve Dis 9:123–129.

- Burstein F, Williams JK, Hudgins R, Boydston W, Reisner A, Stevenson K, Cohen S (2006) Hydroxyapatite cement in craniofacial reconstruction: experience in 150 patients. Plast Reconstr Surg 118: 484-489.

- Busscher HJ, Ploeg RJ, Van der Mei HC (2009) SnapShot: biofilms and biomaterials; mechanisms of medical device related infections. Biomater 30:4247-4248.

- Busscher HJ, Rinastiti M, Siswomihardjo W, van der Mei HC (2010) Biofilm formation on dental restorative and implant materials. J Dent Res 89:657-665.

- Cabraja M, Klein M, Lehmann TN (2009) Long-term results following titanium cranioplasty of large skull defects. Neurosurg Focus 26(6):E10.

- Cahn RW, Haasen P and E. J. Kramer EJ (Eds) (1992) Materials science and technology - a comprehensive treatment, Vol 14: Medical and Dental Materials: Williams DF, (Vol Eds), VCH Verlagsgeselschaft mbH, Weinheim, Germany, ISBN 3-527-26827-8.

- Campoccia D, Lucio Montanaro L, Carla Renata Arciola CR (2006) The significance of infection related to orthopedic devices and issues of antibiotic resistance. Biomater 27:2331–2339.

- Cao W, Hench LL (1996) Bioactive materials. Ceram Int 22:493–507.

- Chang KLB, Tai M, Cheng F (2001) Kinetics and products of the degradation of chitosan by hydrogen peroxide. J Agric Food Chem 49: 4845-4851.

- Chiarini L, Figurelli S, Pollastri G, Torcia E, Ferrari F, Albanese M, Nocini PF (2004) Cranioplasty using acrylic material: a new technical procedure. J Craniomaxillofac Surg 32:5–9.

- Chen X, Schluesener HJ (2008) Nanosilver: a nanoproduct in medical application. Toxicolol Lett 176:1–12.

- Cheng Y-J, Zeiger DN, Howarter JA, Zhang X, Lin NJ, Antonucci JM, Lin-Gibson S (2011) In situ formation of silver nanoparticles in photocrosslinking polymers. J Biomed Mater Res B 97:124–131.

- Chim H, Gosein AK (2009) Biomaterials in Craniofacial Surgery - Experimental Studies and Clinical Application. J Craniofac Surg 20:29-33.

- Cho YR, Gosain AK (2004) Biomaterials in craniofacial reconstruction. Clin Plast Surg 31:377-385.

- Chow TW, Cheng YY, Ladizesky NH (1993) Polyethylene fibre reinforced poly(methyl methacrylate) - water sorption and dimensional changes during immersion. J Dent 21:367-372.

- Costerton JW, Stewart PS, Greenberg EP (1999) Bacterial biofilms: A common cause of persistent infections. Science 284:1318-1322.

- Cristofolini L, Viceconti M, Cappello A, Toni A (1998) Mechanical validation of whole bone composite femur models. J Biomech 29:525-535.

- Darouiche RO (1999) Anti-infective efficacy of silver-coated medical prostheses. Clin Infect Dis 29:1371-1377.

- Darouiche RO (2003) Antimicrobial approaches for preventing infections associated with surgical implants. Clin Infect Dis 36:1284–1289.

- Darvell BW (2002) Materials Science for Dentistry. 7th edition, ISBN 962-85391-5-9.

- De Aza AH, Velásquez P, Alemany MI, Pena P, De Aza PN (2007) In situ bone-like apatite formation from a bioeutectic® ceramic in SBF dynamic flow. J Am Ceram Soc 90:1200–1207.

- De Oliveira-Marques V, Cyrne L, Marinho HS, Antunes F (2007) A quantitative study of NF-κB activation by H2O2: Relevance in inflammation and synergy with TNF-α. J Immunol 178: 3893–3902.

- Deng C, Chen J, Fan H, Zhang X (2005) Effect of flowing speed on bone-like apatite formation in porous calcium phosphate in dynamic RSBF. J Mater Sci Lett 40:1809–1812.

- Dhert WJA Jansen, JA (2000) The Validity of a single pushout test. In: An YH, Draughn RA (Eds.), Mechanical testing of bone and the bone-implant interface. CRC Press LLC, Boca Raton, Florida, pp 477-488.

- Dlapka M, Danninger H, Gierl C, Lindqvist B (2010) Technical trends: Defining the pores in PM components. Metal Powder Report 65:30-33.

- Donati I, Stredanska S, Silvestrini G, Vetere A, Marcon P, Marsich E, Mozetic P, Gamini A, Paoletti S, Vittur F (2005) The aggregation of pig articular chondrocyte and synthesis of extracellular matrix by a lactose-modified chitosan. Biomater 26:987-998.

- Donati I, Haug IJ, Scarpa T, Borgogna M, Draget KI, Skjåk- Bræk G, Paoletti S (2007) Synergistic Effects in semidilute mixed solutions of alginate and

lactose-modified chitosan (chitlac). Biomacromolec 8:957-962.

- Duan Y, Zhang Z, Wang C, Chen J, Zhang X (2004) Dynamic study of calcium phosphate formation on porous HA/TCP ceramics. J Mater Sci Mater M 15:1205–1211.

- Ducheyne P (1987) Biocheramics: Material characteristics versus *in vivo* behaviour. J Biomed Mater Res A 2:219-236.

- Ducheyne P, Qiu Q (1999) Bioactive ceramics: the effect of surface reactivity on bone formation and bone cell function. Biomater 20:2287-2303.

- Dunne WM (2002) Bacterial adhesion: Seen any good biofilms lately? Clin Microbiol Rev 15:155-166.

- Engstrand T (2012) Biomaterials and biologics in craniofacial reconstruction. J Craniofac Surg 23:239–242.

- Eppley BL (2002) Craniofacial reconstruction with computer-generated HTR patient-matched implants: use in primary bony tumor excision. J Craniofac Surg 13:650-657.

- Gilardino MS, Cabiling DS, Bartlett, SP (2009) Long-term follow-up experience with carbonated calcium phosphate cement (Norian) for Cranioplasty in Children and Adults. Plast Reconstr Surg 123:983-994.

- Gosain AK, and the Plastic Surgery Educational Foundation DATA Committee Milwaukee, Wis., and Arlington Heights, Ill. (2004) Bioactive glass for bone replacement in craniomaxillofacial reconstruction (Safety and Efficacy Report), Plast Reconstr Surg 114:590-593.

- Gosheger G, Hardes J, Ahrens H, Streitburger A, Buerger H, Erren M, Gunsel A, Kemper FH, Winkelmann W, von Eiff C (2004) Silver-coated megaendoprostheses in a rabbit model—an analysis of the infection rate and toxicological side effects. Biomater 25:5547–5556.

- Greenspan DC, Zhong JP, LaTorre GP (1994) Effect of surface area to volume ratio on in vitro surface reactions of bioactive glass particulates. In: Bioceramics 7. edited by Andersson, Happonen, YliUrpo. New York: Butterworth–Heinemann. p 55–60.

- Grunlan JC, Choi JK, Lin A (2005) Antimicrobial behavior of polyelectrolyte multilayer films containing cetrimide and silver. Biomacromolec 6:1149-1153.

- Hanson SR, Harker LA (1996) Blood coagulation and blood-materials interaction. In: Biomaterials Science - an introduction to materials in medicine. edited by Ratner BD, Hoffman AS, Schoen FJ, Lemons JE, Academic Press. p 193-199.

- Hardes J, Ahrens H, Gebert C, Streitbuerger A, Buerger H, Erren M, Gunsel A, Wedemeyer C, Saxler G, Winkelmann W, Gosheger G (2007) Lack of toxicological side-effects in silver-coated megaprostheses in humans. Biomater 28:2869–2875.

- He J, Söderling E, Lassila LVJ, Vallittu PK (2012) Incorporation of an antibacterial and radiopaque monomer in to dental resin system. Dent Mater 28:e110–e117.

- Heikkilä JT, Mattila KT, Andersson OH, Knuuti J, Yli-Urpo A, Aho AJ (1995) Behaviour of bioactive glass in human bone. Bioceramics 8:35-40.

- Hench LL, Splinter RJ, Allen WC, Greenlee TK (1971) Bonding mechanisms at the interface of ceramic prosthetic materials. J Biomech Mater Res 5:117-141.

- Hench LL (1995) Clinical used of inorganig biomaterials.In: Materials Chemistry. edited by Interrante LV, Casper LA, Ellis AB, American Chemical Society. p525.

- Hench LL (1996) Ceramics, glasses and glass-ceramics. In: Biomaterials Science - an introduction to materials in medicine. edited by Ratner BD, Hoffman AS, Schoen FJ, Lemons JE, Academic Press. p 73-83.

- Hendriks JGE, van Horn JR, van der Mei HC, Busscher HJ (2004) Backgrounds of antibiotic-loaded bone cement and prosthesis-related infection. Biomater 25:545–556.

- Hersek N, Canay S, Akça K, Çiftçi Y (2002) Tensile strength of type IV dental stones dried in a microwave oven. J Prosthet Dent 87:499-502.

- Ho CH, Tobis J, Sprich C, Thomann R, Tiller JC (2004) Nanoseparated polymeric network with multiple antimicrobial properties. Adv Mater 16:957–961.

- Ho ST, Hutmacher DW (2006) A comparison of with other techniques used in the characterization of scaffolds. Biomater 27:1362-1376.

- Houot L, Watnick PI (2008) A novel role for enzyme I of the vibrio cholerae phosphoenolpyruvate phosphotransferase system in regulation of growth in a biofilm. J Bacteriol 190:311-320.

- Hutmacher DW, Rohner D, Yeow V, Lee ST, Brandwood A, Schantz JT (2002) Craniofacial bone tissue engineering using medical imaging, computational modeling, rapid prototyping, bioresorbable scaffolds and bone marrow aspirates. In Reis R and Cohen D (Eds.), Polymer based systems on tissue engineering, replacement and regeneration. Amsterdam: Kluwer Academic. p 333-354.

- Imazato S, McCabe JF, Tarumi H, Ehara A, Ebisu S (2001) Degree of conversion of composites measured by DTA and FTIR. Dent Mater 17:178-183.
- Itälä AI, Ylänen HO, Ekholm C, Karlsson KH, Aro HT (2001) Pore diameter of more than 100 microm is not requisite for bone ingrowth in rabbits. J Biomed Mater Res 58:679-683.
- Jaeger K, Zenz S, Jüttner B, Ruschulte H, Kuse E, Heine J, Piepenbrock S, Ganser A, Karthaus M (2005) Reduction of catheter-related infections in neutropenic patients: a prospective controlled randomized trial using a chlorhexidine and silver sulfadiazine-impregnated central venous catheter. Ann Hematol 84:258-262.
- Jansen JA, von Rectum AF (2004) Textured and porous materials, In: Biomaterials Science – an introduction to materials in medicine. Second edition, edited by Ratner BD, Hoffman AS, Schoen FJ, Lemons JE, Adademic Press. p 218-224.
- Jee WS (2001) Integrated bone tissue physiology: anatomy and physiology. In: Bone mechanics handbook, edited by Cowin SC, ISBN 0-8493-9117-2, Boca Raton, CRC Press.
- Jones JR, Sepulveda P, Hench LL (2001) Dose-dependent behavior of bioactive glass dissolution. J Biomed Mater Res 58:720-726.
- Jones JR, Ehrenfried LM, Saravanapavan P, Hench LL (2006) Controlling ion release from bioactive glass foam scaffolds with antibacterial properties. J Mater Sci Mater M 17:989-996.
- Kawahara K, Tsuruda K, Morishita M, Uchida M (2000) Antibacterial effect of silver-zeolite on oral bacteria under anaerobic conditions. Dent Mater 16:452–455.
- Kim KJ, Sung WS, Suh BK, Moon SK, Choi JS, Kim JG, Lee DG (2009) Antifungal activity and mode of action of silver nano-particles on Candida albicans. Biometals 22:235-242.
- Kubota N, Tatsumoto N, Sano T, Toya K (2000) A simple preparation of half N-acetylated chitosan highly soluble in water and aqueous organic solvents. Carbohydr Res 324:268–274.
- Kokubo T, Hata K, Nakamura T, Yamamuro T (1991) Apatite formation on ceramics, metals and polymers induced by a CaO SiO2 based glass in a simulated body fluid. Bioceramics 4:113–120.
- Kokubo T, Kim HM, Miyaji F, Takadama H, Miyazaki T (1999) Ceramic–metal and ceramic–polymer composites prepared by a biomimetic process. Composites: Part A 30:405-409.
- Kokubo T, Kim H, Kawashita M (2003) Novel bioactive materials with different mechanical properties. Biomaterials 24:2161-2175.
- Kokubo T, Takadama H (2006) How useful is SBF in predicting in vivo bone bioactivity? Biomater 27:2907–15.
- Kumar, MNVR (2000) A review of chitin and chitosan applications. React Funct Polym 46:1-27.
- Kurtz SM, Devine JN (2007) PEEK biomaterials in trauma, orthopedic, and spinal implants. Biomater 28:4845–4869.
- Kuttenberger JJ, Hardt N, Treumann TC (2001) Long-term results following reconstruction of craniofacial defects with titanium micro-mesh systems. J Craniomaxillofac Surg 29:75-81.
- Lawson M, Hoth K, DeForest C, Bowman C, Anseth K (2010) Inhibition of staphylococcus epidermidis biofilms using polymerizable vancomycin derivatives. Clin Orthop Relat Res 468:2081-2091.
- Lee KY, Ha WS, Park WH (1995) Blood compatibilitv and biodegradability of partially IV-acylated chitosan derivatives. Biomater 16:1211-1216.
- Leppäranta O, Vaahtio M, Peltola T, Zhang D, Hupa L, HupaM, Ylänen H, Salonen JI, Viljanen MK, Eerola E (2008) Antibacterial effect of bioactive glasses on clinically important anaerobic bacteria in vitro. J Mater Sci Mater M 19:547–551.
- Lethaus B, ter Laak MP, Laeven P, Beerens M, Koper D, Poukens J, Kessler P (2011) A treatment algorithm for patients with large skull bone defects and first results. J Craniomaxillofac Surg 39:435-440.
- Liao SS, Cui FZ, W. Zhang W, Feng QL (2004) Hierarchically biomimetic bone scaffold materials: Nano-HA/Collagen/PLA composite. J Biomed Mater Res B 69:158-165.
- Lindfors NC, Hyvönen P, Nyyssönen M, Kirjavainen M, Kankare J, Gullichsen E, Salo J (2010) Bioactive glass S53P4 as bone graft substitute in treatment of osteomyelitis. Bone 47:212-218.
- Lok CN, Ho CM, Chen R, He QY, Yu WY, Sun H, Tam P, Chiu JF, Che CM (2007) Silver nanoparticles: partial oxidation and antibacterial activities. J Biol Inorg Chem 12:527-534.
- Lovald S, Kurtz SM (2012) Applications of polyetheretherketone in trauma, arthroscopy and cranial defect repair. In: Peek Biomaterials Handbook. edited by Kurtz SM (First Edition), William Andrew, p 243 – 260.
- Lu HH, Tang A, Oh SC, Spalazzi JP, Dionisio K (2005) Compositional effects on the formation of a calcium phosphate layer and the response of osteoblast-like cells on polymer–bioactive glass composites. Biomater 26:6323–6334.
- Lu L, Sun RW, Chen R, Hui CK, Ho CM, Luk JM, Lau GK, Che CM (2008) Silver nanoparticles inhib-

it hepatitis B virus replication. Antivir Ther 13:253-262.

- Lucke M, Schmidmaier G, Sadoni S, Wildemann B, Schiller R, Haas NP, Raschke M (2003) Gentamicin coating of metallic implants reduces implant-related osteomyelitis in rats. Bone 32:521–531.

- Malaisrie SC, Malekzadeh S, Biedlingmaier JF (1998) In vivo analysis of bacterial biofilm formation on facial plastic bioimplants. Laryngoscope 108:1733-1738.

- Malcher M, Volodkin D, Heurtault B, André P, Schaaf P, Möhwald H, Voegel JC, Sokolowski A, Ball V, Boulmedais F, Frisch B (2008) Embedded silver ions-containing liposomes in polyelectrolyte multilayers: cargos films for antibacterial agents. Langmuir 24:10209-10215.

- Marcolongo M, Ducheyne P, LaCourse WC (1997) Surface reaction layer formation in vitro on a bioactive glass fiber/polymeric composite. Journal of Biomed Mater Res 37:440–448.

- Marcolongo M, Ducheyne P, Garino J, Schepers E (1998) Bioactive glass fiber/polymeric composites bond to bone tissue. J Biomed Mater Res 39:161-170.

- Marsich E, Travan A, Donati I, Turco G, Kulkova J, Moritz N, Aro HT, Crosera M, Paoletti S (2013) Biological responses of silver-coated thermosets: An in vitro and in vivo study. Acta Biomater 9:5088-5099.

- Matsuno A, Tanaka H, Iwamuro H, Takanashi S, Miyawaki S, Nakashima M, Nakaguchi H, Nagashima T (2006) Analyses of the factors influencing bone graft infection after delayed cranioplasty. Acta Neurochir 148:535-540.

- Mattila RH, Puska MA, Lassila LVJ, Vallittu PK (2006) Fibre-reinforced composite implant: in vitro mechanical interlocking with bone model material and residual monomer analyses. J Mater Sci Mater M 41:4321-4326.

- Mattila RH, Laurila P, Rekola J, Gunn J, Lassila LVJ, Mäntylä T, Aho AJ, Vallittu PK (2009) Bone attachment to glass-fibre-reinforced composite implant with porous surface. Acta Biomater 5:1639-1646.

- McElhaney JH, Fogle JL, Melvin JW, Haynes RR, Roberts VL, Alem NM (1970) Mechanical properties of cranial bone. J Biomech 3:495-511.

- Molinaro G, Leroux J, Damas J, Adam A (2002) Biocompatibility of thermosensitive chitosan-based hydrogels: an in vivo experimental approach to injectable biomaterials. Biomater 23:2717–2722.

- Monzón M, García-Alvarez F, Laclériga A, Garcia E, Leiva J, Oteiza C, Amorena B (2001) A simple infection model using pre-colonized implants to reproduce rat chronic Staphylococcus aureus osteomyelitis and study antibiotic treatment. J Orthop Res 19:820-826.

- Moojen DJF, Vogely HC, Fleer A, Verbout AJ, Castelein RM, Dhert WJA (2009) No efficacy of silver bone cement in the prevention of methicillin-sensitive staphylococcal infections in a rabbit contaminated implant bed model. J Orthop Res 27:1002–1007.

- Moreira-Gonzalez A, Jackson IT, Miyawaki T, Barakat K, DiNick V (2003) Clinical outcome in cranioplasty: critical review in long-term follow-up. J Craniofac Surg 14:144-153.

- Moritz N, Vedeel E, Ylänen H, Jokinen M, Peltola T, Areva S, Hupa M, Yli-Urpo A (2003) Bioactive glass and sol-gel-derived TiO2 coatings. Mat Tech Adv Perf Mat 18:29-32.

- Morones JR, Elechiguerra JL, Camacho A, Holt K, Kouri JB, Ramirez JT, Yacaman MJ (2005) The bactericidal effect of silver nanoparticles. Nanotechnol 16:2346–53.

- Motherway JA, Verschueren P, Van der Perre G, Vander Sloten J, Gilchrist MD (2009) The mechanical properties of cranial bone: the effect of loading rate and cranial sampling position. J Biomech 42:2129-2135.

- Murata J, Ohya Y, Ouchi T (1996) Possibility of application of quaternary chitosan having pendant galactose residues as gene delivery tool. Carbohydr Polym 29:69–74.

- Murphy J (1998) Reinforced Plastics Handbook. Second edition, Elsevier advanced technology, ISBN 1 85617 348 8.

- Muzzarelli RAA, Tanfani F, Emanuelli M, Mariotti S (1982) N-(carboxymethylidene) chitosans and N-(carboxymethyl) chitosans: novel chelating polyampholytes obtained from chitosan glyoxylate. Carbohydr Res 107:199–214.

- Nganga S, Ylä-Soininmäki A, Moritz N, Vallittu PK (2011) Wettability of porous glass-fibre reinforced composite implant material with blood. Eur Cells Mater Suppl 1 21:49.

- Nordtveit RJ, Vårum KM, Smidsrød O (1994) Degradation of fully water-soluble, partially N-acetylated chitosans with lysozyme. Carbohydr Polym 23:253-260.

- Peltola MJ, Vallittu PK, Vuorinen V, Aho AAJ, Puntala A, Aitasalo KMJ (2012) Novel composite implant in craniofacial bone reconstruction. Eur Arch Otorhinolaryngol 269:623–628.

- Peutzfeldt A (1997) Resin composites in dentistry: the monomer systems. Eur J Oral Sci 105:97-116.

- Pietrzak WS, Eppley BL (2005) Antibiotic elution from hydroxyapatite cement cranioplasty materials. J Craniofac Surg 16:228-233.
- Prein J, Rahn BA, Plappert C, Perren SM (1998) Scientific and technical background - Manual of fixation in the cranio-facial skeleton. Edited by Prein J, AO Publishing, ISBN 3-540-61810-4, Springer Verlag, Berlin.
- Prendergast PJ, van der Meulen MCH (2001) Mechanics of bone regeneration. In: Bone mechanics handbook. edited by Cowin SC, ISBN 0-8493-9117-2, Boca Raton, CRC Press.
- Puska M, Aho AJ, Tirri T., Yli-Urpo A, Vaahtio M, Vallittu PK (2006) Glass fibre reinforced porous bone cement implanted in rat tibia or femur: histological and histomorphometric analysis. Key Eng Mater 309 - 311:809-812.
- Queiroz AC, Santos JD, Monteiro FJ, Prado da Silva MH (2003) Dissolution studies of hydroxyapatite and glass-reinforced hydroxyapatite ceramics. Mater Charact 50:197–202.
- Ramakrishna S, Mayer J, Wintermantel E, Leong KW (2001) Biomedical applications of polymer-composite materials - a review. Compos Sci Technol 61:1189-1224.
- Rámila A, Vallet-Regí M (2001) Static and dynamic in vitro study of a sol–gel glass bioactivity. Biomater 22:2301–2306.
- Rawlings RD (1993) Bioactive Glasses and Glass-Ceramics. Clin Mater. 14:155-179.
- Retuert J, Fuentes S, Gonzalez G, Benavente R (2000) Thermal effect on the microhardness of chitosan films. Bol Soc Chil Quim 45:323-327.
- Ripamonti U, Crooks J, Kirkbride AN (1999) Sintered porous hydroxyapatites with intrinsic osteoinductive activity: Geometric induction of bone formation. S Afr J Sci 95:335-343.
- Ródenas-Rochina J, Gómez Ribelles JL, Lebourg M (2013) Comparative study of PCL-HAp and PCL-bioglass composite scaffolds for bone tissue engineering. J Mater Sci Mater M 24:1293-1308.
- Ronderos JF, Wiles DA, Ragan FA, Dempesy CW, Culicchia FC, Fontana CJ, Donald E. Richardson DE (1992) Cranioplasty using gentamicin-loaded acrylic cement: A test of neurotoxicity. Surg Neurol 37:356-360.
- Ruyter IE (1995) Physical and chemical aspects related to substances released from polymer materials in an aqueous environment. Advanced Dent Res 9:344.
- Sanus GZ, Tanriverdi T, Ulu MO, Kafadar AM, Tanriover N, Ozlen F (2008) Use of Cortoss as an alternative material in calvarial defects: the first clinical results on cranioplasty. J Craniofac Surg 19:88-95.
- Schierholz JM, Lucasj LJ, Rump A, Pulverer G (1998) Efficacy of silver-coated medical devices. J Hosp Infect. 40:257-262.
- Schierholz JM Beuth J (2001) Implant infections: a haven for opportunistic bacteria. J Hosp Infect 49:87–93.
- Schmitz JP, Hollinger JO (1986) The critical size defect as an experimental model for craniomandibulofacial non-union. Clin Orthop 205:299-308.
- Seitz H, Tille C, Irsen S, Bermes G, Sader R, Zeilhofer HF (2004) Rapid prototyping models for surgical planning with hard and soft tissue representation. CARS2004. Int Congr Ser 1268:567-572.
- Shapiro SA (1991) Cranioplasty, vertebral body replacement, and spinal fusion with tobramycin-impregnated methylmethacrylate. Neurosurg 28:789-791.
- Shi M, Kretlow JD, Nguyen A, Young S, Scott Baggett L, Wong ME, Kasper FK, Mikos AG (2010) Antibiotic-releasing porous polymethylmethacrylate constructs for osseous space maintenance and infection control. Biomater 31:4146-4156.
- Shirazi-Adl A, Forcione A (1992) Finite element stress analysis of a push-out test part II: Free interface with nonlinear friction properties. J Biomech Eng 114:155-161.
- Simoncic B, Tomsic B (2010) Structures of novel antimicrobial agents for textiles - a review. Text Res J 80:1721-1737.
- Søballe K, Hansen ES, Rasmussen HB, Jørgensen PH and Bünger C (1992) Tissue ingrowth into titanium and hydroxyapatite-coated implants during stable and unstable mechanical conditions. J Orthopaed Res 10:285–299.
- Sommers MB, Fitzpatrick DC, Madey SM, Corey Vande Zanderschulp CV, Bottlang M (2007) A surrogate long-bone model with osteoporotic material properties for biomechanical testing of fracture implants. J Biomech 40:3297–3304.
- Stanić V, Dimitrijević S, Antić-Stanković J, Mitrić M, Jokić B, Plećas IB, Raičević S (2010) Synthesis, characterization and antimicrobial activity of copper and zinc-doped hydroxyapatite nanopowders. Appl Surf Sci 256:6083–6089.
- Stebounova L, Guio E, Grassian V (2011) Silver nanoparticles in simulated biological media: a study of aggregation, sedimentation, and dissolution. J Nanopart Res 13:233–244.
- Stevens A, Lowe J (1997) Musculosceletal system. In: Human histology, Mosby. p 227.

- Stone JR, Yang S (2006) Hydrogen peroxide: a signaling messenger. Antioxid Redox Sign 8:243−270.
- Stoor P, Söderling E, Salonen JI (1998) Antibacterial effects of bioactive glass paste on oral microorganisms. Acta Odontol Scand 56:161–165.
- Subbiahdoss G, Fernández IC, Domingues JF, Kuijer R, van der Mei HC, Busscher HJ (2011) In vitro interactions between bacteria, osteoblast-like cells and macrophages in the pathogenesis of biomaterial-associated infections. PLoS One 6(9):e24827. doi: 10.1371/journal.pone.0024827.
- Swords, G (2006) Composite surgical implant made from macroporous synthetic resin and bioglass particles. US patent no. US 7,066,962 B2.
- Taboas JM, Maddox RD, Krebsbach PH, Hollisterc SJ (2003) Indirect solid free form fabrication of local and global porous, biomimetic and composite 3D polymer-ceramic scaffolds. Biomater 24:181-194.
- Tang T, Brooks R, Rushton N, Best S (2010) Production and characterization of HA and SiHA coatings. J Mater Sci Mater M 21:173-181.
- Tang J, Xiong L, Wang S, Wang J, Liu L, Li J, Yuan F, Xi T (2009) Distribution, translocation and accumulation of silver nanoparticles in rats. J Nanosci Nanotechnol 9:4924–4932.
- Tanner J, Vallittu PK, Söderling E (2000) Adherence of Streptococcus mutans to an E-glass fiber-reinforced composite and conventional restorative materials used in prosthetic dentistry. J Biomed Mater Res 49:250-256.
- Tanner J, Vallittu PK, Söderling E (2001) Effect of water storage of E-glass fiber-reinforced composite on adhesion of Streptococcus mutans. Biomater 22:1613-1618.
- Thompson JI, Gregson PJ, Revell PA (1999) Analysis of push-out test data based on interfacial fracture energy. J Mater Sci Mater M 10:863-868.
- Travan A, Pelillo C, Donati I, Marsich E, Benincasa M, Scarpa T, Semeraro S, Turco G, Gennaro R, Paoletti S (2009) Non-cytotoxic silver nanoparticle-polysaccharide nanocomposites with antimicrobial activity. Biomacromolec 10:1429–1435.
- Travan A, Donati I, Marsich E, Bellomo F, Achanta S, Toppazzini M, Semeraro S, Scarpa T, Spreafico V, Paoletti S (2010) Surface modification and polysaccharide deposition on BisGMA/TEGDMA thermoset. Biomacromolec 11:583−592.
- Travan A, Marsich E, Donati I, Benincasa M, Giazzon M, Felisari L, Paoletti S (2011) Silver–polysaccharide nanocomposite antimicrobial coatings for methacrylic thermosets. Acta Biomater 7:337−346.
- Travan A, Marsich E, Donati I, Foulc M-P, Moritz N, Aro HT, Paoletti S (2012) Polysaccharide-coated thermosets for orthopedic applications: from material characterization to in vivo tests. Biomacromolec 13:1564−1572.
- Tuusa SM, Peltola MJ, Tirri T, Lassila LVJ, Vallittu PK (2007) Frontal bone defect repair with experimental glass-fiber-reinforced composite with bioactive glass granule coating. J Biomed Mater Res Part B 82:149−155.
- Tuusa S, Peltola M, Tirri T, Lassila L, Vallittu PK (2007a) A review of two animal studies dealing with biological responses to glass-fibre-reinforced composite implants in critical size calvarial bone defects in rabbits. Key Eng Mater. (Vol. 361-363), Bioceramics 20:471-474.
- Tuusa SM, Peltola MJ, Tirri T, Puska MA, Röyttä M, Aho H, Sandholm J, Lassila LVJ, Vallittu PK (2008) Reconstruction of critical size calvarial bone defects in rabbits with glass-fiber-reinforced composite with bioactive glass granule coating. J Biomed Mater Res B 84:510-519.
- Uctasli S, Tezvergil A, Lassila L, Vallittu P (2005) The degree of conversion of fiber- reinforced composites polymerized using different light-curing sources. Dent Mater 21:469-475.
- Vallittu PK (1996) A review of fiber-reinforced denture base resins. J Prostodont 5:270-276.
- Vallittu PK (1999) Flexural properties of acrylic resin polymers reinforced with unidirectional and woven glass fibers. J Prosthet Dent 81:318–326.
- Vallittu PK (2001) Strength and interfacial adhesion of FRC-tooth system. In: The second international symposion on fibre-reinforced plastics in dentistry, edited by Vallittu PK, Turku University.
- Varin RA (2001) On the fracture toughness of intermetallics estimated from work of fracture. Scripta Mater 45:1357-1363.
- Vårum KM, Myhr MM, Hjerde RJN, Smidsrød O (1997) In vitro degradation rates of partially N-acetylated chitosans in human serum. Carbohydr Res 299:99-101.
- Vincent JF, Bogatyreva OA, Bogatyrev NR, Bowyer A and Pahl AK (2006) Biomimetics: its practice and theory. J R Soc Interface 3:471-482.
- Walenkamp GHIM, Vree TB(1981) Treatment of a patient with impaired renal function with gentamicin-PMMA-beads. Arch Orthop Traumat Surg 99:137-141.
- Wilkinson LJ, White RJ, Chipman JK (2011) Silver and nanoparticles of silver in wound dressings: a review of efficacy and safety. J Wound Care 20:543-549.

- Williams DF (1987) Definitions in biomaterials. Proceedings of a consensus conference of the European Society of biomaterials, Chester, England, March 3-5 1986, Vol. 4 Elsevier, New York.
- Wintermantel E, Ha SW (1998) Biokompatible Werkstoffe und Bauweisen: Implantate für Medizin und Umwelt. Berlin, Germany: Springer-Verlag.
- Wood JL (1971) Dynamic response of human cranial bone. J Biomech 4:1-12.
- Wurm G, Tomancok B, Holl K, Trenkler J (2004) Prospective study on cranioplasty with individual carbon fiber reinforced polymere (CFRP) implants produced by means of stereolithography. Surgic Neurol 62:510–521.
- Wylen EL, Willis BK, Nanda A (1999) Infection rate with replacement of bone fragment in compound depressed skull fractures. Surgic Neurol 51:452–457.
- Yang TC, Chou CC, Li CF (2005) Antibacterial activity of N-alkylated disaccharide chitosan derivatives. Int J Food Microbiol 97:237-245.
- Yoshida K, Tanagawa M, Atsuta M (1999) Characterization and inhibitory effect of antibacterial dental resin composites incorporating silver-supported materials. J Biomed Mater Res 47:516-522.
- Yuan Y, Chesnutt BM, Wright L, Haggard WO, Bumgardner JD (2008) Mechanical property, degradation rate, and bone cell growth of chitosan coated titanium influenced by degree of deacetylation of chitosan. J Biomed Mater Res B 86:245–252.
- Yue S, Lee PD, Poologasundarampillai G, Jones JR (2011) Evaluation of 3-D bioactive glass scaffolds dissolution in a perfusion flow system with X-ray microtomography. Acta Biomater 7:2637–2643.
- Zhao DS, Moritz N, Laurila P, Mattila R, Lassila LVJ, Strandberg N, Mäntylä T, Vallittu PK, Aro HT (2009) Development of a multi-component fibre-reinforced composite implant for load-sharing conditions. Med Eng Phys 31:461−469.
- Zhang D, Leppäranta O, Munukka E, Ylänen H, Viljanen MK, Eerola E, Hupa M, Hupa L (2010) Antibacterial effects and dissolution behavior of six bioactive glasses. J Biomed Mater Res A 93:475–483.